
**UNIVERSIDAD NACIONAL AUTÓNOMA DE MÉXICO**

PROGRAMA DE MAESTRÍA Y DOCTORADO EN INGENIERÍA

INGENIERÍA ELÉCTRICA - TELECOMUNICACIONES

# PERFORMANCE ANALYSIS OF LINK ADAPTATION IN LTE-BASED VEHICULAR NETWORKS

# T E S I S

QUE PARA OPTAR POR EL GRADO DE:

DOCTOR EN INGENIERÍA

**PRESENTA:**

PAÚL ANDRÉS BURBANO ABRIL

**TUTOR PRINCIPAL:**

DR. VÍCTOR RANGEL LICEA, FI UNAM

**COMITÉ TUTOR:**

DR. JAVIER GÓMEZ CASTELLANOS, FI UNAM

DR. MIGUEL LOPEZ GUERRERO, DIE UAM-I

CIUDAD UNIVERSITARIA, CD. MX., MARZO 2022

**JURADO ASIGNADO:**

Presidente: Dr. Ramón Gutiérrez Castrejón

Secretario: Dr. Javier Gómez Castellanos

1$^{er}$ Vocal: Dr. Víctor Rangel Licea

2$^{do}$ Vocal: Dr. Miguel López Guerrero

3$^{er}$ Vocal: Dr. Michael Pascoe Chalke

Lugar donde se realizó la tesis: FACULTAD DE INGENIERÍA, UNAM.

**TUTOR DE TESIS:**

DR. VÍCTOR RANGEL LICEA

---

**FIRMA**

*To my wife Priscila, for her unconditional love and support.*

*To my son Bruno, for being my biggest inspiration.*

*To my parents and brother, for always being there for me.*

**Andrés**

# Acknowledgments

First and foremost, I would like to express my gratitude to my main advisor, Dr. Victor Rangel Licea for his continuous support through this journey.

I would also like to thank my co-advisors, Dr. Miguel Lopez Guerrero and Dr. Javier Gomez Castellanos for their invaluable guidance and encouragement.

Finally, I would like to thank the *Consejo Nacional de Ciencia Y Tecnología (CONACYT)*, for the financial support during my studies.

# Abstract

Vehicular communication systems are expected to revolutionize the transport & mobility sector, enabling improved safety and traffic efficiency. These systems rely on wireless communication technologies to enable vehicular communication. One of these technologies is Long Term Evolution (LTE), which has become one of the most promising solutions for vehicular communications.

The performance of LTE for vehicular communications depends on its ability to adapt to the highly variable propagation conditions of vehicular environments. To achieve this, LTE implements a link adaptation mechanism, which adapts the transmission parameters based on the channel conditions. To this end, link adaptation needs to be able to operate under different communication scenarios, where the transmission conditions depend on whether vehicles communicate with the network infrastructure (LTE-V2I) or with other vehicles (LTE-V2V).

One of the parameters that can be adjusted by link adaptation is the Modulation and Coding Scheme (MCS), which defines the combination of modulation and coding rate. The MCS is particularly relevant, as it has deep implications on both the resource management process and the robustness of the transmissions. Given these implications, it is crucial to understand the effects MCS adaptation on the performance of vehicular communication systems based on LTE. Moreover, this analysis has to be done separately for different communication scenarios in order to provide a broad perspective of its operation.

This thesis addresses this challenge by providing a comprehensive study of the operation and performance of MCS adaptation in vehicular communication systems based on LTE. To this end, the study is performed separately for the LTE-V2I and LTE-V2V, where vehicles communicate with the LTE network infrastructure and with other vehicles in ad hoc fashion, respectively. The study also makes use of different methodologies in each case, using a data-driven and a simulation-based approach for each scenario, respectively.

The results are presented for each communication scenario and provide valuable insights

into the effects of MCS adaptation on the performance of LTE-V2I and LTE-V2V. In the case of LTE-V2I, the results show that MCS adaptation is capable of maintaining high levels of connectivity between the network infrastructure and the vehicles, which could be beneficial for some applications. In turn, in the case of LTE-V2V, the results indicate that MCS adaptation can be useful to reduce interference in the channel and lays the ground for other studies that can leverage the implementation of this mechanism for other applications in LTE-V2V.

# Resumen

Se espera que los sistemas de comunicación vehicular revolucionen los sectores de transporte y movilidad, permitiendo mejorar la seguridad y la eficiencia en el tráfico. La implementación de estos sistemas se basa a su vez en tecnologías de comunicación inalámbricas, las cuales habilitan la comunicación vehicular. Una de estas tecnologías es Long Term Evolution (LTE), la cual se ha convertido en una de las soluciones mas promisiorias para comunicaciones vehiculares.

El rendimiento de LTE para comunicaciones vehiculares depende de su capacidad para adaptarse a las condiciones de propagación altamente variables de los entornos vehiculares. Para lograrlo, LTE implementa un mecanismo de adaptación del enlace, el cual adapta los parámetros de transmisión en función de las condiciones de canal. Para esto, el mecanismo de adaptación del enlace debe ser capaz de operar en diferentes escenarios de comunicación, en donde las condiciones de transmisión dependen si la comunicación se establece entre vehículos y la infraestructura de red (LTE-V2I) o con otros vehículos (LTE-V2V).

Uno de los parámetros que puede ser ajustado por el mecanismo de adaptación del enlace es el esquema de modulación y codificación (MCS). El MCS es particularmente relevante, ya que tiene implicaciones tanto en el proceso de asignación de recursos como en la robustez de la transmisión. Debido a estas implicaciones, es crucial entender los efectos de adaptar el MCS en el rendimiento de sistemas de comunicación vehicular basados en LTE. Además, este análisis debe ser realizado por separado para diferentes escenarios de comunicación con el objetivo de proveer una mejor perspectiva de su operación.

Esta tesis aborda este desafío a través de un análisis exhaustivo de la operación y rendimiento de la adaptación del MCS en sistemas de comunicación vehicular basados en LTE. Para esto, el estudio es realizado de manera separada para LTE-V2I y LTE-V2V, en donde los vehículos se comunican con la infraestructura de red LTE y con otros vehículos de manera directa, respectivamente. El estudio además hace uso de metodologías diferentes en cada caso, usando enfoques basados en datos reales y simulaciones para cada escenario,

respectivamente.

Los resultados son presentados para cada escenario de comunicación y proveen información valiosa con respecto a los efectos de la adaptación del MCS en el rendimiento de LTE-V2I y LTE-V2V. En el caso de LTE-V2I, los resultados muestran que la adaptación del MCS es capaz de mantener altos niveles de conectividad entre la infraestructura de red y los vehículos, lo cual puede resultar beneficioso para determinadas aplicaciones. En cambio, en el caso de LTE-V2V, los resultados indican que la adaptación del MCS puede ser útil para reducir la interferencia en el canal y establece los fundamentos para otros estudios que pueden aprovechar la implementación de este mecanismo para otras aplicaciones en LTE-V2V.

# Contents

# List of Figures

# List of Tables

# List of Acronyms

**3GPP** 3rd Generation Partnership Project
**5G** Fifth generation technology standard for mobile communications
**BPS** Bits Per Second
**AODV** Ad-hoc On-demand Distance Vector
**BLER** Transport Block Error Rate
**CBR** Channel Busy Ratio
**CP** Cycle Prefix
**CQI** Channel Quality Indicator
**CR** Channel Occupancy Ratio
**CRS** Cell-Specific Reference Signals
**CSR** Candidate Subframe Resources
**D2D** Device-to-Device communications
**DMRS** Demodulation Reference Signals
**eNodeB** LTE base station or Evolved Node B
**EPC** Evolved Packet Core
**E-UTRAN** Evolved UMTS Terrestrial Radio Access Network
**FDD** Frequency Division Duplex
**FSMC** Finite-State Markov Chain
**HARQ** Hybrid Automatic Repeat Request
**HSS** Home Subscriber Server
**IDE** Integrated Development Environment
**IEEE** Institute of Electrical and Electronics Engineers
**IP** Internet Protocol
**LTE** Long-Term Evolution
**MAC** Medium Access Control
**MBSFN-RS** Multimedia Broadcast Single Frequency Network Reference Signals

**MCS** Modulation and Coding Scheme
**MME** Mobile Management Entity
**NED** Network Definition
**NIC** Network Interface Card
**OFDMA** Orthogonal Frequency Division Multiple Access
**OSPF** Open Shortest Path First
**PBCH** Physical Broadcast Channel
**PCFICH** Physical Control Format Indicator Channel
**PHICH** Physical Hybrid ARQ Indicator Channel
**PDCCH** Physical Downlink Control Channel
**PDCP** Packet Data Convergence Protocol
**PDN** Packet Data Network
**PDR** Packet Delivery Rate
**PDU** Packet Data Unit
**P-GW** Packet Data Network Gateway
**PSD** Power Spectral Density
**PSS** Primary Synchronization Signals
**PSCCH** Physical Sidelink Control Channel
**PSSCH** Physical Sidelink Shared Channel
**QAM** Quadrature Amplitude Modulation
**QPSK** Quadrature Phase Shift-Keying
**RAN** Radio Access Network
**RB** Resource Block
**RE** Resource Element
**RIP** Routing Information Protocol
**RLC** Radio Link Control
**RRC** Radio Resource Control
**RRC** Resource Reselection Counter
**RRI** Resource Reservation Interval
**RSRP** Reference Signal Received Power
**RSRQ** Reference Signal Received Quality
**RSSI** Reference Signal Strength Indicator
**SB-SPS** Sensing-Based Semi-Persistent Scheduling
**SC-FDMA** Single-Carrier Frequency Division Multiple Access
**SCI** Sidelink Control Information

**S-GW** Serving Gateway
**SINR** Signal-to-Interference-plus-Noise Ratio
**SNR** Signal-to-Noise Ratio
**SUMO** Simulation of Urban MObility
**SSS** Secondary Synchronization Signals
**TB** Transport Block
**TDD** Time Division Duplex
**TraCI** Traffic Control Interface
**TTI** Time Transmission Interval
**UMTS** Universal Mobile Telecommunications System
**UE** User Equipment
**V2I** Vehicle-to-Infrastructure communications
**V2P** Vehicle-to-Pedestrian communications
**V2V** Vehicle-to-Vehicle communications
**V2X** Vehicle-to-Everything communications
**VUE** Vehicular User Equipment
**Wi-Fi** Wireless Fidelity

# Chapter 1

# Introduction

## 1.1 Vehicular networks

The growing demand for an improved driving experience, in combination with the recent advances in wireless communication technologies have been the main driver for the development of vehicular communication systems. In these systems, vehicular networks play a critical role, as they allow vehicles to communicate with other vehicles and their environment.

Through these networks, vehicles can exchange relevant information related to their location, speed or heading direction with their environment. This information can be further leveraged to enable applications that share information [1], improve traffic efficiency [2] and enhance vehicular safety [3], as well as more advanced applications such as autonomous [4] or remote driving [5]. Multiple communication scenarios can arise within vehicular communications environments. For instance, there are scenarios where direct communication between vehicles (V2V) occur, as well as scenarios where vehicles communicate with the network infrastructure (V2I) or with pedestrians (V2P). In vehicular communication systems, all these scenarios are usually referred with the term vehicle-to-everything (V2X) communications [6].

V2X communications can be enabled with the support of different wireless technologies. The following section focuses on the LTE technology as a solution for V2X communications [7].

## 1.2 LTE for vehicular networks

LTE is a mobile communication standard developed by the 3rd Generation Partnership Project (3GPP) [8]. The first version of LTE, known as release 8 [9], was standardized in 2008 and since then it has become the main standard for mobile communications worldwide. Driven by its wide adoption and continuous development, LTE has also become one of the main enablers of 5G communication systems [10].

One of the main applications of 5G systems are V2X communications [11, 12], which are officially supported by LTE since 2017, when release 14 of the standard was finalized [13]. Starting at release 14, LTE has been developed to support multiple communication scenarios, including V2I (LTE-V2I), V2V (LTE-V2V) and V2P (LTE-V2P).

The emergence of LTE as a solution for V2X communications has been driven by technical and financial limitations of the main standard for vehicular communications, that is IEEE 802.11p [14, 15, 16]. The technical limitations addressed by LTE are related to reliability and scalability, both of which are critical in vehicular communications [17, 18]. In addition, LTE has provided a clearer business plan, which has motivated the adoption of LTE in multiple countries as the main standard for vehicular communications [19].

This adoption has driven the continuous development of LTE during the recent years in comparison with the IEEE 802.11p standard [20]. During this period, V2X communications have been a priority in newer releases of the LTE technology, such as releases 15 [21] and 16 [22]. This highlights the importance of vehicular communication systems for the present and future of mobile communications.

## 1.3 Problem statement

The performance of vehicular communication systems depends heavily on their ability to adapt their operation in response to the dynamic characteristics of vehicular environments. In LTE-V2X, the procedure in charge of adapting the operation of the communication system is known as link adaptation. The main goal of this procedure is to adjust the parameters of the LTE-V2X transmitter to allow it to better respond to the dynamic nature of the communication channel.

Link adaptation can modify different transmission parameters to achieve this goal. Among these parameters are the transmission power, the number of transmission antennas or the MCS. The last one is particularly relevant to the operation of LTE-V2X, as it

modifies both the amount of information that can be carried by the available resources as well as the robustness of the transmission.

The MCS defines the modulation method and coding rate, which determine the amount of bits that can be carried per frequency unit. Therefore, adapting the MCS has a direct influence on the resource management process performed by the Medium Access Control (MAC) layer and ultimately on the transmission capacity of the system. In addition, adapting the MCS affects the performance of the transmissions at the link level, where the selected combination of modulation method and coding rate determines the robustness of the transmission against propagation effects such as pathloss, shadowing and interference.

Moreover, the operation of MCS adaptation in LTE-V2X varies depending on the communication scenario. For instance, in LTE-V2I the operation of MCS adaptation depends on whether it is implemented at the LTE base station or at the vehicle, both of which have different transmission characteristics. Furthermore, in LTE-V2I transmissions between the LTE base station (eNodeB) and the Vehicular User Equipment (VUE) are commonly unicast, while LTE-V2V supports broadcast transmission only. The operation of MCS adaptation in LTE-V2I is different in comparison to LTE-V2V also because in the latter both transmitters are vehicles that can experience highly variable conditions in the communication channel due to their mobility.

As discussed above, adapting the modulation method and the coding rate as a mechanism to cope with the dynamic characteristics of the communication channel has multiple implications in the operation of LTE-V2X. Moreover, this implications can be considerably different depending if the mechanism is executed either in the LTE-V2I or the LTE-V2V communication scenarios.

Therefore, it is crucial to understand the effects of adapting the modulation and coding rate on the performance of data transmissions in LTE-V2X, in order to assess its suitability as a link adaptation mechanism. Moreover, to analyze these effects accurately, the study must be performed separately for both LTE-V2I and LTE-V2V, given the differences between transmitter characteristics and mobility conditions of each scenario. The study further requires the development of models that characterize the operation of MCS adaptation in LTE-V2X. The implementation of such models is critical to accurately analyze the effects of MCS adaptation in the operation of LTE-V2X.

This thesis addresses all these challenges by studying the effects of MCS adaptation in LTE-V2X in detail. To this end, the study is performed separately for LTE-V2I and LTE-V2V and proposes different models for each communication scenario, providing a comprehensive perspective of the impact of MCS adaptation on LTE-V2X.

## 1.4 Objectives and methods

The main objective of this thesis is to evaluate the performance of the MCS adaptation in LTE-V2X. Specifically, to study the performance of MCS adaptation, given its wider implications on the operation of the LTE-V2X system.

To this end, two specific objectives have been proposed. The first objective focuses on analyzing the performance of MCS adaptation in the downlink channel of the LTE-V2I communication scenario. In turn, the second objective focuses on the performance of MCS adaptation but in the sidelink channel of the LTE-V2V communication scenario. Both of these scenarios have been evaluated separately in order to provide an accurate assessment of the performance of MCS adaptation in LTE-V2X, where both scenarios are expected to arise.

The methodology followed in this thesis has also been selected depending on the specific objective. In both cases, the methodology proposes the development of models that characterize the operation of MCS adaptation in LTE-V2I and LTE-V2V scenarios as a mechanism to evaluate the performance of this procedure.

Specifically, the methodology to analyze the performance of MCS adaptation in the LTE-V2I scenario is based on the analysis of a dataset containing channel quality measurements collected by LTE users in a real-world vehicular environment. From this dataset, a model that characterizes the channel quality experienced by the vehicles is developed. The model is then used to generate the information required by MCS adaptation in LTE-V2I in order to select the combination of modulation method and coding rate and to evaluate its performance in terms of the maximum transmission capacity.

In turn, the methodology to analyze the performance of MCS adaptation in the LTE-V2V scenario is based on simulation models. The models are developed in an open source discrete-event simulator to replicate the operation of MCS adaptation in LTE-V2V and the vehicular communication environment. The simulation models are then used to evaluate the performance of MCS adaptation in LTE-V2V, where the procedure is used to select a combination of modulation method and coding rate in response to the levels of interference in the channel.

## 1.5 Related literature

In this section, the literature related to the study of link adaptation and MCS adaptation in LTE-V2X is discussed. The literature has been reviewed separately for the LTE-V2I and LTE-V2V communications scenarios.

In LTE-V2I, link adaptation can be performed either by the eNodeB or by the LTE User Equipment (UE) in the downlink and uplink channels, respectively and the operation of the procedure depends on where it is executed. The first part of this section focuses on the literature related to the analysis of link adaptation in the downlink of LTE-V2I, which corresponds to the first objective of this thesis.

The performance of link adaptation in LTE-V2I has been analyzed in different studies. The following studies made use of real-world measurements collected during unicast transmissions in the downlink channel of an LTE network that was deployed in a vehicular environment. These studies have been selected as they follow a similar methodology to the one implemented in the first part of this thesis, where the performance of link adaptation in the downlink channel of LTE-V2I is analyzed.

In [23], the performance of MCS adaptation is evaluated by analyzing metrics such as throughput, number of transmission errors and channel quality in the downlink direction. These metrics are analyzed through real-world measurements collected by commercial UEs in a vehicular environment. The results show that the quality of the downlink channel is significantly degraded due to the high mobility of the vehicles. The results also show how MCS adaptation in LTE-V2I adapts the MCS to cope with the degraded channel conditions, resulting in a reduction of the transmission capacity.

A similar study is presented in [24], where measurements are collected from an LTE network using specialized equipment installed in vehicles. The measurements are collected under different levels of mobility for metrics such as the Signal-to-Noise Ratio (SNR), throughput and the power levels of control signals in the downlink direction. The results show that executing MCS adaptation in LTE-V2I can reduce the transmission capacity in the downlink channel up to 70% when vehicles are moving at higher speeds in order to adapt the transmission parameters to the channel conditions.

Similarly, a more recent study is presented in [25], where channel quality and performance metrics like throughput are collected in an LTE network. The measurements are also collected by commercial UEs under vehicular mobility conditions. The results show that even though the analyzed LTE network implements a higher bandwidth in the downlink channel by using carrier aggregation [26], the transmission capacity is considerably reduced

at higher levels of mobility due to the implementation of MCS adaptation.

Another study in [27] shows a more detailed analysis of the downlink channel quality under high mobility conditions. The study extracts the channel quality reports sent by the UEs that are required to perform MCS adaptation at the eNodeB. The results indicate that UEs moving at relatively high speeds report considerable worse channel conditions compared to UEs that are static or moving at lower speeds. Interestingly, the results show that channel quality reports remain stable during a shorter period for moving UEs, resulting in unstable transmission capacity as a result of the execution of MCS adaptation.

Other studies like [28, 29] also make use of measurements collected in vehicular environments to assess the performance of LTE-V2I. Even though these studies do not focus specifically on the performance of MCS adaptation, they show the effects of high mobility in the downlink of LTE-V2I in terms of shadowing or channel losses, both of which have an impact on the operation of MCS adaptation in LTE-V2I.

It is important to note that the studies discussed above analyze the operation of LTE-V2I as well as MCS adaptation through measurements collected from real-world deployments of commercial LTE networks. Therefore, they provide valuable insights in the operation of LTE-V2I under realistic conditions, where vehicular networks are expected to operate.

However, different from these works, the study presented in the first part of this thesis focuses not only on analyzing the performance of MCS adaptation of LTE-V2I but also on characterizing the reports collected by UEs, which are required to execute the procedure. This information is critical for the operation of MCS adaptation in LTE-V2I [30, 31, 32], as it allows the eNodeB to accurately track the channel and execute the procedure in vehicular environments where the propagation conditions vary rapidly.

Different from LTE-V2I, in LTE-V2V the link adaptation procedure is performed only by vehicles. Since vehicles (also known as VUEs) are usually moving, the transmission conditions of the channel in the LTE-V2V scenario can be highly dynamic, making link adaptation critical. In the second part of this section, the literature related to the analysis of link adaptation in the LTE-V2V scenario is discussed.

In LTE-V2V vehicles only support broadcast transmissions. This means that transmissions from any vehicle in the channel can be received by all vehicles within its transmission range. Therefore, link adaptation decisions in LTE-V2V are not based on information reported from the receiving vehicles, as this would be highly inefficient considering that each receiver can experience considerably different channel conditions.

In LTE-V2V, link adaptation can be implemented by adapting the transmission power

or the MCS configuration. By adapting these parameters, link adaptation can be used to improve the performance of broadcast transmissions in LTE-V2V as well as for other applications such as congestion control or the transmission of packets of variable size.

The following part of this section discusses the studies that focus on the operation of link adaptation in LTE-V2V. It is worth mentioning that all these studies have made use of simulation models to analyze the operation of the procedure. This is the same modeling methodology implemented in the second part of this thesis, where the performance of link adaptation in LTE-V2V is evaluated.

Some of the analyzed studies focused on the transmission power as the link adaptation parameter in LTE-V2V. This is the case of [33], where an adaptive transmission power solution is analyzed and compared against fixed transmission power configuration. The solution uses two different transmission power configurations depending on the average distance between the transmitter and receiver. The results show that adapting the transmission power can improve the performance of broadcast transmissions in LTE-V2V for vehicles within the transmission range, in comparison to the fixed configuration.

A similar study is presented in [34], where a mechanism that adapts the transmission power based on the vehicular density is analyzed. The mechanism allows each vehicle to use a higher transmission power when the vehicular density is low, and reduces the power as the density increases. The results show that the proposed solution outperforms fixed transmission power configurations and other adaptive mechanisms, particularly in environments where channel interference increases due to higher vehicular density.

Other studies have evaluated the performance of link adaptation, but as a congestion control mechanism in LTE-V2V. The goal of congestion control is to reduce the channel interference that occurs as a consequence of high vehicular density. To achieve this goal, vehicles can either reduce their transmission power, or limit their channel occupation by reducing the amount of transmissions resources.

The study presented in [35] discusses a transmission power control mechanism for congestion control in LTE-V2V. The mechanism proposes to use lower transmission power under high levels of interference in the channel and shows that some improvements can be achieved, particularly for event-driven message transmissions. Similarly, the study in [36] analyzes a solution based on transmission-power adaptation for congestion control. The mechanism adapts the transmission power based on collision probability estimations and channel measurements, and is able to reduce transmission errors and update delay under high vehicular density.

Link adaptation can also be used for congestion control by increasing the MCS, which

limits the channel interference by reducing the amount of frequency resources required to transmit information. The potential of this mechanism for congestion control has been discussed in several studies [37, 38, 38, 39]. However, different from these works, the study in the second part of this thesis presents a detailed analysis of the operation of MCS adaptation and evaluates its performance for congestion control in LTE-V2V.

Finally, other studies have discussed the implementation of MCS adaptation for other applications in LTE-V2V. Among these are the transmission of packets of variable size in LTE-V2V [40, 41], or more generally the optimization of broadcast transmission in vehicular networks through data rate adaptation, as discussed in works that propose this solution for the 802.11p technology in [42, 43, 44].

## 1.6 Thesis contributions

This thesis makes the following contributions:

1. A method to analyze measurements that are collected by UEs in real-world deployments of LTE in vehicular environments. The methodology can be used to extract useful data collected by commercial LTE UEs in order to evaluate the performance of MCS adaptation in LTE-V2I.

2. A method to model the channel quality experienced by UEs in a vehicular environment by means of a finite-state Markov chain (FSMC). The FSMC is then used to generate the information required to analyze the operation of link adaptation in LTE-V2I.

3. A study of the effects of MCS adaptation on the operation of LTE-V2V. The study includes an analysis of the impact of MCS adaptation on the resource organization, the computation of the power levels in the channel and the resource management process in LTE-V2V.

4. A method to model the operation and analyze the performance implications of adapting the MCS for congestion control in LTE-V2V. The model also provides the foundations for other studies that can leverage the implementation of MCS adaptation for other purposes.

## 1.7 Publications

### Conference Papers

[45] A. Burbano-Abril, B. McCarthy, M. Lopez-Guerrero, V. Rangel and A. O'Driscoll, "MCS Adaptation within the Cellular V2X Sidelink," 2021 IEEE Conference on Standards for Communications and Networking (CSCN), 2021, pp. 111-117, doi: 10.1109/CSCN53733.2021.9686168.

### Refereed Journals

[46] A. Burbano-Abril, R.M. Edwards, V. Rangel-Licea, R. Aquino-Santos, M. Lopez-Guerrero, R.S. Kalawsky, and M. Behjati. Modeling and analysis of lte connectivity in a high mobility vehicular environment. Computers and Electrical Engineering, 68:322–336, 2018.

### Other Publications

[47] Brian McCarthy, Andres Burbano-Abril, Victor Rangel-Licea, and A. O'Driscoll. Opencv2x: Modelling of the v2x cellular sidelink and performance evaluation for aperiodic traffic. CoRR, abs/2103.13212, July 2021.

## 1.8 Thesis organization

The structure of this thesis is organized as follows. Chapter 2 presents the background of LTE-V2X, focusing on the operation of the MCS adaptation at the MAC and physical layers of LTE-V2I and LTE-V2V. Chapter 3 presents a study where the performance of MCS adaption in LTE-V2I is analyzed. To this end, a novel downlink-channel quality model for LTE-V2I is introduced and used to evaluate the performance of MCS adaptation by obtaining the transmission capacity in the downlink channel of LTE-V2I. In Chapter 4 an analysis of the effects of MCS adaptation in the operation of LTE-V2V is presented. To this end, a model for the operation of the mechanism is introduced and used to analyze its performance for congestion control in LTE-V2V. Finally Chapter 5 concludes the thesis.

# Chapter 2

# Background

## 2.1 Introduction

LTE supports multiple V2X communication scenarios. These include communication between the vehicle and the LTE network infrastructure (LTE-V2I), direct communication between vehicles (LTE-V2V) and communication between vehicles and pedestrians (LTE-V2P). All these scenarios are illustrated in Figure 2.1.

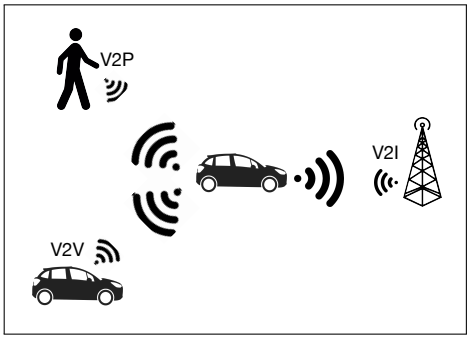


Figure 2.1: LTE-V2X communication scenarios.

This chapter presents the background of LTE-V2X, specifically focusing on the operation of MCS adaptation in LTE-V2I and LTE-V2V. To this end, the remaining of this chapter is organized as follows. Section 2.2 discusses the architecture of LTE-V2I and LTE-V2V, while Sections 2.3 and 2.4 describe the protocol stack and the main concepts of the physical and MAC layers of LTE-V2I and LTE-V2V, respectively.

## 2.2 Architecture

The architecture of LTE-V2X comprises three main components. These are the Evolved Packet Core (EPC), the Evolved UMTS Terrestrial Radio Access Network (E-UTRAN) and the VUE. The architecture of LTE-V2X is shown in Figure 2.2.

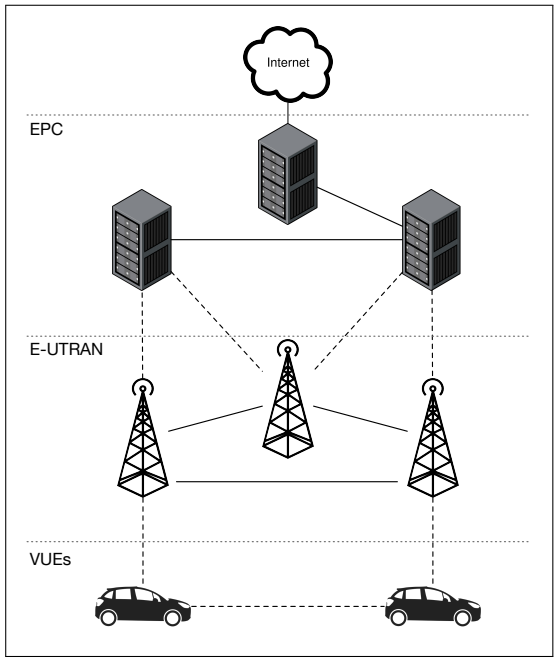


Figure 2.2: LTE-V2X architecture.

### 2.2.1 Evolved Packet Core

At the core of the LTE-V2X architecture is the EPC, which is in charge of packet management throughout the network. The operation at the EPC relies entirely on the Internet Protocol (IP) to transport all services. The EPC comprises different entities, such as the Mobile Management Entity (MME), the Packet Data Network Gateway (P-GW), the Serving Gateway (S-GW), the Home Subscriber Server (HSS) and all the interfaces connecting them. The EPC and its main entities are shown in Figure 2.3.

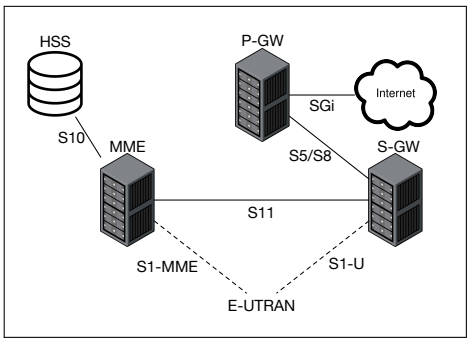


Figure 2.3: EPC.

Each entity at the EPC performs tasks that are critical for the operation of LTE-V2X. For instance, the MME processes all the signaling between the EPC and VUE during mobility procedures and communicates with the HSS, which contains all subscriber information. The connectivity between the VUE and external Packet Data Networks is managed by the P-GW. In turn, the S-GW provides important functionalities at the user-plane, such as routing and mobility management. All the EPC entities interoperate with the E-UTRAN to provide different services as discussed in the next section.

### 2.2.2 Evolved UMTS Terrestrial Radio Access Network

Another component of the LTE-V2X architecture is the access network, also known as E-UTRAN. The E-UTRAN is mainly responsible for managing the radio interface of LTE-V2X through the LTE base station, known as eNodeB. As shown in Figure 2.4, the E-UTRAN usually comprises a network of eNodeBs, interconnected through the X2 interface and distributed across the service area of the operator.

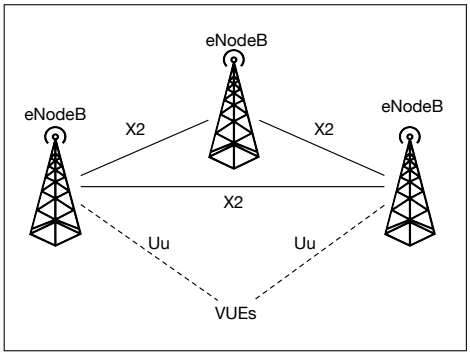


Figure 2.4: E-UTRAN.

Within the E-UTRAN, each eNodeB performs critical control-plane functions such as radio resource management, mobility management and monitoring of all signaling at the radio interface. At the user-plane level, each eNodeB provides data security functions such as encryption and ciphering of all the data sent over the radio interface.

### 2.2.3 Vehicular User Equipment

The user terminal, also known as VUE in LTE-V2X is the final component of the LTE-V2X architecture. This architecture comprises both LTE-V2I and LTE-V2V communications, which are managed independently by different interfaces. This is shown in Figure 2.5, where it can be seen that LTE-V2I communications between the VUE and the EPC are managed by the Uu interface, while LTE-V2V communications among VUEs are managed by the PC5 interface.

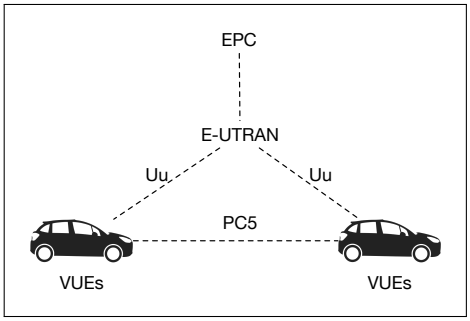


Figure 2.5: VUE.

The VUE plays important functions at the user and control planes of both interfaces. At the Uu interface, the VUE is partially responsible for managing the connection among VUEs and external Packet Data Networks (PDNs). In addition, it performs important functions related to radio resource management, such as the measurements required by mobility procedures or link adaptation. Similarly, at the PC5 interface, the VUE manages the connection with other VUEs and performs radio resource management autonomously or with support of the eNodeB.

One of the main procedures executed at the Uu and PC5 interfaces is link adaptation and specifically MCS adaptation. Since this procedure is the main focus of this thesis, the following sections provide the background required to understand its operation in LTE-V2I and LTE-V2V communications.

## 2.3 LTE-V2I communications

As discussed in Section 2.2.3, the Uu interface is the main point of connection between the VUE and the eNodeB at the radio access network of LTE-V2I. To manage this connection, the Uu interface implements a protocol stack that guarantees reliable communication at the radio interface. This section describes the operation of the protocol stack at the Uu interface, focusing on the physical and MAC layers, where the MCS adaptation procedure is executed.

### 2.3.1 Protocol stack

The protocol stack at the Uu interface is shown in Figure 2.6 and comprises a set of protocols that perform diverse control functions at the radio interface.

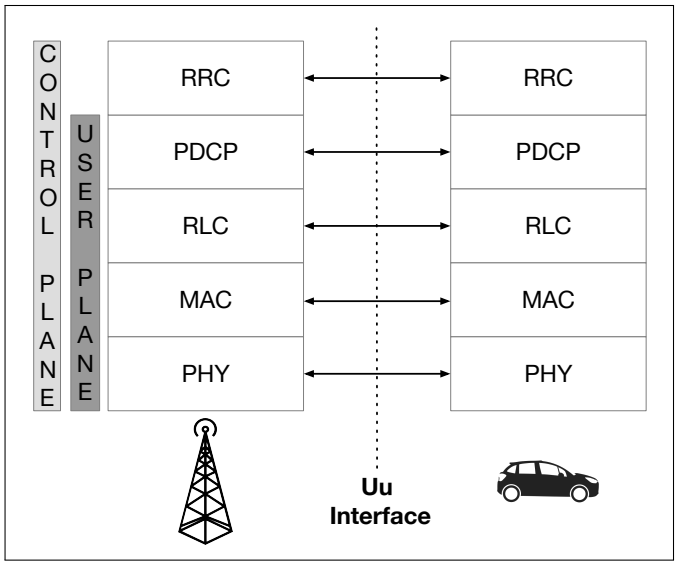


Figure 2.6: Protocol stack for the Uu interface in LTE-V2I.

These protocols, also known as layers, are shared between the user and control planes of the Uu interface and perform specific functions, as described below:

- **Radio Resource Control (RRC):** The RRC protocol performs admission control and manages signaling and control information between VUEs and the eNodeB.
- **Packet Data Convergence Protocol (PDCP):** The PDCP protocol is responsible for encryption and security of user data, IP header compression, control of packet transmission sequence and duplicate detection.

- **Radio Link Control (RLC):** The RLC layer performs different tasks depending on the operation mode, such as broadcasting, segmentation and concatenation or packet retransmission control.
- **MAC layer:** The MAC layer performs radio interface management tasks such as dynamic resource allocation and MCS adaptation as well as error correction through the implementation of Hybrid Automatic Repeat Request (HARQ) [48].
- **Physical layer:** The physical layer is responsible of radio interface-related tasks such as signal processing, synchronization, modulation/demodulation, coding/decoding, error detection and channel quality estimation required for MCS adaptation.

As described above, the operation of MCS adaptation in LTE-V2I is performed by the physical and MAC layers at the protocol stack. Therefore, the main concepts of both layers related to the MCS adaptation procedure are described in the following sections.

### 2.3.2 Physical layer

As previously discussed, LTE-V2I makes use of the Uu interface for the communications between a vehicle and the cellular network infrastructure of LTE. The communication occurs in the uplink and downlink directions, with both directions sharing the same protocol stack described in Subsection 2.3.1. However, even though the protocol stack is the same for downlink and uplink, there are some key differences at the physical layer due to the different transmission characteristics of eNodeBs and VUEs.

This section focuses on the physical layer of the LTE-V2I downlink, where some of the processes required by MCS adaptation are executed.

#### 2.3.2.1 Resource structure

The downlink channel of LTE-V2I implements Orthogonal Frequency Division Multiple Access (OFDMA) at the physical layer [49]. With OFDMA, downlink signals are multiplexed in orthogonally-spaced subcarriers and span over the entire channel bandwidth as illustrated in Figure 2.7.

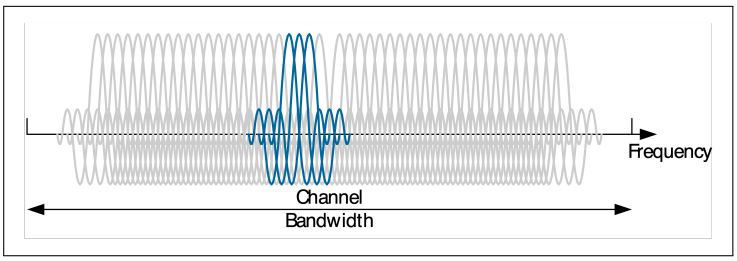


Figure 2.7: Orthogonally-spaced subcarriers multiplexed by OFDMA [50].

These subcarriers have a bandwidth of 15 kHz and the number of subcarriers that are available directly depends on the configured channel bandwidth. In LTE-V2I, the downlink channel bandwidth can be configured to 1.4, 3, 5, 10, 15 and 20 MHz, corresponding to 72, 180, 300, 600, 900 and 1200 subcarriers that can be used for transmission, respectively.

At the physical layer, the subcarrier represents the smallest resource in the frequency domain. However, in LTE-V2I, subcarriers are organized in groups of 12 (180 kHz of total bandwidth) prior to be allocated and correspond to the minimum amount of frequency resources that can be used for data transmissions.

In contrast, in the time domain resources are organized in OFDMA symbols. Similar to the frequency domain, the symbols are further grouped into subframes of 1 ms and frames of 10 ms. Therefore, each subframe can contain up to 14 OFDMA symbols plus a Cycle Prefix (CP), which contains a portion of the first OFDMA symbol in order to reduce the effects of interference caused by the spread delay as illustrated in Figure 2.8.

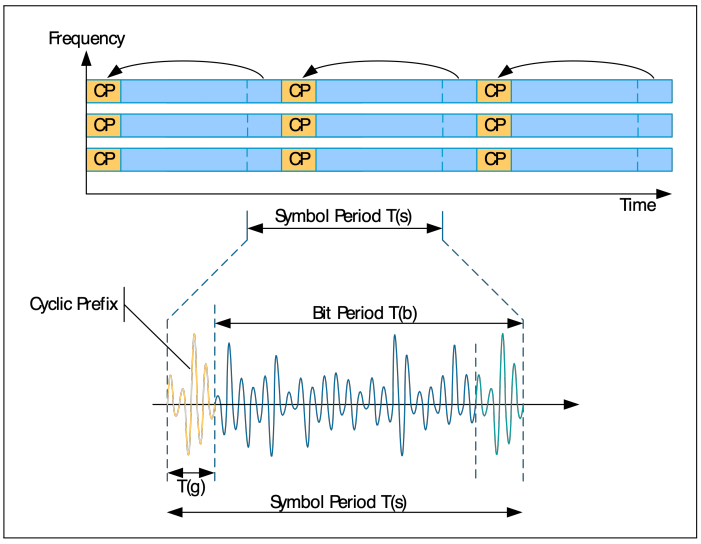


Figure 2.8: OFDMA symbol and CP [50].

In LTE-V2I, a subframe of 1 ms is the minimum amount of time resources that can be allocated. The combination of 12 subcarriers and 1 subframe create a Resource Block (RB), which is depicted in Figure 2.9. The number of RBs in the downlink direction of LTE-V2I depends on the channel bandwidth and there can be 15, 25, 50, 75 and 100 RBs for channel bandwidths of 1.4, 3, 5, 10, 15 and 20 MHz, respectively.

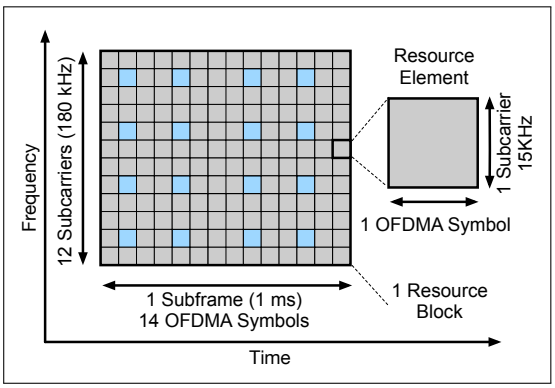


Figure 2.9: Downlink RB structure.

The available RBs create a grid structure of time-frequency resources as depicted in Figure 2.10 for a channel bandwidth of 1.4 MHz and a frame of 10 ms.

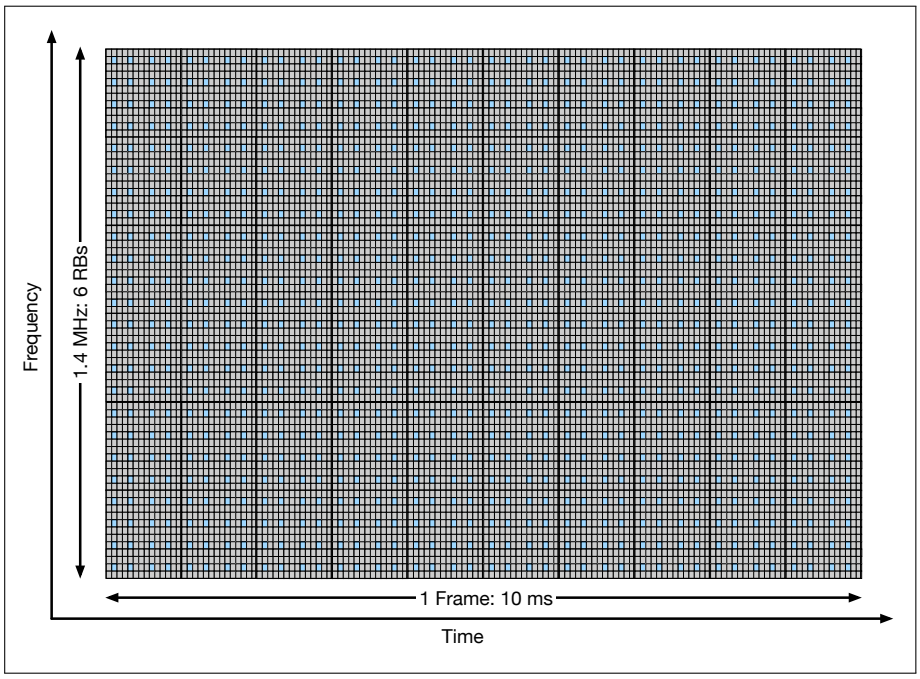


Figure 2.10: Resource grid structure for a 1.5 MHz channel bandwidth.

As shown in Figures 2.9 and 2.10, each RB contains OFDMA symbols in the time domain and subcarriers in the frequency domain. However, within this structure the are smaller time-frequency resources known as Resource Elements (REs), which comprise 1 OFDMA symbol and 1 subcarrier.

The REs are the smallest resource unit where information can be encoded and can be used either for data transmission or for the execution of control procedures in LTE-V2I. In the latter case, REs are used to carry control signals known as reference signals, which are critical for procedures such as cell selection, handovers and MCS adaptation.

#### 2.3.2.2 Downlink reference signals

In LTE-V2I, downlink reference signals are transmitted periodically and in specific REs within each RB of the resource grid. There are different types of downlink reference signals, such as Cell-Specific Reference Signals (CRS), Demodulation Reference Signals (DMRS) and Multimedia Broadcast/Multicast Single Frequency Network Reference Signals (MBSFN-RS) [51].

CRS are transmitted in every subframe and RB within the resource grid and their number depends on the number of antennas at the eNodeB. CRS are used for channel estimation, cell selection/reselection, handovers and MCS adaptation. In turn, DM-RS are used for coherent demodulation at the VUE, while MBSFN-RS are intended for channel estimation of multicast transmissions, which are supported by LTE-V2I.

In LTE-V2I, CRS occupy specific REs within the resource grid depending on parameters such as the cell ID or the antenna configuration at the eNodeB. This is illustrated in Figure 2.11, where the REs occupied by the CRS are shown for the three different cell IDs within the same eNodeB.

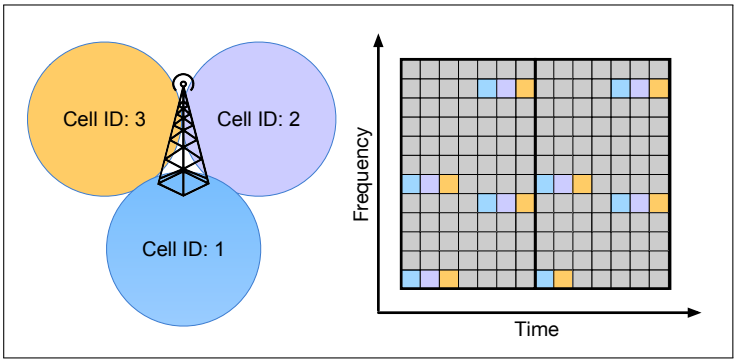


Figure 2.11: Location of CRS in a RB as a function of the Cell ID.

As shown in Figure 2.11, by occupying specific REs, depending on the cell ID, CRS avoid intercell interference in contiguous cells. This allows VUEs to accurately track the downlink channel of each cell, which is critical for channel estimation and MCS adaptation in the downlink direction, as discussed in the following section.

#### 2.3.2.3 Downlink channel quality estimation

In LTE-V2I, VUEs perform channel quality estimation by measuring different metrics in the downlink channel between the eNodeB and the VUE. These measurements are performed independently on the CRS of each cell and provide an estimation of the downlink channel quality. These estimations allow the VUE to track the downlink channel at a cell level and perform mobility procedures such as handovers and MCS adaptation.

Channel estimation is performed independently by each VUE, which computes multiple metrics to measure the quality of the downlink channel. These metrics are the Reference Signal Received Power (RSRP), the Reference Signal Received Quality (RSRQ), the Received Signal Strength Indicator (RSSI) and the Reference Signal SNR.

The RSRP is measured at the antenna port of the VUE by computing the linear average power of all the REs carrying CRS within the measured bandwidth [52]. This parameter is measured for all the cells that are in range, allowing the VUE to select the most suitable cell while moving within the E-UTRAN. In LTE-V2I, the RSRP is used to select the most suitable cell during handovers, when a VUE moves between cells while data is being carried through an active downlink connection.

The VUE reports these RSRP measurements to the eNodeB, which is in charge of coordinating the execution of these mobility procedures. To this purpose, the VUE reports a predefined value based on the RSRP measurement and the intervals shown Table 2.1.

Table 2.1: Reported RSRP values and measurement intervals [53].

| **Reported value** | **Measurement interval (dBm)** |
|---|---|
| RSRP_00 | $RSRP < -140$ |
| RSRP_01 | $-140 <= RSRP < -139$ |
| ... | ... |
| RSRP_96 | $-45 <= RSRP < -44$ |
| RSRP_97 | $-44 <= RSRP$ |

Moreover, the VUE uses the measured RSRP to obtain the SNR by computing the

ratio between the RSRP and the thermal noise, which has a value of -174 dBm for a 15 kHz subcarrier [54]. The value of SNR is then used to compute another parameter, known as the Channel Quality Indicator (CQI). The CQI is reported individually by each VUE to the eNodeB to indicate the quality of the downlink channel and is used by the MAC layer at the eNodeB to perform resource allocation and MCS adaptation in the downlink direction of LTE-V2I.

There is a total of 16 CQI levels (0–15) defined in the standard and each level represents a quantized version of the SNR measured at the antenna port of the VUE. From the 16 possible levels that parameter CQI can take, 1 and 15 represent the worst and the best channel quality, respectively. In addition, CQI 0 corresponds to the out-of-range state, which occurs when the VUE is connected to the eNodeB in the downlink direction but data cannot be transmitted.

The procedure implemented by the VUE to compute the CQI is not defined by the LTE standard and therefore, it is open to chipset manufacturers [25]. Even though the procedure to obtain the CQI is not standardized, the main parameter involved in its computation is the SNR [24] as it provides an accurate estimation of the downlink channel quality from the perspective of the VUE.

CQI reports can be either periodic or aperiodic. Periodic reports are sent automatically by the VUE to the eNodeB and the time between transmissions can be configured with a value between 2 and 100 ms. In contrast, aperiodic reports are sent upon request of the eNodeB. Moreover, there are different types of CQI reports depending on how the downlink bandwidth is measured by the VUE. Specifically, there are wideband, sub-band and user-selected sub-band CQI reports, where a sub-band refers to a group of contiguous RBs where the CQI is computed.

The wideband CQI is obtained by computing the median of the CQIs of all sub-bands in the measured bandwidth and provides an estimation of the overall channel quality. In turn, the sub-band CQI is used to report the CQI of each sub-band and provides a more accurate estimation of the channel quality. Similarly, the user-selected sub-band only reports the CQI of selected sub-bands where the VUE experiences the best channel quality. All types of CQI reports available in the downlink of LTE-V2I are depicted in Figure 2.12.

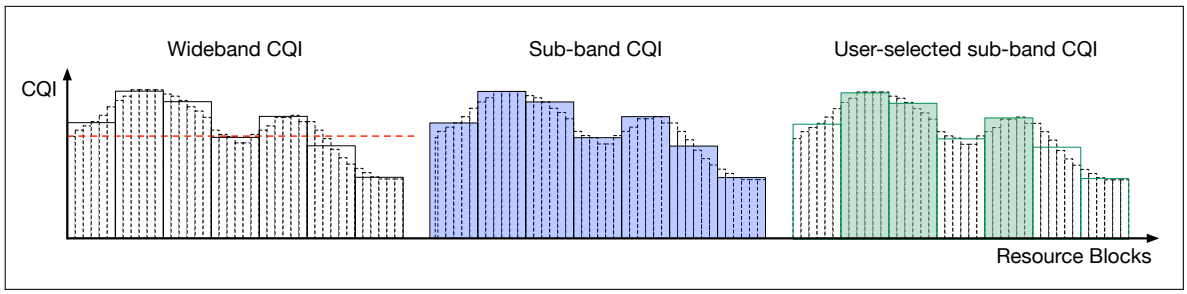


Figure 2.12: Types of CQI reports in LTE-V2I.

Among the three types of CQI reports, the wideband CQI report is the most common in LTE-V2I. This is because, in comparison to the sub-band CQI and user-selected sub-band CQI reports, the wideband CQI is a good trade-off between the channel information that is required by the MAC layer of the eNodeB and the amount of uplink resources required to report it.

The wideband CQI indicates to the eNodeB the combination of modulation method and coding rate that can be supported by the transmission in the downlink direction without exceeding a predefined error rate [55]. In the downlink of LTE-V2I there are two modulation methods available to support data transmissions including Quadrature Phase Shift-Keying (QPSK) and two variants of Quadrature Amplitude Modulation (QAM). QPSK is able to carry 2 bits per modulated symbol, while QAM can be configured to carry 4 bits per symbol (16QAM) or 6 bits per symbol (64QAM).

After a modulation method is selected, the physical layer of LTE-V2I implements coding to protect the data against the transmission errors at the radio interface. Specifically, LTE-V2I implements turbo coding [56] as the coding method, which introduces redundant bits in addition to the data in order to improve the decoding probability at the VUE.

Therefore, in addition to the modulation method, the reported CQI level also indicates to the eNodeB the coding rate that can be supported by the downlink transmissions of the corresponding VUE. The supported combinations of modulation method and coding rate for all the CQI levels are shown in Table 2.2, with the exception of CQI 0, which represents the out-of-range state where data cannot be transmitted in the downlink direction.

By providing the supported modulation method and coding rate, the CQI reports also play a key role in the resource management process. In the downlink direction of LTE-V2I, this process is performed by the MAC layer at the eNodeB and its operation is described in the following section.

Table 2.2: Supported modulation method and coding rate per CQI level [55]

| CQI | Modulation method | Coding rate |
|---|---|---|
| 0 | Out-of-Range | |
| 1 | QPSK | 0.08 |
| 2 | QPSK | 0.12 |
| 3 | QPSK | 0.19 |
| 4 | QPSK | 0.30 |
| 5 | QPSK | 0.44 |
| 6 | QPSK | 0.59 |
| 7 | 16QAM | 0.37 |
| 8 | 16QAM | 0.48 |
| 9 | 16QAM | 0.60 |
| 10 | 64QAM | 0.46 |
| 11 | 64QAM | 0.55 |
| 12 | 64QAM | 0.65 |
| 13 | 64QAM | 0.75 |
| 14 | 64QAM | 0.85 |
| 15 | 64QAM | 0.93 |

### 2.3.3 Medium Access Control layer

The MAC layer of LTE-V2I is in charge of managing the resources in the uplink and downlink channels. This process is performed at the eNodeB side, where the MAC layer allocates the available resources to VUEs. At the MAC layer, resource management is performed through two procedures known as MCS adaptation and resource allocation. The operation of these procedures is described in the following sections.

#### 2.3.3.1 Resource allocation

Resource allocation, also known as scheduling, is one of the most critical procedures executed at the MAC layer of the eNodeB. This procedure is performed by a scheduling algorithm, whose main goal is to effectively allocate the available time and frequency resources in the downlink and uplink channels to each VUE while maximizing the overall performance of system [57].

Due to the resource organization at the radio interface of LTE-V2I, the scheduling algorithm allocates resources in both the time and frequency domains. In the time domain, resources can be allocated every 1 ms, which is the minimal Time Transmission Interval

(TTI) in LTE-V2I. In turn, in the frequency domain resources are allocated using the RB as the resource unit. Under this resource organization, the minimum amount of resources that can be allocated to a VUE is 1 RB in 1 TTI.

The number of RBs to be allocated in the downlink direction by the scheduling algorithm to each VUE depends on different performance criteria. Specifically spectral efficiency, fairness and QoS provisioning are used during the resource allocation process to guide the scheduling decisions at the MAC layer of LTE-V2I. Therefore, the scheduling algorithm is designed to either prioritize one of these parameters or more generally, to achieve a good trade-off between them in order to guarantee an adequate performance of the system [58].

For instance, if the scheduling algorithm is designed to improve the spectral efficiency, the resource allocation process is prioritized to VUEs that support the highest transmission rates according to their reported channel quality. In turn, fairness can achieved if the algorithm allocates the available RBs to all VUEs independently of their supported transmission rates, although at the expense of reducing the overall spectral efficiency. Finally, QoS provisioning can be prioritized by overriding both spectral efficiency and fairness criteria in order to guarantee that resources are allocated to specific VUEs based on predefined QoS policies [59].

Once the scheduling strategy has been defined and the RBs are allocated to each VUE, the MAC layer of the eNodeB needs to select the modulation method and coding rate in order to encode the information in the downlink direction. To achieve this goal, the MAC layer makes use of the information provided by the CQI reports from each VUE, which indicate to the eNodeB the maximum data rate that can be supported by their downlink transmissions according to the reported channel quality. The process to select the combination of modulation and coding rate for downlink transmissions is defined by the operation of the MCS adaptation procedure, which is described detail in the following section.

#### 2.3.3.2 MCS selection and MCS adaptation

The main goal of link adaptation in LTE-V2I is to adjust the transmission parameters to better respond to the dynamic nature of the communication channel. There are different techniques that can be implemented for this purpose, such as adapting the transmission power, varying the number of transmission antennas or adapting the Modulation and Coding Scheme (MCS) [60].

The latter consist on adapting the MCS of the downlink transmissions depending on

the channel conditions experienced by the VUEs. This procedure is executed for each VUE and allows the eNodeB to dynamically adapt the data rate of the downlink transmissions based on the channel quality experienced by each VUE. The CQI reports play a key role in the execution of this procedure, as they provide an estimation of the channel quality in the downlink direction. More importantly, they indicate to the eNodeB the combination of modulation method and coding rate that can be supported by the downlink transmission of each VUE.

The wideband CQI (Commonly referred only as CQI) is the main input at the MAC layer of the eNodeB required to select the MCS configuration for the downlink transmission. The selection is made from a total of 29 values that are available in the downlink of LTE-V2I. Once selected, the value of MCS specifies the modulation method and is used to compute the coding rate.

The coding rate is computed as the ratio between the size of the Packet Data Unit (PDU) in bits passed from the MAC to the physical layer and the number of bits to be effectively transmitted through the radio interface. In LTE, the MAC layer PDU is known as the Transport Block (TB) and consist of the header required by the MAC layer plus the MAC payload. The latter contains the data from the application plus all the control information required for operation of the the upper layers of the protocol stack of LTE-V2I.

To compute the exact size of the TB in Bits, the MAC layer at the eNodeB uses the selected MCS configuration and the number of RBs allocated by the scheduling algorithm. By using the MCS, the MAC layer can define the modulation method (Which also specifies the number of bits per modulated symbol) and a TB Size Index ($I_{TBS}$), which is required to compute the size of the TB. The values of ($I_{TBS}$) for all the available MCS configurations are shown in Table 2.3.

Using the $I_{TBS}$ obtained from Table 2.3 and the number of allocated RBs, the MAC layer at the eNodeB can obtain the TB size through Table 7.1.7.2.1-1 in [61]. For the sake of clarity, Table 2.4 presents a portion of Table 7.1.7.2.1-1, where the size of the TB is shown for all the available MCS configurations when the number of allocated RBs is between 1 and 10.

Table 2.3: Modulation method, bits per modulated symbol and $I_{TBS}$ per MCS in the downlink channel of LTE-V2I [61].

| **MCS** | **Modulation method** | **Bits per modulated symbol** | $I_{TBS}$ |
|---|---|---|---|
| 0 | QPSK | 2 | 0 |
| 1 | QPSK | 2 | 1 |
| 2 | QPSK | 2 | 2 |
| 3 | QPSK | 2 | 3 |
| 4 | QPSK | 2 | 4 |
| 5 | QPSK | 2 | 5 |
| 6 | QPSK | 2 | 6 |
| 7 | QPSK | 2 | 7 |
| 8 | QPSK | 2 | 8 |
| 9 | QPSK | 2 | 9 |
| 10 | 16QAM | 4 | 9 |
| 11 | 16QAM | 4 | 10 |
| 12 | 16QAM | 4 | 11 |
| 13 | 16QAM | 4 | 12 |
| 14 | 16QAM | 4 | 13 |
| 15 | 16QAM | 4 | 14 |
| 16 | 16QAM | 4 | 15 |
| 17 | 64QAM | 6 | 15 |
| 18 | 64QAM | 6 | 16 |
| 19 | 64QAM | 6 | 17 |
| 20 | 64QAM | 6 | 18 |
| 21 | 64QAM | 6 | 19 |
| 22 | 64QAM | 6 | 20 |
| 23 | 64QAM | 6 | 21 |
| 24 | 64QAM | 6 | 22 |
| 25 | 64QAM | 6 | 23 |
| 26 | 64QAM | 6 | 24 |
| 27 | 64QAM | 6 | 25 |
| 28 | 64QAM | 6 | 26 |

Table 2.4: TB Size (Bits) per $I_{TBS}$ and number of allocated RBs in the downlink channel of LTE-V2I [61].

| | Number of resource blocks | | | | | | | | | |
|---|---|---|---|---|---|---|---|---|---|---|
| $I_{TBS}$ | 1 | 2 | 3 | 4 | 5 | 6 | 7 | 8 | 9 | 10 |
| 0 | 16 | 32 | 56 | 88 | 120 | 152 | 176 | 208 | 224 | 256 |
| 1 | 24 | 56 | 88 | 144 | 176 | 208 | 224 | 256 | 328 | 244 |
| 2 | 32 | 72 | 144 | 176 | 208 | 256 | 296 | 238 | 376 | 424 |
| 3 | 40 | 104 | 176 | 208 | 256 | 328 | 392 | 440 | 504 | 568 |
| 4 | 56 | 120 | 208 | 256 | 328 | 408 | 488 | 552 | 632 | 696 |
| 5 | 72 | 144 | 224 | 328 | 424 | 504 | 600 | 680 | 776 | 872 |
| 6 | 328 | 176 | 256 | 392 | 504 | 600 | 712 | 808 | 936 | 1032 |
| 7 | 104 | 224 | 328 | 472 | 584 | 712 | 840 | 968 | 1096 | 1224 |
| 8 | 120 | 256 | 392 | 536 | 680 | 808 | 968 | 1096 | 1256 | 1384 |
| 9 | 136 | 296 | 456 | 616 | 776 | 936 | 1096 | 1256 | 1416 | 1544 |
| 10 | 144 | 328 | 504 | 680 | 872 | 1032 | 1224 | 1384 | 1544 | 1736 |
| 11 | 176 | 376 | 584 | 776 | 1000 | 1192 | 1384 | 1608 | 1800 | 2024 |
| 12 | 208 | 440 | 680 | 904 | 1128 | 1352 | 1608 | 1800 | 2024 | 2280 |
| 13 | 224 | 488 | 744 | 1000 | 1256 | 1544 | 1800 | 2024 | 2280 | 2536 |
| 14 | 256 | 552 | 84 | 1128 | 1416 | 1736 | 1992 | 2280 | 2600 | 2856 |
| 15 | 280 | 600 | 904 | 1224 | 1544 | 1800 | 2152 | 2472 | 2728 | 3112 |
| 16 | 328 | 632 | 968 | 1288 | 1608 | 1928 | 2280 | 2600 | 2984 | 3240 |
| 17 | 336 | 696 | 1064 | 1416 | 1800 | 2152 | 2536 | 2856 | 3240 | 3624 |
| 18 | 376 | 776 | 1160 | 1544 | 1992 | 2344 | 2792 | 3112 | 3624 | 4008 |
| 19 | 408 | 840 | 1288 | 1736 | 2152 | 2600 | 2984 | 3496 | 3880 | 4264 |
| 20 | 440 | 904 | 1384 | 1864 | 2344 | 2792 | 3240 | 3752 | 4136 | 4584 |
| 21 | 488 | 1000 | 1480 | 1992 | 2472 | 2984 | 3496 | 4008 | 4584 | 4968 |
| 22 | 520 | 1064 | 1608 | 2152 | 2664 | 3240 | 3752 | 4264 | 4776 | 5352 |
| 23 | 552 | 1128 | 1736 | 2280 | 2856 | 3496 | 4008 | 4584 | 5160 | 5736 |
| 24 | 584 | 1192 | 1800 | 2408 | 2984 | 3624 | 4264 | 4968 | 5544 | 5992 |
| 25 | 616 | 1256 | 1864 | 2536 | 3112 | 3752 | 4392 | 5160 | 5736 | 6200 |
| 26 | 712 | 1480 | 2216 | 2984 | 3752 | 4392 | 5160 | 5992 | 6712 | 7480 |

Finally, by using the number of allocated RBs and the TB size, the MAC layer at the eNodeB can compute the coding rate using Equation (2.1),

$$Coding\ Rate = \frac{TB\ Size + CRC\ Bits}{Allocated\ RBs * REs\ per\ RB * Bits\ per\ Symbol} \tag{2.1}$$

Where:

- *TB Size*: Transport Block Size obtained from Table 2.4.
- *CRC Bits*: Cyclic Redundancy Check added to the TB by the MAC layer (24 bits).
- *Allocated RBs*: Number of RBs allocated by the scheduling algorithm.
- *REs per RB*: Number of REs per RB, computed as the product of the number of OFDMA symbols and the number of subcarriers per RB.
- *Bits per symbol*: Number of bits per modulated symbol depending on the selected MCS obtained from Table 2.3.

The computed coding rate for the selected MCS cannot exceed the limit defined by the reported CQI shown in Table 2.2. This limit is used by the eNodeB to select the "best" MCS configuration, which is the MCS that can maintain the coding rate within the limit while achieving the highest spectral efficiency.

In summary, the resource management procedure in LTE-V2I is performed through the following steps:

- The eNodeB transmits CRS in the downlink direction on a cell basis.
- Each VUE estimates the CQI by measuring the SNR on the CRS.
- Each VUE reports the CQI to the eNodeB in the uplink direction.
- The scheduling algorithm at the MAC layer of the eNodeB allocates RBs.
- The MAC layer at the eNodeB performs MCS adaptation by selecting the MCS configuration following the procedure described in Subsection 2.3.3.2.
- Data is transmitted in the downlink channel using the selected MCS configuration.

## 2.4 LTE-V2V communications

As discussed in Subsection 2.2.3, the PC5 interface is the main point of connection between VUEs in LTE-V2V communications. The PC5 interface was originally introduced in LTE to support direct Device-To-Device (D2D) communications [62]. However, the newest versions of LTE have introduced modifications to the PC5 interface to enable V2V communications.

At the PC5 interface, the communication channel among VUEs can be either managed by the eNodeB or autonomously by each VUE. When the eNodeB manages the channel resources, LTE-V2V operates in mode 3 [63]. Conversely, when resources are managed autonomously by the VUEs, LTE-V2V operates in mode 4 [37]. This section describes the operation of the protocol stack at the PC5 interface when LTE-V2V operates in mode 4, which is the default mode of operation of LTE-V2V. The section focuses particularly on the physical and MAC layers, where the MCS adaptation procedure is executed.

### 2.4.1 Protocol stack

The PC5 interface comprises a set of protocols to manage the radio interface in LTE-V2V mode 4. This set of protocols is shared between the control and user planes, where the control information and user data are managed separately. The protocol stack is shown in Figure 2.13.

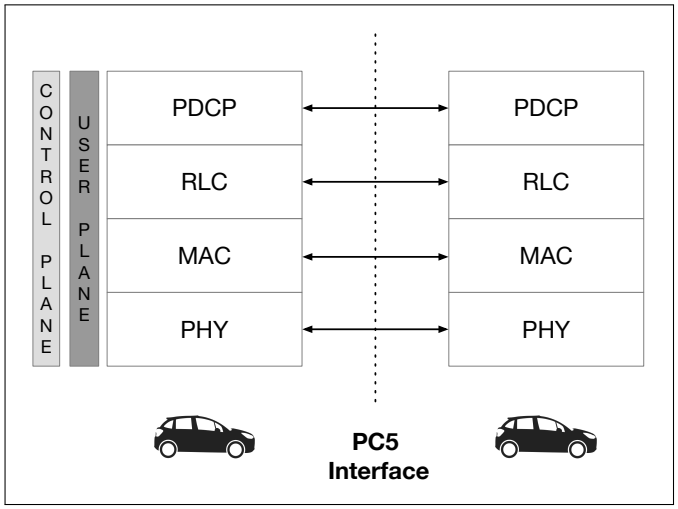


Figure 2.13: Protocol stack for the PC5 interface in LTE-V2V

These protocols, also known as layers, support the operation of the PC5 interface by

performing the following functions in the control plane:

- **Packet Data Convergence Protocol (PDCP):** The PDCP layer is responsible for encryption and security of data packets, transmission sequence control and duplicate detection.
- **Radio Link Control (RLC):** In LTE-V2V, the RLC layer operates in Unacknowledged Mode (UM), where transmissions are broadcasted without acknowledgment from the receivers.
- **MAC layer:** The MAC layer performs resource selection and re-selection by implementing a Sensing Based Semi-Persistent Scheduling (SB-SPS) mechanism as well as MCS adaptation.
- **Physical layer:** The physical layer performs signal processing, synchronization, modulation/demodulation and coding/decoding. It also performs the channel measurements required by the MAC layer to perform resource selection and MCS adaptation.

Since the operation of MCS adaptation is performed at the physical and MAC layers of LTE-V2V mode 4, the main concepts of both layers are described in the following sections.

### 2.4.2 Physical layer

In LTE-V2V mode 4, the communication channel is known as the sidelink channel. In comparison to the downlink and uplink, the physical layer of the sidelink channel has been exclusively designed to support V2V communications. This section describes the main features of the sidelink channel physical layer, particularly focusing on its resource structure and the channel estimation process in LTE-V2V mode 4.

#### 2.4.2.1 Resource structure

At the physical layer, the sidelink channel implements Single-Carrier Frequency Division Multiple Access (SC-FDMA). There are some key differences between the OFDMA method implemented in the downlink of LTE-V2I and SC-FDMA in LTE-V2V. The most relevant difference is the way in which each method maps the modulated data to the subcarriers in the frequency domain. This is illustrated in Figure 2.14, where it can be seen that

OFDMA (left) maps the modulated data symbol to a single subcarrier, while SC-FDMA (right) maps the modulated data symbol to a group of subcarriers.

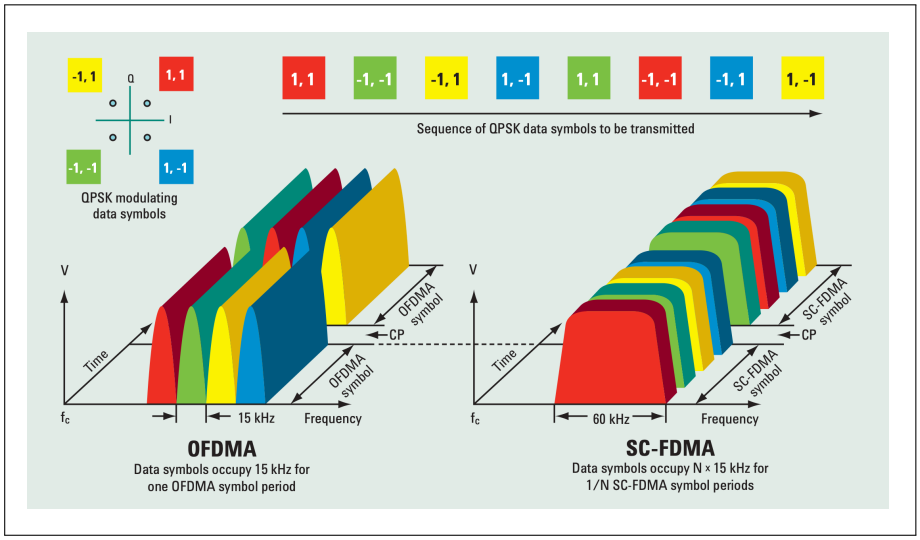


Figure 2.14: OFDMA (left) vs SC-FDMA (right) [64].

With this modification, SC-FDMA is able to maintain the subcarrier power constant over the duration of each SC-FDMA symbol. The main advantage of this method is that SC-FDMA transmitters have lower power peaks during transmission with respect to OFDMA, which translates into a lower the Peak-To-Average Power Ratio [65]. This allows SC-FDMA transmitters to reduce their transmit power requirements, which can be beneficial in the case of VUEs.

Despite the differences between OFDMA and SC-FDMA, the resource structure in the time and frequency domains remains mostly the same. Therefore, in the time domain, the sidelink channel maintains the same structure by organizing resources in subframes of 1 ms and frames of 10 ms. The only difference is that each subframe in the sidelink channel contains a total of 14 SC-FDMA symbols where 5 symbols are dedicated exclusively to control functions required to support V2V communications.

In the frequency domain the resource structure of the sidelink channel is the same as the downlink channel, where subcarriers of 15 kHz are organized in groups of 12. Similarly, in the sidelink channel, the combination of 14 SC-FDMA symbols (1 subframe) in the time domain and 12 subcarrier (180 kHz) in the frequency domain creates a RB, as shown in Figure 2.15.

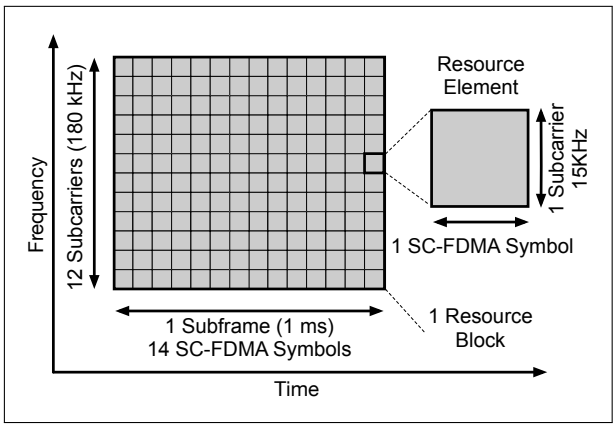


Figure 2.15: Sidelink channel RB structure.

The number of RBs in the sidelink channel depends on the allocated bandwidth, which can be configured to either 10 MHz or 20 MHz. With these configurations, the number of available RBs is 50 and 100, respectively. The sidelink channel can be deployed either in a commercial band allocated to an operator or in the 5.8 GHz band. The latter is a band exclusively reserved for vehicular communications, where LTE-V2V is expected to operate [66].

In contrast to the downlink channel in LTE-V2I where resources are allocated in RBs, the physical layer at the sidelink channel groups the available RBs into structures known as subchannels [37]. The number of RBs per subchannel and the total number of subchannels are configurable but limited by the allocated bandwidth. Therefore, in LTE-V2V the available resources are allocated on a subchannel basis every TTI, which has a duration of 1 ms.

The sidelink channel resources are further divided into two separate physical channels known as the Physical Sidelink Control Channel (PSCCH) and the Physical Sidelink Shared Channel (PSSCH). The PSCCH is used to transmit all the information required by the receiver for decoding. This information is known as the Sidelink Control Information (SCI) and occupies 2 RBs within the the PSCCH. The SCI contains information such as the implemented MCS, the frequency resource location of the transmission and other scheduling information.

Conversely, The PSSCH is used to transmit the data contained in the TB from the MAC layer and can also be used to transmit the SCI, depending on how the channel is configured. The available RBs in the PSSCH are grouped into subchannels, whose size depends on the available bandwidth and the transmission scheme.

There are two transmission schemes depending if the the PSCCH and the PSSCH use contiguous RBs or separate RB pools. In the former case the PSCCH and PSSCH use an adjacent scheme and in the latter a non-adjacent scheme. Independently of the configured transmission scheme, both the PSSCH and PSCCH are always transmitted in the same subframe.

Each transmission scheme also defines the size of the subchannels in the PSSCH. In the adjacent scheme, the number of RBs per subchannel can be of 5, 6, 10, 20, 25, 50, 75 and 100. Conversely, the number of RBs per subchannel in the non-adjacent scheme can be of 4, 5, 6, 8, 9, 10, 12, 15, 16, 18, 20, 30, 48, 72 and 100. Despite the number of available configurations, the LTE-V2V standard [67] specifies that the sidelink channel should implement the adjacent mode with subchannels of 10 RBs for both 10 MHz and 20 MHz bandwidths [67]. An illustration of the sidelink channel configurations for both transmission schemes is depicted in Figure 2.16.

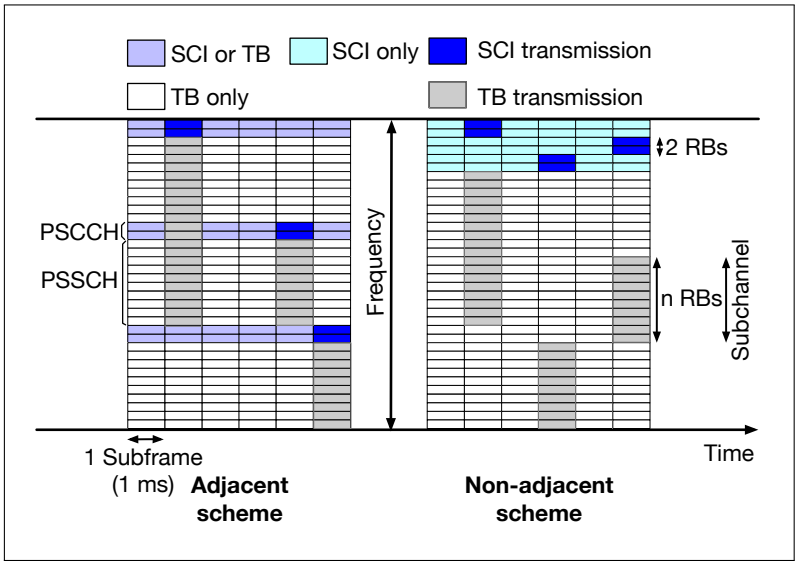


Figure 2.16: Sidelink channel structure and transmission schemes.

As previously discussed, each subframe in the sidelink channel contains additional SC-FDMA symbols required to support vehicular communications. Similar to LTE-V2I, these symbols are used to transmit reference signals in LTE-V2V, which are critical for the execution of multiple control functions. These reference signals are described in the following section.

#### 2.4.2.2 Sidelink reference signals

Within each subframe of the sidelink channel, 5 SC-FDMA symbols are used as reference signals [55]. Of these 5 symbols, 4 are DMRS, which are used for coherent channel demodulation and synchronization between the receiver and the broadcasting VUE. The remaining symbol is left as a guard period at the end of the subframe and allows each VUE to switch between transmission and reception. In LTE-V2V these symbols occupy fixed positions within each RB, as shown in Figure 2.17.

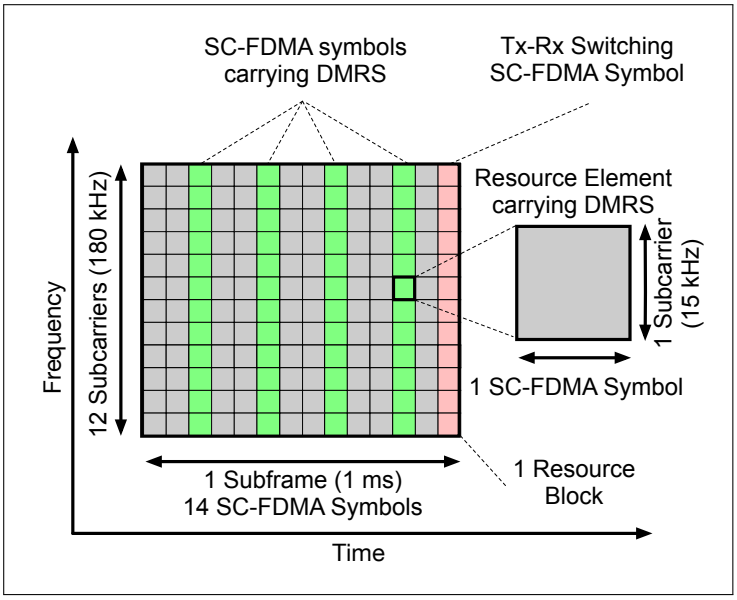


Figure 2.17: Sidelink reference signals.

Reference signals and specifically DMRS are critical to the performance of LTE-V2V mode 4 in the sidelink channel, where both transmitter and receiver are under high mobility conditions. DMRS are also used to perform channel sensing in LTE-V2V mode 4, as discussed in the following section.

#### 2.4.2.3 Channel sensing

In LTE-V2V mode 4 each VUE selects resources in the PSSCH autonomously, without coordination from the eNodeB. Therefore, VUEs must perform channel sensing prior to select the required resources. The goal of this process is that VUEs select resources that are less likely to be occupied by other transmissions and therefore avoid harmful interference [37].

The amount of resources that can be selected in the PSSCH is measured in groups of RBs known as subchannels. The number of subchannels to be selected is defined by the MAC layer of the VUE and depends on two parameters, the size of the packet from the application and the MCS.

After both parameters have been set, the MAC layer indicates to the physical layer the number of subchannels to be selected. At the physical layer, this information is used to sense the channel by measuring the power levels in the symbols carrying DMRS according to the number of subchannels indicated by the MAC layer. Through this process VUEs compute two metrics, the RSRP and the RSSI.

The RSRP is defined as the linear average over the power contribution of the resource elements (REs) carrying DMRS computed in the RBs contained in the specified subchannels. Conversely, the RSSI is defined as the linear average of the total received power per SC-FDMA symbol observed by the VUE. The RSSI is computed in all the symbols carrying DMRS as well as in other symbols within the RB. In the same way as the RSRP, the RSSI is computed in all the RBs contained in the specified subchannels.

The information provided by the RSRP and RSSI helps the MAC layer at the VUE to avoid subchannels that are already selected. For instance, a high value of RSRP indicates that a subchannel is selected by a another VUE in close proximity, that can potentially cause higher interference. Similarly, a high value of RSSI indicates that the subchannel is subject to high levels of interference and should therefore be avoided. After the channel sensing process is performed by the physical layer, the resource selection process continues at the MAC layer. This process is discussed in the following section.

### 2.4.3 Medium Access Control layer

In LTE-V2V mode 4, the MAC layer is in charge of selecting the subchannels in the sidelink channel. This process is performed autonomously by each VUE and it is based on channel sensing. The selection process also depends on other parameters such as the packet size or the MCS, which define the amount of subchannels required for any given transmission. This section describes the resource selection process of LTE-V2V mode 4 in detail.

#### 2.4.3.1 Resource selection

The MAC layer at each VUE in LTE-V2V mode 4 implements a SB-SPS mechanism to select resources. The operation of the SB-SPS mechanism is mainly designed for the

transmission of Cooperative Awareness Messages (CAMs). CAMs are highly periodic messages of relatively fixed size, that are used in vehicular networks to share basic kinetic information among VUEs [68].

With the SB-SPS mechanism, each VUE is first required to sense the sidelink channel by measuring the power levels of all the available subchannels. After sensing, the VUE selects one or multiple subchannels and reserve them on a semi-persistent basis. This means that after a number of consecutive transmissions, the VUE can either maintain the same reservation or restart the process and select new resources.

The operation of the SB-SPS mechanism starts with the reception of a packet from the application at the MAC layer. Every time a packet arrives at the MAC layer and a reservation is not in place, the SB-SPS mechanism generates a new resource grant. The resource grant is a control structure containing information such as the number of subchannels to be selected, the number of consecutive transmissions the subchannels will be reserved and the period of time between those transmissions (considering that packets are transmitted periodically).

The number of subchannels to be selected is defined by multiple parameters such as the size of the packet and the MCS. In turn, the number of consecutive transmissions the subchannels will be reserved is selected at random as an integer value between 5 and 15 and it is set in the Resource Reselection Counter (RRC) field in the grant. Finally, the periodicity between transmissions is selected based on application requirements and it is also set in the grant in the Resource Reservation Interval (RRI) field.

All the information contained in the resource grant is then passed from the MAC to the physical layer. In there, a list of subchannels that fit the grant specifications, known as Candidate Subframe Resources (CSR), is created. This list contains all possible CSR that can be selected within a selection window, defined between the time the packet arrives at the MAC layer plus the RRI set by the application.

The MAC layer then selects a single CSR within the selection by first discarding all the possible CSR based on the information received during a sensing window. The sensing window starts 1 s before the time the packet arrived at the MAC layer and contains relevant information of the CSR received during this period, such as previously received SCIs as well as RSRP and RSSI values recorded during previous receptions.

In order to better explain the selection process, Figure 2.18 depicts the structure of the sensing and selection windows, assuming that a new packet arrives at the MAC layer at time $t$. Upon reception, the MAC layer generates a resource grant indicating that the packet requires a number of subchannels, to be reserved for a number of $RRC$ transmissions

and with a $RRI$ period between transmissions. This information is passed from the MAC to the physical layer, which defines a selection window between $t$ and $t + RRI$ and creates a list with all the possible CSR within this period.

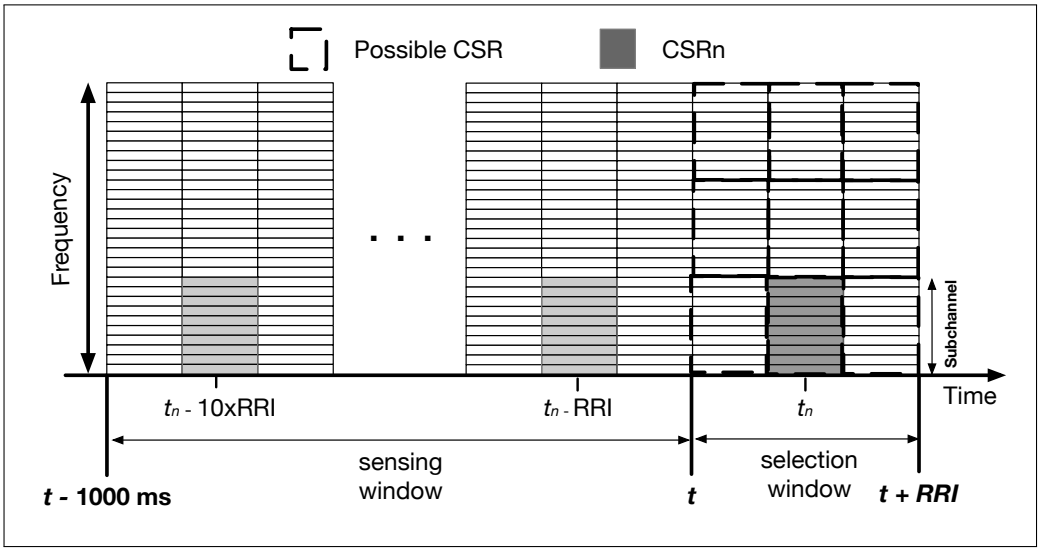


Figure 2.18: Illustration of the selection process in SB-SPS.

The physical layer then defines a sensing window between $t - 1000$ ms (1s) and $t$, as shown in Figure 2.18. The information received during the sensing window is used to select a single CSR within the upcoming selection window. This process is performed by first discarding possible CSRs based on their previously received information.

For instance, assuming that $CRS_n$ is a possible CSR within the selection window at time $t_n$, it will be discarded if either of these two conditions are met: (a) the latest received SCI of $CSR_n$ recorded at time $t_n - RRI$ indicates that $CSR_n$ will be reserved during the selection window at time $t_n$ or (b) the computed RSRP of $CSR_n$ recorded at time $t_n - RRI$ exceeds a predefined RSRP threshold.

The process described above is repeated for each of the possible CSRs within the selection window in Figure 2.18 until at least 20% of the possible CSRs are available for selection. Otherwise, the process is repeated by increasing the RSRP threshold by 3 dB until at least the 20% is available. When this condition is met, the physical layer selects only 20% of the possible CSRs with the lowest average RSSI. In the case of $CSR_n$, the average RSSI is computed by taking into account the latest ten receptions between $t_n - RRI$ and $t_n - 10xRRI$ and this process is repeated for all the possible CSRs within the selection window.

The filtered list of possible CSRs is then sent to the MAC layer, where a single CSR is selected at random. Finally, the MAC layer indicates the physical layer to use the selected CSR to transmit the packet and decreases the RRC by one after each transmission. With this mechanism, all upcoming packets are transmitted using the same CSR until the RRC reaches zero. When this occurs, the MAC layer can maintain the same reservation with a probability of $P$ that can be chosen between $[0, 0.8]$ or restart the entire process to generate a new resource grant and select new resources.

As shown, the SB-SPS mechanism is designed to allow VUEs to select subchannels on a semi-persistent basis. However, VUEs implementing SB-SPS can still modify some of their transmission parameters such as the transmission power or the MCS while maintaining the same reservation and perform link adaptation in LTE-V2V mode 4. The operation of this procedure is described in the following section.

#### 2.4.3.2 MCS selection and MCS adaptation

Similar to LTE-V2I, in LTE-V2V mode 4 VUEs are able to modify their transmission parameters in order to adapt to the variable conditions of the sidelink communication channel. To this purpose, VUEs can adapt parameters such as the transmission power or in the case of MCS adaptation, the MCS configuration.

In LTE-V2V mode 4, MCS adaptation is performed autonomously by each VUE in the sidelink channel, without support from the eNodeB. This contrasts with the downlink of LTE-V2I, where the eNodeB is in charge of executing this procedure for each VUE. Moreover, in LTE-V2V, MCS adaptation does not require any type feedback report from receivers like in LTE-V2I, where each VUE reports the quality of the downlink channel to the eNodeB. This occurs because in LTE-V2V mode 4 transmissions are broadcasted to all the receivers within the transmission range, making feedback unnecessary and highly inefficient.

Therefore, in LTE-V2V mode 4 MCS adaptation is not used to modify modulation and coding rate as a function of the channel conditions experienced by the receivers. Instead, MCS adaptation is used for other purposes such as congestion control [69], whose main goal is to adapt the MCS in order to reduce the interference and resource occupation when the sidelink channel is highly congested.

However, prior to perform MCS adaptation, VUEs must select a default MCS configuration to transmit in the sidelink channel. In LTE-V2V there is a total of 17 MCS configurations available, with each MCS defining a modulation method, the number of

bits per modulated symbol and a TB Size Index $I_{TBS}$, as shown in Table 2.5.

Table 2.5: Modulation method, bits per modulated symbol and $I_{TBS}$ per MCS [61] in the sidelink channel of LTE-V2V.

| **MCS** | **Modulation method** | **Bits per modulated symbol** | $I_{TBS}$ |
|---|---|---|---|
| 0 | QPSK | 2 | 0 |
| 1 | QPSK | 2 | 1 |
| 2 | QPSK | 2 | 2 |
| 3 | QPSK | 2 | 3 |
| 4 | QPSK | 2 | 4 |
| 5 | QPSK | 2 | 5 |
| 6 | QPSK | 2 | 6 |
| 7 | QPSK | 2 | 7 |
| 8 | QPSK | 2 | 8 |
| 9 | QPSK | 2 | 9 |
| 10 | QPSK | 2 | 10 |
| 11 | 16QAM | 4 | 10 |
| 12 | 16QAM | 4 | 11 |
| 13 | 16QAM | 4 | 12 |
| 14 | 16QAM | 4 | 13 |
| 15 | 16QAM | 4 | 14 |
| 16 | 16QAM | 4 | 15 |

Once a default MCS configuration is selected, the MCS can be used to obtain the amount of information that can be carried per RB. To this end, the selected MCS is first mapped to a TB size index $I_{TBS}$ through Table 2.5. Then, the corresponding $I_{TBS}$ can used to obtain the amount of bits carried per RB using Table 7.1.7.2.1-1 from [61]. For the sake of clarity, Table 2.6 presents a portion of Table 7.1.7.2.1-1, which shows the amount of bits that can be transmitted per $I_{TBS}$ when the number of RBs is between 1 and 10.

The amount of bits per $I_{TBS}$ and per MCS can then be used to define the number of RBs (TB size) required for transmission. To this end, the MAC layer uses the information in Table 7.1.7.2.1-1 from [61] and the size of the packet to be transmitted to select the number of required RBs. This information is also used to define the number of required subchannels, which is critical for the operation of the SB-SPS mechanism.

However, despite the number of available MCS configurations in LTE-V2V mode 4, the specification defines a range of configurations that can be selected depending if the transmission corresponds to the SCI or the data. In the case of the SCI, the specification

Table 2.6: Transport Block Size (Bits) per $I_{TBS}$ and number of selected RBs in the sidelink channel of LTE-V2V [61].

| | Resource Blocks | | | | | | | | | |
|---|---|---|---|---|---|---|---|---|---|---|
| $I_{TBS}$ | 1 | 2 | 3 | 4 | 5 | 6 | 7 | 8 | 9 | 10 |
| 0 | 16 | 32 | 56 | 88 | 120 | 152 | 176 | 208 | 224 | 256 |
| 1 | 24 | 56 | 88 | 144 | 176 | 208 | 224 | 256 | 328 | 244 |
| 2 | 32 | 72 | 144 | 176 | 208 | 256 | 296 | 238 | 376 | 424 |
| 3 | 40 | 104 | 176 | 208 | 256 | 328 | 392 | 440 | 504 | 568 |
| 4 | 56 | 120 | 208 | 256 | 328 | 408 | 488 | 552 | 632 | 696 |
| 5 | 72 | 144 | 224 | 328 | 424 | 504 | 600 | 680 | 776 | 872 |
| 6 | 328 | 176 | 256 | 392 | 504 | 600 | 712 | 808 | 936 | 1032 |
| 7 | 104 | 224 | 328 | 472 | 584 | 712 | 840 | 968 | 1096 | 1224 |
| 8 | 120 | 256 | 392 | 536 | 680 | 808 | 968 | 1096 | 1256 | 1384 |
| 9 | 136 | 296 | 456 | 616 | 776 | 936 | 1096 | 1256 | 1416 | 1544 |
| 10 | 144 | 328 | 504 | 680 | 872 | 1032 | 1224 | 1384 | 1544 | 1736 |
| 11 | 176 | 376 | 584 | 776 | 1000 | 1192 | 1384 | 1608 | 1800 | 2024 |
| 12 | 208 | 440 | 680 | 904 | 1128 | 1352 | 1608 | 1800 | 2024 | 2280 |
| 13 | 224 | 488 | 744 | 1000 | 1256 | 1544 | 1800 | 2024 | 2280 | 2536 |
| 14 | 256 | 552 | 84 | 1128 | 1416 | 1736 | 1992 | 2280 | 2600 | 2856 |
| 15 | 280 | 600 | 904 | 1224 | 1544 | 1800 | 2152 | 2472 | 2728 | 3112 |
| 16 | 328 | 632 | 968 | 1288 | 1608 | 1928 | 2280 | 2600 | 2984 | 3240 |

mandates that transmission should implement the lowest MCS of 0. With this MCS configuration, the SCI requires 2 RBs to transmit a total of 32 bits.

In contrast, data can be transmitted using a minimum MCS of 0 or 3 and a maximum of 11 if the VUE travels at a speed less than 160 km/h [67]. The specification does not mandate the use of a specific MCS within this range as a default configuration. However, it encourages to implement an MCS of QPSK with a coding rate of 0.5 as a baseline, or alternatively an MCS of QPSK with a coding rate of 0.7 or 16QAM with a coding rate of 0.5 [70].

The coding rate can be computed using the number of required RBs in combination with the information provided by Tables 2.6 and 2.5 using Equation (2.2),

$$Coding\ Rate = \frac{TB\ Size + CRC\ Bits}{Selected\ RBs * REs\ per\ RB * Bits\ per\ Symbol} \tag{2.2}$$

Where:

- *TB Size*: Transport Block Size obtained from Table 2.6.
- *CRC Bits*: Cyclic Redundancy Check added to the TB by the MAC layer (24 bits).
- *Selected RBs*: Total number of RBs selected by the MAC layer at the VUE as a function of the packet size from the application.
- *REs per RB*: Number of REs per RB, computed as the product between the number of SC-FDMA symbols and the number of subcarriers per RB.
- *Bits per symbol*: Number of bits per modulated symbol depending on the selected MCS obtained from Table 2.5.

After selecting an initial MCS configuration, each VUE can adapt the MCS within the specified ranges. However, adapting the MCS in LTE-V2V is a challenging task due to the constraints in the channelization scheme of the sidelink channel in terms of the available subchannel configurations. This is also due to the impact of MCS adaptation on the selection of subchannels, since changing the MCS directly modifies the number of required RBs. Therefore, MCS adaptation has implications in the operation of the physical layer, where parameters such as the RSRP and RSSI are computed. The operation of MCS adaptation and its implications in LTE-V2V is discussed in detail in Chapter 4, where the performance of MCS adaptation is discussed.

# Chapter 3

# Modeling and performance analysis of MCS adaptation in LTE-V2I

## 3.1 Introduction

One of the procedures that can have an impact on the performance of downlink transmissions in LTE-V2I is MCS adaptation, where the MCS configuration is adapted by the eNodeB to respond to the dynamic nature of the communication channel. In order to execute MCS adaptation, the eNodeB requires information regarding the quality of the communication channel. In the downlink direction of LTE-V2I this information is provided by the VUEs, which estimate the quality of the downlink channel and report it to the eNodeB.

This estimation is performed through measurements of CRS. Specifically, to estimate the channel quality, the VUE computes the SNR of the received CRS and converts such reading to a value of CQI. In turn, the computed CQI value is reported to the eNodeB, where the MAC layer uses it as the main input to execute the MCS adaptation procedure. For reference, the channel quality estimation process and the operation of the MCS adaptation procedure in LTE-V2I are described in detail in Subsections 2.3.2.3 and 2.3.3.2, respectively.

Given the relevance of the MCS adaptation procedure, a methodology for evaluating its impact on the performance of transmissions in LTE-V2I is required. Therefore, this chapter presents a study where its performance is evaluated for transmissions in the downlink direction of LTE-V2I. To this end, the study first introduces a novel downlink-channel

quality model for LTE-V2I that characterizes the CQI values reported by VUEs in a real-world vehicular environment. The model is then used to evaluate the performance of MCS adaptation by obtaining the transmission capacity in the downlink channel of LTE-V2I.

The remaining of this chapter is organized as follows. Section 3.2 discusses the methodology used to develop the downlink channel quality model and Section 3.3 describes the process to develop the proposed model. Then, Section 3.4 presents the performance analysis of the MCS adaptation procedure in LTE-V2I, where the proposed model is implemented. Finally, Section 3.5 presents the conclusions.

## 3.2 Modeling methodology

The performance of MCS adaptation in the downlink channel of LTE-V2I is analyzed through a model that characterizes the quality of the communication channel. The creation of such a model requires a large number of measurements of the downlink channel quality, which must be recorded by VUEs in a vehicular environment.

One method to collect such data is to make use of specialized software and hardware in extensive measurement campaigns. This approach is often used in related studies that analyze the performance of transmission in the downlink channel of LTE-V2I systems [23, 24].

In an alternative way, smartphones can be used to collect measurements in a distributed and cooperative manner. This is the basis of the crowdsourcing-based approach for data collecting and it is becoming a feasible alternative due to the wide availability of smartphones with adequate computing power, low cost and reasonable measurement accuracy [71].

However, extracting valid measurements from crowdsourced data is challenging regardless of the application. This is also the case of data collected in vehicular environments, where users are subject to high mobility conditions. For this reason, the first part of this chapter proposes an analysis methodology of measurements collected through a crowdsourcing application in order to obtain data that can be used to evaluate the performance of MCS adaptation in LTE-V2I.

The following sections present the various aspects related to the data collection and filtering process. This includes a description of the collection method, the vehicular environment, the characteristics of the collected data and the implemented filtering method.

### 3.2.1 Vehicular scenario and collection method

The original dataset used in this chapter was provided by the developers of the OpenSignal platform [72]. The OpenSignal platform is implemented as both a smartphone application as well as a website for collecting and retrieving network performance statistics, respectively.

The data was collected during a period of six months (from June to November 2016) through the crowdsourcing application implemented by OpenSignal, which allows smartphones to record performance statistics for both Wi-Fi and cellular networks.

In the case of cellular networks, the smartphone application records the performance statistics of connections between LTE users and the eNodeB in the downlink direction, since the data is recorded by at the application at the UE side. In addition, OpenSignal implements a website that provides aggregated statistics presented in the form of coverage maps that can be used by the general public to assess the coverage characteristics in the corresponding area.

Due to the characteristics of the crowdsourcing application, the collected dataset contained samples from all the available mobile operators in the surveyed area. However, for this study, the subset corresponding to the mobile operator with the largest number of collected samples was extracted from the original dataset. The resulting dataset consisted of approximately 300,000 samples, which contained several parameters related to the quality of the downlink channel.

From the selected subset, the samples were filtered based on the location reported by the LTE users at the moment of recording. According to information provided by the application, the location was obtained either by users through the built-in GPS or by triangulation of known eNodeBs. Therefore, from the collected samples, only users with a reported location constrained to be on a vehicular environment were considered. Specifically, the environment corresponds to the M1 motorway in the UK, which is the longest motorway covering a south-north route with a length of 193.6 miles (311.6 kilometers) that connects London to Leeds, as shown in Figure 3.1.

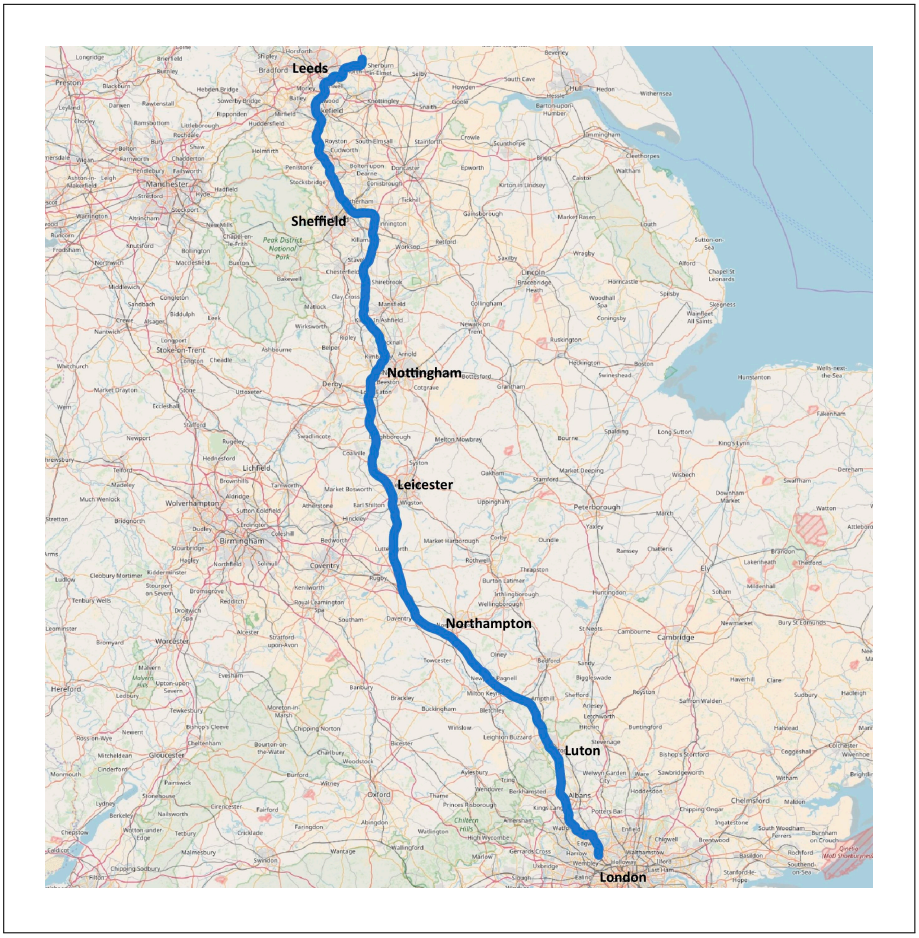


Figure 3.1: Map of the M1 motorway [73]

In order to assess the location precision of the samples, Figure 3.2 (left) shows a 1.3 km section of the M1 motorway, where the road layout can be observed. Within this section, there were approximately 1650 samples, which are shown in Figure 3.2 (right). In this Figure, the location precision of the samples is illustrated by the radius of the circles, with smaller circles representing a more accurate location estimation.

In Figure 3.2, a few houses can be observed at the north-west of the section. However, this type of scenarios is not usual in the analyzed motorway. This is due to the fact that planning laws for motorways in the UK prevent buildings from being built close to major roads as a measure to avoid the negative effects of noise and pollution on people's health.

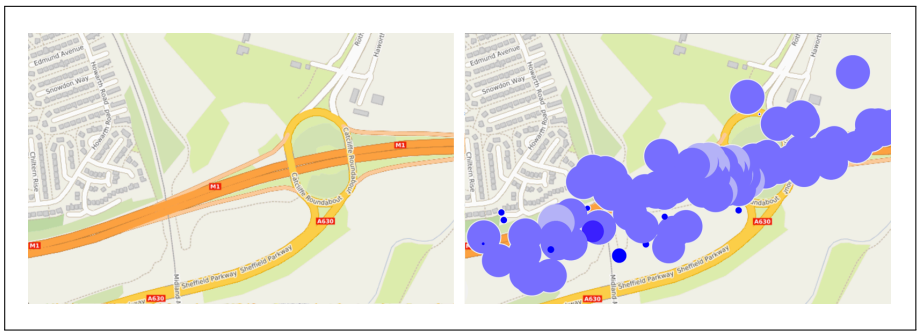

Figure 3.2: M1 section of approximately 1.3 km long. Road layout (left). Approximately 1650 samples (right) [73].

With this constraint, it can be reasonably assumed that the majority of samples were most likely collected by LTE users in vehicles. With this assumption samples were considered to be collected by vehicles that were either moving at average speeds for motorways or temporarily stopped in traffic jams. In either case, the samples were collected by VUEs in the downlink channel of an LTE system.

### 3.2.2 Collected data

As previously mentioned, the dataset corresponding to the selected operator consists of approximately 300,000 records. Among the different parameters contained in the dataset, only those related to CRS were considered as they are used to quantify the quality of the downlink channel in LTE-V2I.

Each of the records in the dataset contained several parameters related to CRS. Among these, the SNR was analyzed, considering that it is the main parameter involved in channel quality estimation. The observed SNR values were found to lie within the interval from -20 dB to 30 dB. Although the range for this parameter is not defined in the standard, measurements performed in other studies such as in [24] and [25] agree with these values.

The time and location of the samples were also specified in the records. They contained timestamps rounded to the nearest minute and location in terms of latitude and longitude. In order to show the temporal characteristics of the samples, Figure 3.3 presents the time distribution of the collected samples, where it can be seen that the majority of them were taken during working hours, with peaks in the morning (7 to 9 a.m.) and in the evening (4 to 5 p.m.) during the rush hours.

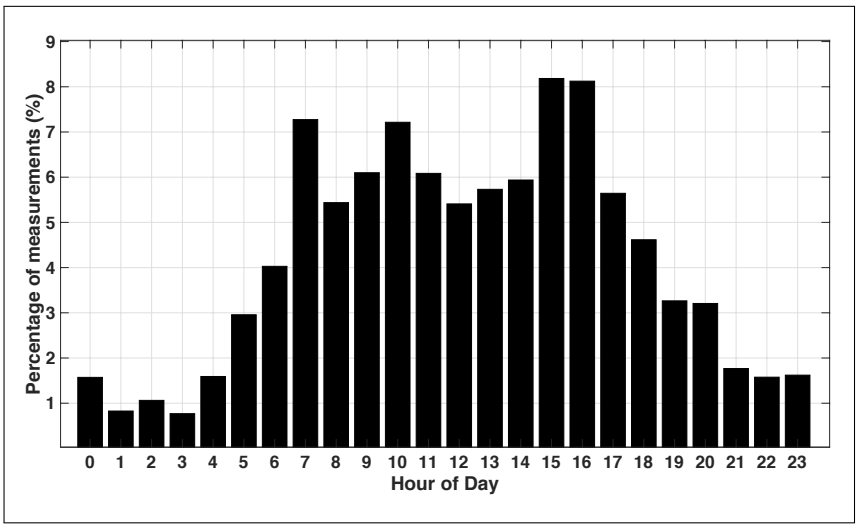


Figure 3.3: Distribution of samples per hour of day in the motorway.

As for location, Figure 3.4 indicates the percentage of samples collected in each km along the motorway. From this figure, it can be observed that apart from London, which is the major city in the UK, there is a roughly similar number of samples per km. This is particularly relevant, as it indicates that samples were uniformly collected along the motorway.

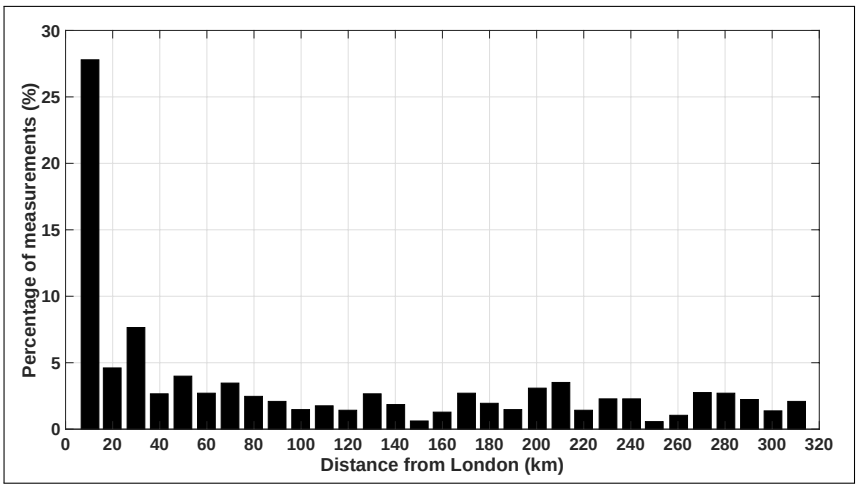


Figure 3.4: Spatial distribution of samples in the motorway.

These data were filtered in order to ensure that they were collected by VUEs prior to be used in the development of the the proposed model. The following sections describe the implemented filtering method as well as the proposed model.

### 3.2.3 Filtering method

As previously described, the original dataset was provided by OpenSignal according to the geographic location of the samples. Therefore, only samples with coordinates (latitude and longitude) constrained to be within a range of 200 meters from each side of the motorway were provided. This range corresponds to the smallest resolution (in terms of location) that can be provided by the OpenSignal platform.

From this dataset, only the records from a single LTE operator were selected for the proposed analysis. This was done to avoid inconsistencies and improve the reliability of the results, given the differences between operators in terms of infrastructure, transmission parameters and operation bands. In order to perform the filtering process, the location, type of connection of the VUE, and SNR values of each sample were analyzed as described below.

In the first step of the filtering process, the samples that were assumed to be collected by static LTE users were discarded. For this reason, the samples with a reported location within a range of 200 meters near the 12 service stations along the M1 motorway [74] were excluded. These samples were discarded because it was assumed that they came from VUEs that were either on a fixed location or moving at relatively slow speeds near the service stations.

In the second step, the samples were filtered based on the type of connection (Wi-Fi or mobile) recorded by the VUE at the moment of the reading. In this step, all samples from users reporting a Wi-Fi connection at the time of recording were discarded. The reason is that it is likely that these VUEs were able to establish a Wi-Fi connection while located at a fixed location, increasing the probability that the SNR measurement was not recorded by a moving VUE.

Finally, samples containing SNR values falling out of the normal operating range were discarded. To discard these samples, the studies performed in [24] and [25] were used as a reference given that the standard does not indicate a specific range of values for the SNR. These inconsistent SNR values were likely recorded while VUEs performed cell-reselection or handovers between LTE eNodeBs or between LTE and other radio access technologies and were therefore not considered for analysis.

The filtering method was applied to all the samples. It is important to mention that other subsets of data corresponding to different periods of time were also analyzed during the study and no significant differences among the statistical properties of the compared subsets were found.

After applying the filtering method, 92,525 samples scattered over 16,000 locations on the motorway were obtained. This dataset was then used to develop a model of the downlink channel quality, based on SNR measurements of CRS along the analyzed motorway. The methodology to develop the model is described in the following section.

## 3.3 Modeling MCS adaptation in LTE-V2I

This section describes the methodology for analyzing the SNR measurements collected by VUEs in the analyzed scenario. For the sake of clarity, the methodology is discussed in three parts. The first part explains the method used for resampling the original SNR measurements. In turn, the second part describes the mapping process between the SNR measurements and CQI levels. Finally, the third part describes the process to develop a model for the obtained CQI levels.

### 3.3.1 Resampling method

In the first step, the motorway was divided into $r$ regularly spaced zones of the same area. The area of these zones was chosen as to contain a number of samples large enough to allow the extraction of its statistical properties and it was also considered that all points within each zone should share similar statistical properties. For this reason, the diameter of each zone in all cases was set to 1 km, yielding a total of 310 zones.

From the 310 zones that were created, 241 of them had 50 or more samples. In these cases, it was theorized that the distribution of the observed values within zone $n$ (where $n = 1, \ldots, r$) could be represented by using a Gaussian distribution whose mean value $\mu_n$ and variance $\sigma_n^2$ could be estimated from the observations corresponding to that zone.

This statement was used as the null hypothesis to be tested by the Kolmogorov-Smirnov test [75] to determine the goodness of fit of our assumption in each zone. The results showed that 225 out of the 241 zones passed the test, at the 0.05 significance level, meaning that they contained samples with SNR values that can be considered to come from a Gaussian distribution.

Based on these results, each of the zones with more than 50 samples was modeled as a Gaussian distribution while allowing to preserve the statistical properties of each section of the motorway. In the case of zones with less than 50 samples their mean and variance were not estimated from the sample set. In such cases both statistical descriptors were

interpolated from adjacent zones as follows.

Let $X_1$, $Z$ and $X_2$ be three random variables representing the statistics of three contiguous zones, being $Z$ the one in the middle whose PDF is unknown. Let us also consider that $X_1$ and $X_2$ are Gaussian whose parameters are known, that is $X_1 \sim N(m_1, \sigma_1^2)$ and $X_2 \sim N(m_2, \sigma_2^2)$. It is proposed to consider that the statistical properties of $Z$ can be estimated as the average of $X_1$ and $X_2$, i.e.

$$Z = \frac{X_1 + X_2}{2}. \tag{3.1}$$

It can be easily shown, from the theory of jointly Gaussian random variables [76], that $Z$ is also Gaussian (i.e., $Z \sim N(m_Z, \sigma_Z^2)$) with mean

$$m_Z = \frac{1}{2}m_1 + \frac{1}{2}m_2 \tag{3.2}$$

and variance

$$\sigma_Z^2 = \frac{1}{4}\sigma_1^2 + \frac{1}{2}COV(X_1, X_2) + \frac{1}{4}\sigma_2^2. \tag{3.3}$$

In this way, the parameters of $Z$ can be estimated from the ones corresponding to adjacent zones. This procedure was applied to zones with less than 50 samples surrounded by zones with more than 50 samples. In total 38 zones were interpolated in this way, which in addition to the 241 zones mentioned before, accounted for 90% of the total length of the motorway.

In cases where two or more consecutive zones with less than 50 samples were found (i.e., 31 zones), it was assumed that LTE coverage was unavailable. In the analysis, these zones were assigned the SNR for CQI 0, which is used by VUEs to report the out-of-coverage state.

Having modeled each zone, the resampling was performed considering a total of $m$ regularly spaced sampling points $SP_i$ for $i = 1, \ldots, m$ for the entire motorway. The resampling distance was set to 20 meters, yielding a total of 50 SNR samples per zone and, therefore, 15500 SNR samples in total. Each one of these points represents a single SNR measurement, as illustrated in Figure 3.5.

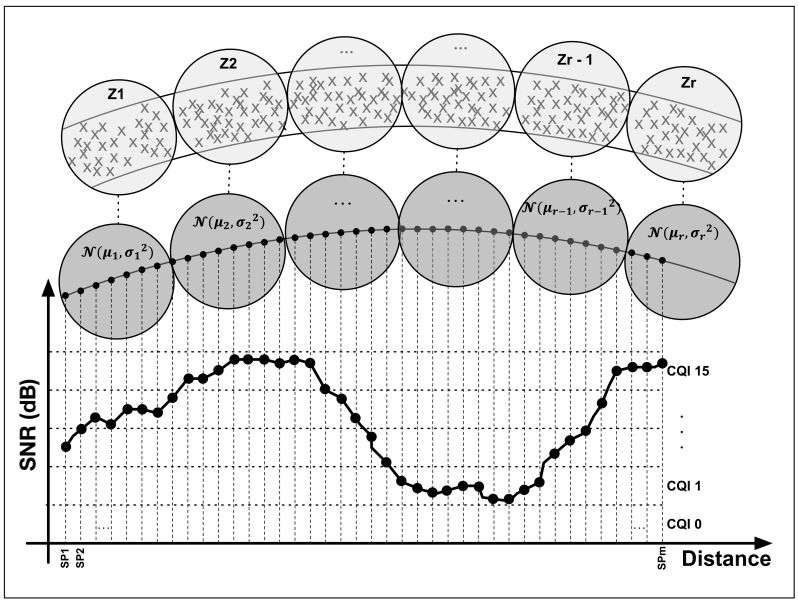


Figure 3.5: Illustration of the resampling process. *Top*, zones along the motorway; *middle*, sampling points within zones whose statistical properties are modeled as normally distributed random variables; *bottom*, SNR sampling points and CQI levels along the motorway.

Each one of the resampled SNR measurements was then mapped to a corresponding CQI level, since it is the parameter used to model the channel quality in the analyzed scenario. The process to map the SNR measurements to CQI levels is described in the following section.

### 3.3.2 SNR to CQI mapping

In LTE-V2I the CQI is reported by the VUE to the eNodeB to indicate the quality of the communication channel in the downlink direction and indicate the supported modulation method and coding rate. In turn, these reports are used by the MAC layer at the eNodeB to perform MCS adaptation by modifying the MCS as a function of the CQI value, as described in Subsection 2.4.3.2.

Since the collected samples did not contained the CQI values reported from VUEs, the methodology described in [77] was used to obtain the required CQI values. In [77], the process is carried out in three steps. In the first step, an averaging window is applied to the SNR measurements collected by the VUE. In the second step, the average SNR is

mapped to the supported MCS through modulation curves and in the third step the MCS is converted to a CQI level.

To follow this process, first an averaging window of five SNR measurements was applied. The use of the average SNR instead of single SNR measurements reduces variations in the reported CQI, which can lead to inaccurate CQI reports. This process also reduces errors during the selection of the MCS, which can increase the number of transmission errors in the downlink channel [77].

In the second step, the average SNR value was mapped to an MCS configuration through the use of modulation curves. These curves describe the Transport Block Error Rate (BLER) of each MCS configuration as a function of the SNR, as shown in Figure 3.6. To use these curves, a BLER limit of 10% is set as specified in [77]. With this limit in place, the average SNR can be readily used to select an MCS configuration.

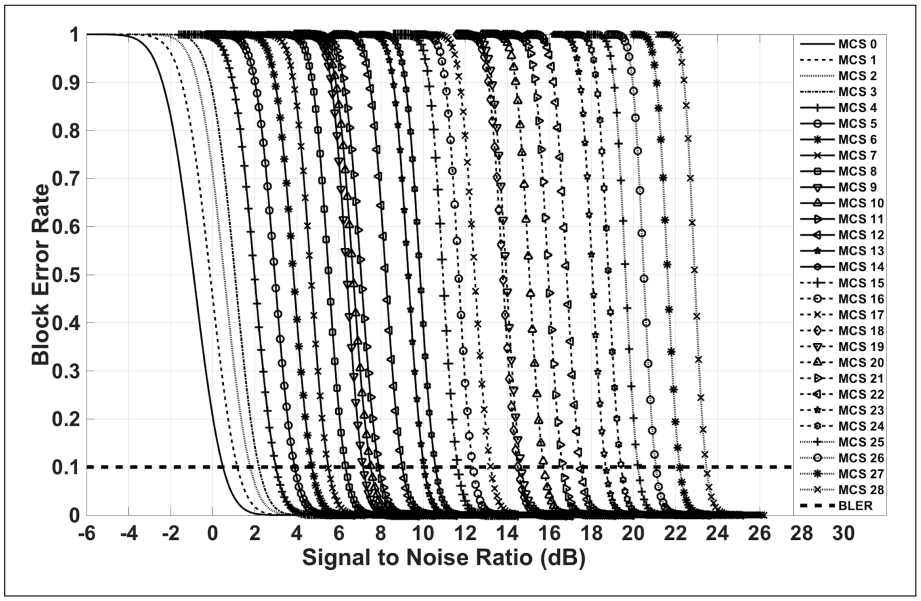


Figure 3.6: Modulation curves for the 29 MCS configurations available in the downlink channel of LTE-V2I [77].

In order to select a specific MCS through the modulation curves in Figure 3.6, only the MCS configurations that obtained a BLER below the 10% limit were considered. From these configurations, the highest MCS was selected, as it corresponds to the combination of modulation method and coding rate that achieves the highest spectral efficiency.

Finally, the mapping between MCS and CQI was performed. For this process, Table 3.1 [77], which describes the equivalence between the 29 values of MCS and the 16 CQI

levels was used. This process was repeated for all the average SNR values in order to obtain their corresponding CQI levels. It is worth mentioning that during the process, the average SNR values below the SNR threshold for MCS 0 were mapped to CQI level 0 and considered as the out-of-range state. The obtained CQI values where then used to generate the proposed model as described in the following section.

Table 3.1: MCS to CQI equivalence in the downlink channel of LTE-V2I. [77]

| **MCS** | **CQI** |
|---|---|
| 0 | 1 |
| 1-2 | 2 |
| 3-4 | 3 |
| 5-6 | 4 |
| 7-8 | 5 |
| 9-10 | 6 |
| 11-12 | 7 |
| 13-14 | 8 |
| 15-16 | 9 |
| 17-18 | 10 |
| 19-20 | 11 |
| 21-22 | 12 |
| 23-24 | 13 |
| 25-26 | 14 |
| 27-28 | 15 |

### 3.3.3 Markov modeling

The evolution of the reported CQI values along the analyzed scenario is modeled through a FSMC. This model is developed under the assumption that the CQI values can be characterized as a discrete random process $X = \{X_m; m \in \mathbb{N}\}$ that complies with the Markov property. This property establishes that the probability of the system being at a given state $j$ at index $m + 1$, is conditioned only on the knowledge that the process is at state $i$ at index $m$, and therefore, it is independent of all previous states [78].

In this case, to assume that this property holds is equivalent to consider that the space distribution of observed CQI values is such that the probability of measuring a certain CQI value in a nearby location along a route, only depends on the value observed at the present location. Note that the chain index in this case represents position instead of time, which is the most frequent case.

For the proposed Markov model, a finite state space $S_{cqi} = \{0, 1 \dots 15\}$ is defined, where each state represents one of the 16 levels of CQI (1 to 15) plus the out-range-state (CQI 0). In order to define the transition probability between states $i$ and $j$, i.e. $P_{i,j}$, this FSMC is considered to be space-homogeneous, therefore its transition probabilities are independent of the actual value of $m$ and thus, $P_{i,j}$ can be defined as

$$\boldsymbol{P_{cqi}} = \begin{bmatrix} P_{0,0} & & \dots & & P_{0,15} \\ & \ddots & \ddots & \ddots & \\ \vdots & \ddots & P_{i,j} & \ddots & \vdots \\ & \ddots & \ddots & \ddots & \\ P_{15,0} & & \dots & & P_{15,15} \end{bmatrix}; i, j \in S_{cqi}. \tag{3.4}$$

Recall that the transition probability matrix $\boldsymbol{P_{cqi}}$ is a stochastic matrix, meaning that the total sum of the transition probabilities for state $i$, represented by the $i_{th}$ row of matrix $\boldsymbol{P_{cqi}}$, must be equal to 1. Therefore,

$$\sum_{j=0}^{15} P_{i,j} = \sum_{j=0}^{15} P(X_{m+1} = j | X_m = i) = 1; \forall i \in S_{cqi}. \tag{3.5}$$

The transition probability matrix $\boldsymbol{P_{cqi}}$, could also be represented by means of a state transition diagram as shown in Figure 3.7, with vertices representing the states within the finite state space $S_{cqi}$ and edges representing the transition probability $P_{i,j}$ between states $i$ and $j$.

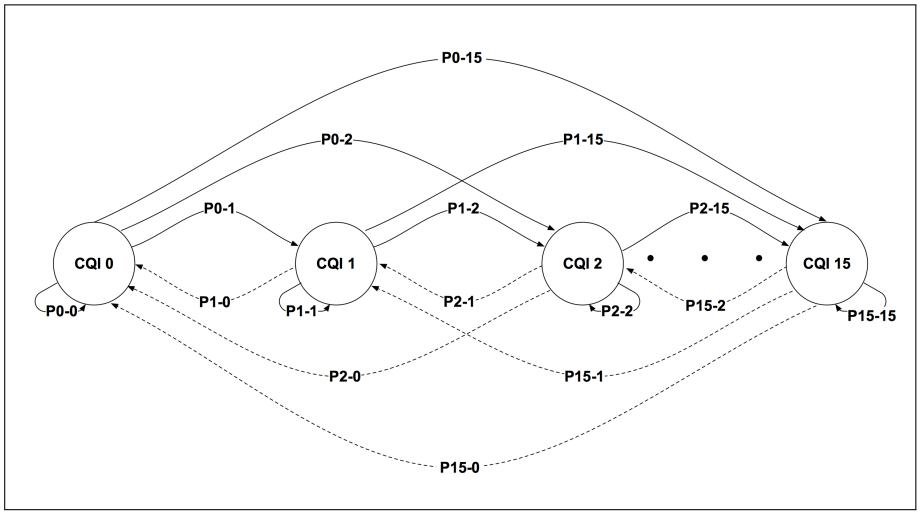


Figure 3.7: Finite-state Markov chain model for CQI transitions.

In order to obtain the transition probabilities $P_{i,j}$ from the resampled data, the following procedure was applied. The number of times the CQI changed from state $i$ to state $j$ was counted (i.e., $n_{i,j}$) when considering two consecutive sampling points along the road (i.e., $m$ and $m+1$) and this procedure was repeated for all sampling points depicted in Figure 3.5. Thus, the set of transition probabilities $P_{i,j}$ were computed as

$$P_{i,j} = \frac{n_{i,j}}{\sum_{j=0}^{15} n_{i,j}}; \forall i, j \in S_{cqi}. \tag{3.6}$$

The set of transition probabilities were found as described above. The resulting transition probabilities $P_{i,j}$ for all states $i$ and $j$, of the transition probability matrix $\boldsymbol{P_{cqi}}$, are shown in Table 3.2.

From the probability matrix $\boldsymbol{P_{cqi}}$ it can be seen that the use of averaged SNR measurements causes the CQI levels to remain the same or move only to nearby levels, as expected in a usual situation. As a result of this, the higher values of transition probabilities are the ones close to the main diagonal in Table 3.2. In contrast, the probability of CQI changing two or more levels from its current value is considerably lower as it can be observed from the transition probabilities outside such main diagonal.

Table 3.2: Transition probability matrix $\boldsymbol{P_{cqi}}$.

| **CQI level** | **0** | **1** | **2** | **3** | **4** | **5** | **6** | **7** | **8** | **9** | **10** | **11** | **12** | **13** | **14** | **15** |
|---|---|---|---|---|---|---|---|---|---|---|---|---|---|---|---|---|
| **0** | 0.718 | 0.081 | 0.079 | 0.085 | 0.033 | 0.004 | 0 | 0 | 0 | 0 | 0 | 0 | 0 | 0 | 0 | 0 |
| **1** | 0.24 | 0.144 | 0.194 | 0.244 | 0.139 | 0.039 | 0 | 0 | 0 | 0 | 0 | 0 | 0 | 0 | 0 | 0 |
| **2** | 0.126 | 0.159 | 0.183 | 0.325 | 0.134 | 0.065 | 0.004 | 0.004 | 0 | 0 | 0 | 0 | 0 | 0 | 0 | 0 |
| **3** | 0.054 | 0.048 | 0.077 | 0.384 | 0.253 | 0.155 | 0.023 | 0.006 | 0 | 0 | 0 | 0 | 0 | 0 | 0 | 0 |
| **4** | 0.011 | 0.014 | 0.02 | 0.115 | 0.453 | 0.298 | 0.068 | 0.018 | 0.002 | 0.001 | 0 | 0 | 0 | 0 | 0 | 0 |
| **5** | 0.001 | 0.002 | 0.006 | 0.024 | 0.143 | 0.502 | 0.226 | 0.073 | 0.022 | 0.001 | 0 | 0 | 0 | 0 | 0 | 0 |
| **6** | 0 | 0.001 | 0.001 | 0.005 | 0.047 | 0.175 | 0.485 | 0.192 | 0.089 | 0.004 | 0.001 | 0 | 0 | 0 | 0 | 0 |
| **7** | 0 | 0 | 0 | 0.001 | 0.011 | 0.058 | 0.153 | 0.534 | 0.224 | 0.015 | 0.004 | 0 | 0 | 0 | 0 | 0 |
| **8** | 0 | 0 | 0 | 0 | 0.001 | 0.006 | 0.039 | 0.23 | 0.542 | 0.135 | 0.043 | 0.004 | 0 | 0 | 0 | 0 |
| **9** | 0 | 0 | 0 | 0 | 0.001 | 0.001 | 0.009 | 0.084 | 0.227 | 0.505 | 0.144 | 0.027 | 0.002 | 0 | 0 | 0 |
| **10** | 0 | 0 | 0 | 0 | 0 | 0 | 0.001 | 0.011 | 0.05 | 0.397 | 0.387 | 0.133 | 0.016 | 0.005 | 0 | 0 |
| **11** | 0 | 0 | 0 | 0 | 0 | 0 | 0 | 0.004 | 0.011 | 0.225 | 0.17 | 0.463 | 0.094 | 0.029 | 0.004 | 0 |
| **12** | 0 | 0 | 0 | 0 | 0 | 0 | 0 | 0 | 0 | 0.07 | 0.108 | 0.338 | 0.39 | 0.061 | 0.019 | 0.014 |
| **13** | 0 | 0 | 0 | 0 | 0 | 0 | 0 | 0 | 0 | 0 | 0.071 | 0.153 | 0.294 | 0.4 | 0.047 | 0.035 |
| **14** | 0 | 0 | 0 | 0 | 0 | 0 | 0 | 0 | 0 | 0 | 0 | 0 | 0.333 | 0.381 | 0.286 | 0 |
| **15** | 0 | 0 | 0 | 0 | 0 | 0 | 0 | 0 | 0 | 0 | 0 | 0 | 0.111 | 0.111 | 0.445 | 0.333 |

As an example of the information provided in matrix $\boldsymbol{P_{cqi}}$, it can be mentioned that

the first row presents the transition probabilities for CQI level 0, which is used by the VUE to report the out-of-coverage state. The value of 0.718 for CQI 0 means that a VUE without coverage is more likely to remain in the same state in the next sampling point.

Furthermore, it is interesting to note that some transition probabilities in the main diagonal, i.e. $P_{i,i}$, are significantly higher than the other probabilities in the same row. Thus, the CQI value is very likely to remain in the same value for the next sampling point. This is more noticeable for CQI levels 4 through 9, meaning that a VUE is more likely to have a stable LTE connection when reaching these CQI levels.

By observing the characteristics of the transition probability matrix $\boldsymbol{P_{cqi}}$, it can also be inferred that the process can move back and forth among all states belonging to $S_{cqi}$ in an arbitrary (random) number of steps. Therefore, it can be concluded that the FSMC is irreducible and its steady state probabilities can be calculated [79]. The steady state probabilities for the transition probability matrix $\boldsymbol{P_{cqi}}$ can be calculated through

$$\boldsymbol{\pi_{cqi}} = \lim (\boldsymbol{P_{cqi}})^n \text{ when } n \to \infty. \tag{3.7}$$

For a large enough $n$, the results are presented in Table 3.3.

Table 3.3: Steady state probability vector $\boldsymbol{\pi_{cqi}}$.

| **CQI level** | **0** | **1** | **2** | **3** | **4** | **5** | **6** | **7** | **8** | **9** | **10** | **11** | **12** | **13** | **14** | **15** |
|---|---|---|---|---|---|---|---|---|---|---|---|---|---|---|---|---|
| **Probability** | 0.018 | 0.007 | 0.009 | 0.029 | 0.069 | 0.129 | 0.144 | 0.199 | 0.193 | 0.114 | 0.051 | 0.026 | 0.008 | 0.003 | 0.001 | 0 |

In the steady state probability vector $\boldsymbol{\pi_{cqi}}$, the probability for CQI level 0 is particularly relevant. As mentioned above, CQI 0 is reported by the VUE to indicate the out-of-coverage state. Therefore, the value for the steady probability of this level could be interpreted as the outage probability of the LTE connection. In the analyzed scenario, this accounts for 1.8%.

The steady state probability values for the upper levels of CQI can also be observed in Table 3.3. For CQI levels 10 through 15, the total probability is around 9%. This would mean that there is less than 10% probability that a VUE can achieve the highest levels of channel quality in the downlink. This is a logical outcome, since these levels are only achieved when a VUE is really close to the eNodeB and the propagation conditions are ideal in terms of noise and interference.

It is also worth pointing out that the steady state probability values for CQI levels 4 through 9 account for around 85% of the total probability. This result suggests that most

of the coverage along the motorway is good enough to maintain stable LTE connections.

In the following section, the performance on MCS adaptation in the downlink channel of LTE-V2I is analyzed through the developed CQI model. To this end, the transition probabilities of the CQI FSMC from Table 3.2 are used to obtain the corresponding MCS configurations and to estimate the transmission capacity of the downlink channel in the analyzed scenario.

## 3.4 Performance analysis

As previously discussed in Subsections 2.3.3.2 and 2.3.2.3, MCS adaptation in LTE-V2I consist on adapting the MCS of the downlink transmissions based on the CQI reports from VUEs. These reports indicate to the MAC layer at the eNodeB the combination of modulation method and coding rate that can be supported by the VUEs in the downlink channel. These two parameters have a direct impact on the amount of information that can be transmitted in the channel and therefore on the overall transmission capacity.

Therefore, this section evaluates the performance of MCS adaptation in LTE-V2I by obtaining the maximum transmission capacity of the downlink channel when MCS adaptation is in operation. To this end, the model presented in Subsection 3.3.3 is used to generate the CQI reports required by MCS adaptation. These reports are then used to model the operation of the procedure by selecting the MCS and computing the transmission capacity.

In order to perform this analysis, first the generated CQI values are converted into MCS configurations through the procedure described in Subsection 3.3.2. The obtained MCS configurations are then used to compute the maximum transmission capacity of the downlink channel in LTE-V2I. To perform this computation, the amount of resources in the downlink channel that are exclusively dedicated to transmit data to VUEs need to be estimated. For this reason, the following section describes the process to compute these resources.

### 3.4.1 Number of resources for data transmission

In this section, the amount of resources available for the transmission of dedicated traffic in the physical downlink channel of LTE-V2I is obtained. In LTE-V2I, these resources are known as the Physical Downlink Shared Channel (PDSCH) and consist of a set of

$REs$ ($Data_{RE}$). To compute $Data_{RE}$, first, the number of $REs$ allocated to all the control channels in the downlink ($Control_{RE}$) are first subtracted from the total number of $REs$ available ($Total_{RE}$). Therefore $Data_{RE}$ is computed on a frame basis as

$$Data_{RE} = Total_{RE} - Control_{RE}. \tag{3.8}$$

The following sections describe the process to compute $Total_{RE}$ and $Control_{RE}$.

#### 3.4.1.1 $Total_{RE}$ computation

In order to compute $Total_{RE}$, the resources were analyzed in both frequency and time domains. In the frequency domain, resources were computed in terms of the number of the subcarriers within the available bandwidth. The downlink channel of LTE-V2I supports six different bandwidth configurations of 1.4, 3, 5, 10, 15 and 20 MHz, containing a total of 72, 180, 300, 600, 900 and 1200 subcarriers, respectively. The number of subcarriers is obtained by multiplying the 12 subcarriers contained in a RB by the number of RBs in the available bandwidth, which are 6, 15, 25, 50, 75 and 100, respectively.

In turn, in the time domain resources were computed in terms of OFDM symbols. In order to estimate the maximum transmission capacity, a total of 14 OFDM symbols per frame was considered, which is the maximum number that can be configured in LTE-V2I considering a normal Cycle Prefix [80]. The product between the total number of subcarriers in the frequency domain and OFDM symbols in the time domain results in the total number of available $REs$ in the downlink channel of LTE-V2I, as previously described in Subsection 2.3.2.1.

Another factor determining the number of available resources is the transmission mode. There are two modes available in LTE-V2I, Frequency Division Duplex (FDD) and Time Division Duplex (TDD). The FDD mode allocates different bands for the uplink and downlink channels, while in the TDD mode, the same bandwidth is shared between the downlink and uplink during different periods of time. For this analysis, TDD was chosen as the transmission mode, as it allows to select the proportion of resources for downlink transmissions with higher precision in comparison with FDD.

TDD supports seven different frame configurations and each configuration defines the number of subframes within the frame that can be dedicated to downlink ($D_{SF}$) and uplink ($U_{SF}$) transmissions. TDD also supports the implementation of a Special Subframe ($SS$) within the frame for switching between downlink and uplink transmissions. Within this

$SS$, there are OFDM symbols that can be used for downlink ($D_{SS}$) and uplink ($U_{SS}$) transmissions or as a guard period ($GP$). Given that this analysis focuses of the number of $REs$ for downlink transmissions, only $D_{SF}$ subframes and $D_{SS}$ symbols per $SS$ were considered. With these considerations, the total number of $REs$ available in the downlink channel $Total_{RE}$ can be computed on a frame basis as

$$Total_{RE} = RBs \times S(\frac{subcarriers}{RB}) \times (D_{SF} \times O(\frac{OFDM}{Frame}) + SS \times D_{SS}(\frac{OFDM}{Frame})), \quad (3.9)$$

where:

- $RBs$: Number of available RBs.
- $S$: Number of subcarriers per RB.
- $D_{SF}$: Number of downlink subframes per frame.
- $O$: Number of OFDM symbols per downlink subframe.
- $SS$: Number of special subframes per frame.
- $D_{SS}$: Number of downlink OFDM symbols per special subframe.

#### 3.4.1.2 $Control_{RE}$ computation

In turn, the computation of $Control_{RE}$ is performed by accounting for all the $REs$ required by the control and signaling channels in the downlink of LTE-V2I. To this end, the following physical downlink control channels were considered: Physical Downlink Control Channel (PDCCH), Physical Broadcast Channel (PBCH), Physical Control Format Indicator Channel (PCFICH) and Physical Hybrid ARQ Indicator Channel (PHICH). In addition to these channels, Primary Synchronization Signals (PSS), Secondary Synchronization Signals (SSS) and $CRS$ were also considered.

The $PDCCH$ is the control channel that occupies the larger amount of resources in the downlink channel, as it extends along the entire channel independently of the bandwidth configuration [81]. The number of $REs$ required by the $PDCCH$ on a frame basis ($PDCCH_{RE}$) is obtained as

$$PDCCH_{RE} = RBs \times S(\frac{subcarriers}{RB}) \times (D_{SF} \times OC(\frac{OFDM}{Frame}) + SS \times OCSS(\frac{OFDM}{Frame})), \quad (3.10)$$

where:

- $RBs$: Number of available RBs.
- S: Number of subcarriers per RB.
- $D_{SF}$: Number of downlink subframes per frame.
- $OC$: Number of OFDM symbols required by the PDCCH per $DL_{SF}$.
- $SS$: Number of special subframes per frame.
- $OCSS$: Number of OFDM symbols required by the PDCCH per $SS$.

The number of $REs$ required by the $PBCH$ ($PBCH_{RE}$), the PSS ($PSS_{RE}$) and the SSS ($SSS_{RE}$) was set to a fixed value of 240, 120 and 120 per frame, respectively. In turn, the $REs$ required by the $PCFICH$, $PHICH$, $PSS$ and $SSS$ were accounted in Eq. (3.10), as they overlap with $PDCCH_{RE}$ and therefore, they were not considered in the overall computation. Finally, the number of $REs$ required for the transmission of $CRS$ ($CRS_{RE}$) was obtained. $CRS$ are transmitted in every subframe and RB within the available bandwidth and depend on the number of transmission antennas at the eNodeB, as discussed in Subsection 2.3.2.2. Therefore $CRS_{RE}$ was computed as:

$$CRS_{RE} = RBs \times DL_{SF} \times C \times \frac{3}{4} \times A, \tag{3.11}$$

where:

- $RBs$: Number of available RBs.
- $D_{SF}$: Number of downlink subframes per frame.
- $C$: Number of $CRS$ per $RB$.
- 3/4: Overlapping factor to account for the 1/4 of $REs$ that overlap with the $PDCCH$.
- $A$: Number of antennas at the eNodeB.

After accounting for all the REs required by the control channels in the downlink channel of LTE-V2I, $Control_{RE}$ can be computed on a frame basis as

$$Control_{RE} = PDCCH_{RE} + PBCH_{RE} + PSS_{RE} + SSS_{RE} + CRS_{RE}. \tag{3.12}$$

#### 3.4.1.3 Downlink transmission capacity computation

Having obtained $Total_{RE}$ and $Control_{RE}$, $Data_{RE}$ can be computed through Eq. (3.8) on a frame basis. Then, the obtained $Data_{RE}$ can then be used to compute the maximum transmission capacity in the downlink channel of LTE-V2I in bits per second as

$$Throughput_{bps} = Data_{RE}(RE) \times B(\frac{Bits}{RE}) \times Coding\,Rate \times \frac{1}{Frame\,Duration(s)}, \quad (3.13)$$

where:

- $Data_{RE}$: Number of RE available for data transmission.
- $B$: Number of bits per RE depending on the MCS, as shown in Table 2.3.
- $CR$: Coding rate.
- $Frame\,Duration$: Duration of the frame in seconds.

### 3.4.2 Downlink transmission capacity results

In this section, the performance of MCS adaptation in LTE-V2I is evaluated by obtaining the transmission capacity of the downlink channel. The results are obtained through the CQI values generated by the model presented in Subsection 3.3.3 in combination with the number of resources available for data transmission in the downlink channel ($Data_{RE}$).

In order to obtain $Data_{RE}$, first $Total_{RE}$ and $Control_{RE}$ need to be computed. To this end, Table 3.4 shows the values of the parameters required to compute both parameters through Eq. (3.9) and Eq. (3.12), respectively.

Table 3.4: Configuration parameters.

| **Parameter** | **Value** |
|---|---|
| Number of available RBs ($RBs$) | 25, 50, 100 |
| Number of subcarriers per RB ($S$) | 12 |
| Number of downlink subframes per frame ($D_{SF}$) | 6,7,8 |
| Number of OFDM symbols per downlink subframe ($O$) | 14 |
| Number of special subframes per frame ($SS$) | 1 |
| Number of downlink OFDM symbols per special subframe ($D_{SS}$) | 12 |
| Number of OFDM symbols required by the PDCCH ($OC$) | 1 |
| Number of CRS per RB ($C$) | 8 |
| Number of antennas at the eNodeB ($A$) | 1 |

With the values from Table 3.4, $Data_{RE}$ can be computed through Eq. (3.8) and the result can be used to obtain the downlink transmission capacity through Eq. (3.13). In turn, the values of $B$ and $CR$ in Eq. (3.13) can be obtained from the MCS values that correspond to the CQI reports generated by the proposed model. Following, Table 3.5 shows the downlink transmission capacity results for the configuration parameters in Table 3.4.

Table 3.5: Downlink transmission capacity results

| $RBs$ | $D_{SF}$ | **Min (Mb/s)** | **Max (Mb/s)** | **Mean (Mb/s)** |
|---|---|---|---|---|
| 25 | 6 | 0.248 | 9.056 | 2.572 |
| | 7 | 0.369 | 13.472 | 3.833 |
| | 8 | 0.483 | 17.638 | 5.017 |
| 50 | 6 | 0.504 | 18.388 | 5.222 |
| | 7 | 0.746 | 27.220 | 7.735 |
| | 8 | 0.975 | 35.552 | 10.104 |
| 100 | 6 | 1.016 | 37.052 | 10.533 |
| | 7 | 1.500 | 54.715 | 15.545 |
| | 8 | 1.957 | 71.38 | 20.283 |

The results in Table 3.5 show that the mean transmission capacity that can be achieved is around 20 Mb/s. This value is achieved when 100 RBs are available in the downlink channel and is considerably lower in comparison to the maximum transmission capacity of 70 Mb/s. These results indicate that MCS adaptation considerably reduces the transmission capacity in the downlink channel of LTE-V2I in order to adapt to the channel conditions in the analyzed scenario.

In order to perform a more detailed analysis, Figure 3.8 shows the probability distribution for the downlink transmission capacity in LTE-V2I. These results are obtained for the configuration parameters shown in Table 3.4, when the number of $RBs$ and $D_{SF}$ are fixed to 50 and 7, respectively.

In Figure 3.8, the probability distribution has a total of 15 values, corresponding to the total number of MCS configurations selected by MCS adaptation according to the 15 values of CQI. The probability for the transmission capacity of each MCS that corresponds to each CQI is shown from the lowest to the highest CQI, starting with CQI 1 at the left of Figure 3.8.

It can also be observed in Figure 3.8 that in the analyzed scenario, the transmission capacity remains around 4 and 9 Mb/s with higher probability in comparison to values outside this range. These results indicate that MCS adaptation implements lower values

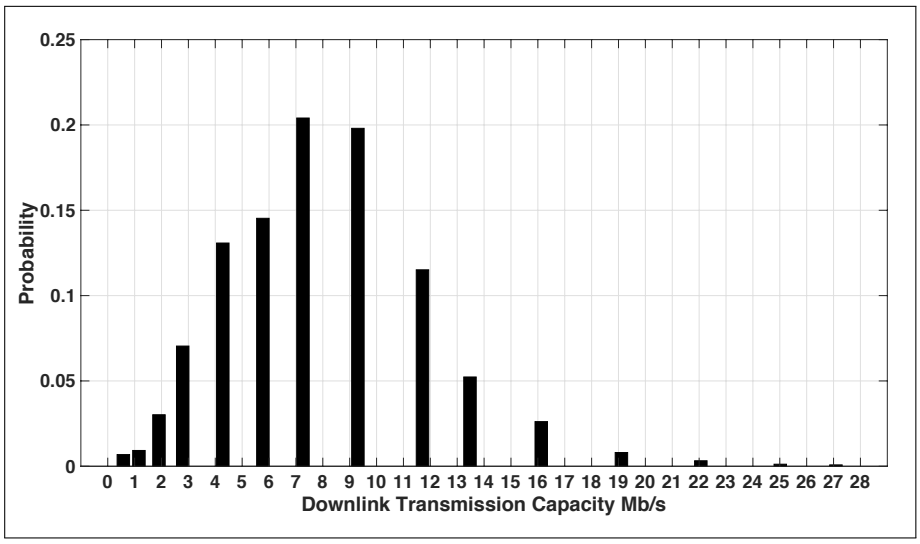


Figure 3.8: Probability distribution of the downlink transmission capacity for configuration parameters in Table 3.4 with 50 $RBs$ and 7 $D_{SF}$.

of MCS with higher probability, which reduces the overall transmission capacity of the downlink channel in LTE-V2I. This is also evident for the probabilities of higher transmission capacity values. In this case, Figure 3.8 shows that the probability for achieving a transmission capacity above 16 Mb/s is almost negligible.

These results can also be analyzed in terms of the implemented modulation methods. In this case, the computed utilization percentages for QPSK, 16QAM and 64QAM are 39%, 52% and 9%, respectively. These results suggest that, as a consequence of the conditions in the analyzed scenario, MCS adaptation implements the lowest modulation methods, i.e. QPSK and 16QAM, along 91% of the motorway in order to cope with the channel conditions. This is done at the expense of reducing the downlink transmission capacity, which can also be observed from the mean transmission capacity values presented in Table 3.5.

## 3.5 Chapter conclusions

In this chapter the performance of MCS adaptation is analyzed in the downlink channel of LTE-V2I. To that end, a model intended to capture the statistical behavior of the downlink channel quality in LTE-V2I is first introduced. The model makes use of a Markov chain to represent how the CQI levels change from point to point along a motorway.

The model is then used to generate the CQI levels required by the MCS adaptation

mechanism in LTE-V2I to select the MCS configurations in the downlink channel. In order to analyze the performance of the mechanism, the obtained MCS configurations were used to estimate the maximum transmission capacity of the downlink channel when MCS adaptation is in operation.

The proposed model is derived from the analysis of a large number of SNR measurements in the downlink channel of a LTE-V2i system, obtained by using a crowdsourcing-based approach. That is, measurements that were recorded and contributed by real users driving along a motorway. However, since the crowdsourcing application was not custom-made, great care had to be put into making the readings suitable for modeling and analysis.

For instance, there were some surveyed areas that did not have an amount of samples large enough to fit a probabilistic model, so that some procedures, described above, had to be applied where possible, in order to estimate the statistical distribution of samples in these cases. Another issue was that information regarding the speed of the vehicle was not included in the records, so that we had to make use of some heuristics in order to reasonably determine when the samples were collected by VUEs.

After filtering the samples, the dataset of SNR measurements was used to estimate the CQI values reported by the VUEs along the analyzed scenario. The obtained CQI values were then used to develop a Markov chain model, where the transition probabilities between the reported CQI levels was computed. Finally, the obtained model was used to generate the CQI values required by MCS adaptation in the downlink channel of LTE-V2I.

The performance of the MCS adaptation mechanism was analyzed by computing transmission capacity of the downlink channel of LTE-V2I in the analyzed scenario. To this purpose the CQI levels were mapped to MCS configurations and were used to estimate the maximum transmission capacity based on the amount of resources available for data transmission in the downlink channel.

The obtained results showed that the the overall transmission capacity of the downlink channel in LTE-V2I is limited by the implementation of MCS adaptation. This was attributed to the use of more robust, but less efficient combinations of modulation methods and coding rates, which allow VUEs to maintain the connectivity required to transmit data over the downlink channel at the expense of reducing the available data rate.

Finally, it is worth noting that the analysis presented in this chapter was limited to the downlink direction of LTE-V2I given that the available measurements were only recorded at the UE side. However, the proposed analysis could also be extended to the the uplink direction of LTE-V2I if the measurements performed by the base station in the uplink channel were available.

# Chapter 4

# Modeling and performance analysis of MCS adaptation in LTE-V2V

## 4.1 Introduction

In LTE, direct communication between vehicles and their environment can be achieved either with the support of the cellular network infrastructure or by allowing vehicles to communicate directly in an ad-hoc fashion. In the former case LTE-V2V operates in mode 3, where vehicles communicate directly while resources are allocated by the eNodeB. Differently, when vehicles communicate directly, without the support of the eNodeB, LTE-V2V operates in mode 4.

When LTE-V2V mode 4 is deployed, vehicles can autonomously select and manage a fixed amount of resources for predefined periods of time using a scheduling mechanism known as SB-SPS. While resources are reserved in a semi-persistent basis, vehicles can still modify parameters like the transmission power or the MCS. Therefore, vehicles can perform link adaptation by adapting these parameters.

However, while adapting the transmission power during ongoing transmissions in the LTE-V2V mode 4 is straightforward because it does not modify the resource occupation, adapting the MCS is a more challenging task. This occurs because the different MCS configurations available in the LTE-V2V mode 4 modify the number of transmission resources in the sidelink channel and consequently, the transmission bandwidth. This has further effects on the computation of the power levels in the channel and on the operation

of SB-SPS, which relies on specific power metrics in order to select and reserve the required resources, as discussed in Subsection 2.4.3.1.

This chapter addresses this challenge by presenting a comprehensive analysis of the effects of MCS adaptation on the operation of LTE-V2V mode 4. Specifically, it analyzes the impact of MCS adaptation on the resource organization of LTE-V2V, as well as on the computation of the power levels in the channel and their effects on the operation of SB-SPS. It further analyzes and accurately models the performance effects of adapting the MCS for congestion control, which is one of the main applications of the mechanism. In addition, the analysis, presented in this chapter, provides the foundations for other applications that can leverage the implementation of MCS adaptation in LTE-V2V mode 4.

The remainder of this chapter is organized as follows. Section 4.2 describes the methodology implemented to model the operation of MCS adaptation in LTE-V2V mode 4. Section 4.3 describes the effects of MCS adaptation on the operation of SB-SPS and discusses the intricacies of modeling this mechanism within LTE-V2V mode 4. Section 4.4 presents the performance of MCS adaptation when the mechanism is used for congestion control in LTE-V2V mode 4. Finally, Section 4.5 provides the conclusions.

## 4.2 Modeling methodology

The performance of MCS adaptation in LTE-V2V mode 4 is analyzed through a simulation model developed by extending the open-source simulator OpenCV2X [47, 82]. OpenCV2X provides a detailed model of LTE-V2V mode 4 and leverages different simulation frameworks and libraries to provide a full protocol stack implementation. In addition, OpenCV2X supports the implementation of frameworks that provide realistic vehicular mobility models, which are critical for the analysis and evaluation of vehicular communication technologies. Figure 4.1 shows the simulation frameworks and libraries leveraged by OpenCV2X.

The following section describes the main features of the simulation frameworks shown in Figure 4.1, which are required to deploy the LTE-V2V mode 4 model developed in OpenCV2X.

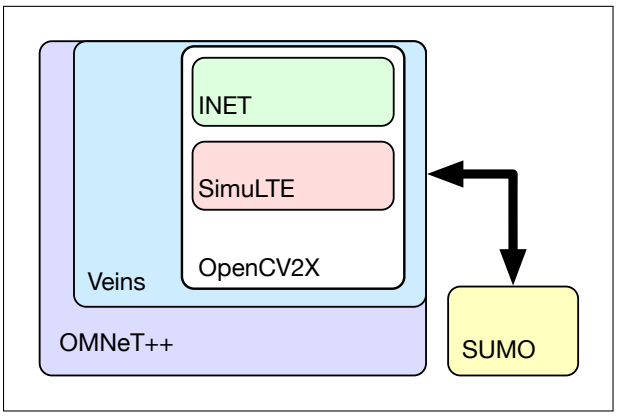


Figure 4.1: Simulation frameworks and libraries leveraged by OpenCV2X.

### 4.2.1 Simulation frameworks

#### 4.2.1.1 OMNet++

OMNeT++ [83] is a simulation framework based on C++ consisting of an extensive model library for building discrete-event network simulations. OMNeT++ is also open source and provides a comprehensive Integrated Development Environment (IDE) that can be deployed in multiple operating systems.

The basic component in every OMNeT++ model is known as a simple module. Simple modules communicate with each other through gates and connections and can be grouped or nested together to create more complex or compound modules. The designer can then map concepts such as network devices, protocols, channels or any other network concept into these modules in order to build the desired simulation. Figure 4.2 below depicts the structure of an OMNeT++ module.

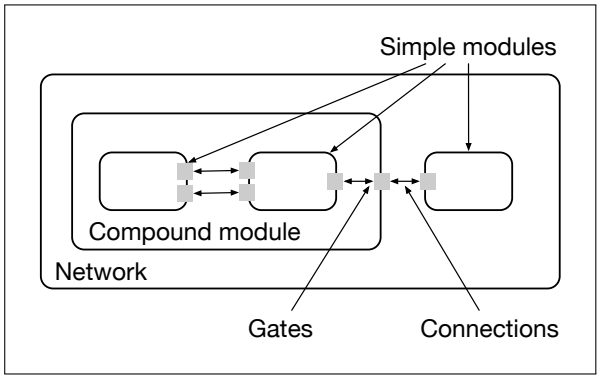


Figure 4.2: OMNeT++ module structure.

OMNeT++ provides a class library for building and programming modules. The module structure and hierarchy required to assemble network simulations is defined through a network definition (NED) language. NED files can be edited through a text editor or in a graphical editor, taking advantage of the OMNeT++ IDE.

Simulations in OMNeT++ can also be to set with different configuration parameters for the same model. This allows to run multiple simulations with different parameter values as well as different seeds in order to obtain statistically valid results. These results are provided in the form of output vectors and scalar files, which can be analyzed with either the native IDE or with other processing software such as Matlab or Python.

In this chapter, OMNeT++ is used as the network simulation platform to compile and build all the simulation frameworks and libraries required by OpenCV2X, which are described in the following sections.

#### 4.2.1.2 INET

INET [84] is a widely used, open source library that provides a variety of models for communication protocols and networks for OMNeT++ simulations. INET provides models for the upper layers of the IP stack, including application, transport and network protocols, as well as for the lower layers, such as link layer and physical layer protocols.

For the upper layers, INET provides application models that can generate traffic based on the TCP and UDP protocols. In the case of TCP, INET provides basic models as well as echo or Telnet models. In the case of UDP, INET provides basic models where the application simply sends UDP packets to an IP destination address, as well as more complex applications such as video streaming or voice transmission. Similarly, at the network layer INET implements protocol models for both wired and mobile networks, such as RIP, OSPF or AODV.

At the link layer, INET offers multiple MAC layer protocols. These include basic MAC protocols that implement simple features such as MAC addressing and dropping of frames. It also includes more realistic protocols such as the IEEE 802.11 [85], which implements more complex procedures such as transmission acknowledgment, request to send and clear to send control and packet fragmentation.

INET also provides realistic models for the radio channel and physical layer protocols. For instance, for the radio channel, it implements signal propagation models that include path loss, shadow fading, multipath fading or background noise. These models are complemented with models of physical layer protocols for both transmitter and receiver,

where different modulation and coding schemes are implemented in order to cope with all the propagation phenomena in the radio channel.

In summary, INET provides a very comprehensive framework that implements a variety of models for network simulations. In the analysis presented in this chapter, some of the INET models are used to perform the analysis of MCS adaptation in LTE-V2V mode 4. These INET models are deployed in combination with other frameworks, which are described in the following sections.

#### 4.2.1.3 Veins and SUMO

Veins [86] is an open source framework designed specifically for OMNeT++ and provides a variety of simulation models for vehicular networking. In OMNeT++, Veins is mainly used as an interface between the network simulation models built in OMNeT++ and vehicular mobility models available from external frameworks.

While the network simulation models are deployed with frameworks such as INET, mobility models for vehicles are implemented by external frameworks specifically designed for vehicular traffic simulation. One of the most used frameworks for this purpose is Simulation of Urban MObility (SUMO) [87]. SUMO provides a comprehensive set of features, allowing to model node mobility in realistic vehicular scenarios.

SUMO models vehicular mobility by defining traffic flows consisting of groups of single vehicles moving through a road network. Traffic flows are simulated by modeling the behavior of each vehicle individually along the road network, which is known as microscopic simulation [88]. In this type of simulation, each vehicle can be configured with different values for parameters like speed or acceleration, as well as certain constraints such as the minimum distance gap to other vehicles. This allows to deploy realistic vehicular scenarios, where mobility can be modeled on a vehicle basis.

In this context, Veins plays a key role, as it handles the interaction between the network simulation in OMNeT++ and the vehicular traffic simulation in SUMO. This is done in Veins through the Traffic Control Interface (TraCI) protocol, which coordinates the communication between the network and vehicular simulations on an event basis. In this chapter, SUMO is used as the vehicular traffic simulation framework. SUMO is implemented in combination with VEINS in order to perform the network and vehicular traffic simulations required to model the operation of LTE-V2V mode 4. Both are further complemented with the implementation of other frameworks that model the operation of LTE as described in the following section.

#### 4.2.1.4 SimuLTE

SimuLTE [89] is a framework of simulation libraries for the data plane of LTE. SimuLTE implements the full LTE architecture, including the core network as well as the radio access network (RAN). At the RAN level, it models the operation of the eNodeB by implementing processes such as resource allocation or MCS adaptation, while providing full connectivity between eNodeBs required to model cell selection or handovers.

SimuLTE is designed for OMNeT++ and is built upon the concept of the Network Interface Card (NIC) in order to implement the full LTE protocol stack. The implementation of the NIC concept abstracts the functionality of LTE from the implementation of upper layers. This allows SimuLTE to leverage other frameworks like INET in order to provide a full range of IP-based applications for the TCP and UDP protocols at the UE, as well as the upper layer protocols at the eNodeB. This is depicted in Figure 4.3.

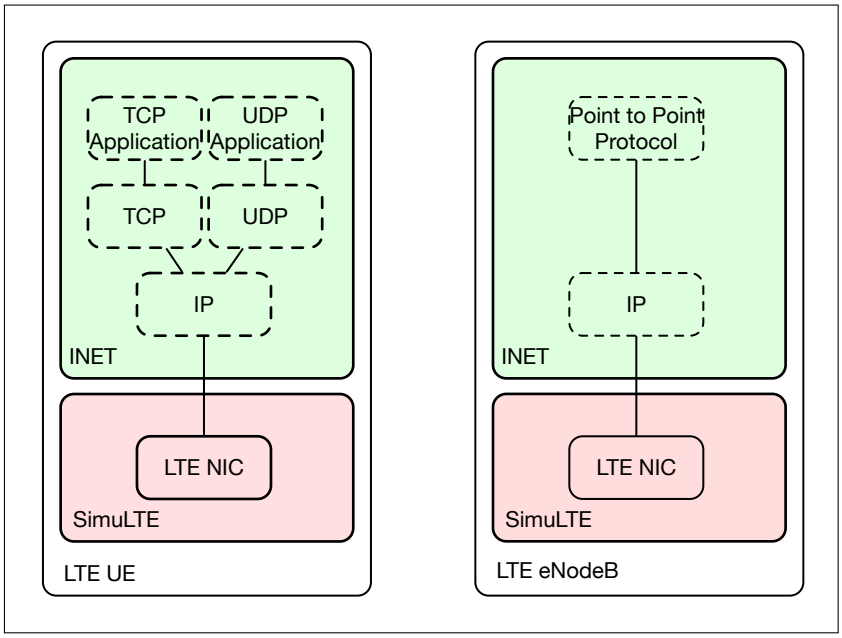


Figure 4.3: LTE NIC abstraction at the UE and eNodeB.

Within the NIC abstraction, SimuLTE implements the full LTE protocol stack, including the PDCP, RRC, RLC, MAC and PHY layer protocols. These are implemented as C++ base classes to allow UE and eNodeB objects to inherit functionalities that are common to both. However, since the layers at the UE and eNodeB perform different operations, SimuLTE implements inherited classes to model the specifics of each layer. Figure 4.4 illustrates the NIC structure and the class inheritance implemented in SimuLTE.

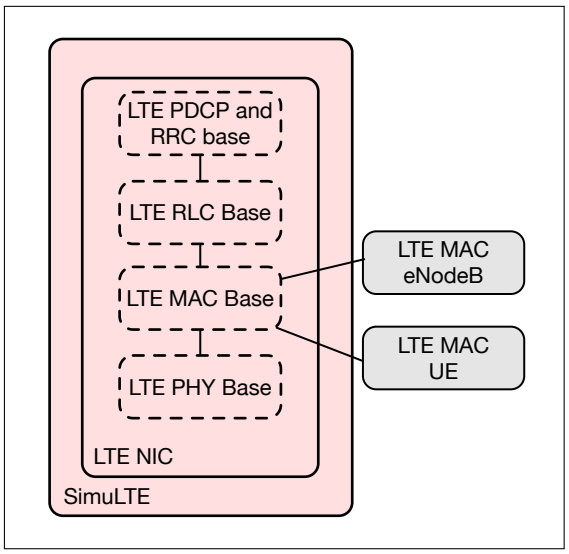


Figure 4.4: LTE NIC structure and class inheritance.

The current version of SimuLTE supports LTE communications at the Uu interface (downlink and uplink channels) as well as the PC5 interface (sidelink channel). At the sidelink channel, SimuLTE provides a standard-compliant implementation of D2D communications, which served as the foundation for the current LTE-V2V standard [37].

The following section describes how the simulation libraries provided by SimuLTE are leveraged by the OpenCV2X framework in order to model the operation of LTE-V2V mode 4 in the sidelink channel.

### 4.2.2 OpenCV2X

OpenCV2X [82] is an open source framework that provides a full protocol stack implementation of LTE-V2V mode 4 in compliance with the standard specifications. OpenCV2X is mainly developed for OMNeT++, but can also be built with any C++ compiler, allowing it to add other frameworks for vehicular communications, such as Artery [90] or Vanetza [91]. In the OMNeT++ version, which is the one used in this chapter, OpenCV2X leverages INET and SimuLTE for network simulation and SUMO and Veins for the implementation of realistic vehicular mobility models. This is illustrated in Figure 4.5, where the architecture of OpenCV2X is shown when the framework is implemented in OMNeT++.

As shown in Figure 4.5, OpenCV2X leverages the INET framework for the upper layers of the protocol stack so that any IP-based application, using either TCP or UDP, can be implemented in the network simulation. OpenCV2X also leverages the SimuLTE framework

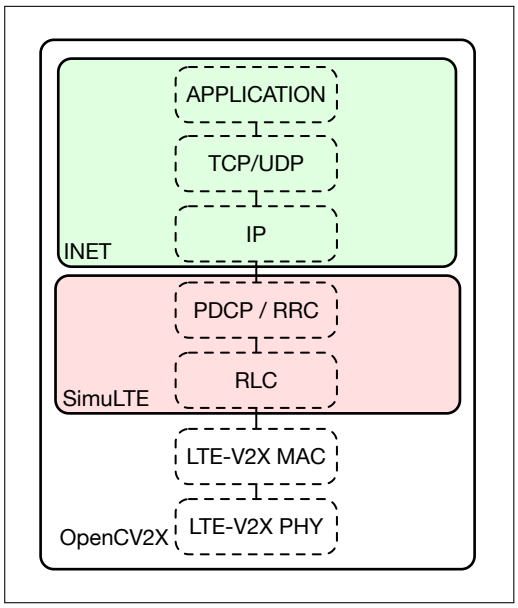


Figure 4.5: OpenCV2X architecture (OMNeT+ version).

by making use of the PDCP, RRC and RLC layers, but implements modifications to the models of these layers in order to comply with the LTE-V2V mode 4 standard.

More notably, OpenCV2X implements new MAC and physical layer models by modifying the current libraries available in the SimuLTE framework. This is required because LTE-V2V mode 4 introduces numerous modifications to the MAC and physical layers of the D2D communication standard, which is available in the current version of SimuLTE. For reference, the operation of the MAC and physical layers of LTE-V2V mode 4 are described in detail in Subsections 2.4.3 and 2.4.2 of Chapter 2, respectively.

Among the most relevant features of OpenCV2X are the following two: the implementation of the SB-SPS mechanism at the MAC layer, in order to allow vehicles to autonomously select resources in the sidelink channel, as well as the implementation of the new resource structure of LTE-V2V mode 4. In turn, at the physical layer, OpenCV2X implements features, such as the WINNER+ B1 channel model [92], which is required to comply with the simulation guidelines from the standard [70], as well as new modulation curves [93], required to accurately model transmissions in the sidelink channel.

In addition, one of the contributions of this thesis are the modifications to the physical layer of OpenCV2X required to accurately model the operation of LTE-V2V mode 4 in the sidelink channel. These modifications are described in the following section.

### 4.2.3 Modifications to the physical layer of OpenCV2X

The first major modification introduced to OpenCV2X has to do with how the power levels are computed at the PHY layer. In the previous version of OpenCV2X, packets were transmitted as groups of RBs and every RB was allocated the total transmission power. Under this model, transmissions at the receiver were evaluated on an RB basis by computing the Signal-to-Interference-plus-Noise Ratio (SINR) also assuming that interferers used the total transmission power for each RB and that the thermal noise was a function of the total number of RBs.

This transmission model is generally accurate as long as the transmission bandwidth is maintained fixed during the simulation and all power ratios are clearly defined. However, if the MCS is adapted during transmission, this results in variations in the transmission bandwidth, which needs to be considered in the model. Therefore, this chapter introduced modifications to OpenCV2X in order to compute parameters such as the received power, interference and thermal noise by distributing the total transmission power across the number of RBs required to transmit each packet, rather than allocating the total transmission power to every RB.

This modification was critical to the correct calculation of key physical layer parameters in LTE-V2V mode 4, such as the RSRP and the RSSI, whose values depend directly on the number of transmitted RBs. This is also the case of other power measurements such as the SINR, which requires an accurate estimation of the interference and thermal noise, which depends on the transmission bandwidth occupied by interferers.

To achieve this, first the transmission bandwidth needs to be computed by estimating the number of RBs required for each transmission. To this end, the new modifications introduced to OpenCV2X consider both the selected MCS and the size of the packet to obtain the TB size, as described in Subsection 2.4.3.1. In addition, the modifications consider the 2 RBs needed to transmit the SCI, which are added to obtain the total number of RBs to be transmitted. At the receiver, the total received power (after accounting for pathloss and shadowing) is divided by the number of transmitted RBs to obtain the received power per RB. This value is then divided by the RB bandwidth to obtain the Power Spectral Density (PSD) of each RB. With these modifications, the PSD becomes the building block upon which key parameters such as RSSI, RSRP and the SINR are computed.

Specifically, to compute the RSRP, the PSD of the RB is multiplied by the bandwidth of each RE. In this computation the PSD is assumed to be constant within each RB

and therefore the power per RE is also assumed to be the same for all REs. With this assumption, the RSRP, which is defined as the average power contribution of each RE, is equal to the power per RE. In turn, for the RSSI the received power per SC-FDMA symbol is obtained by considering all power sources such as the received power, interference, and noise. The received power per SC-FDMA symbol is computed as the sum of the total received power per RB multiplied by the total number of transmitted RBs.

Finally, the SINR per RB is computed as the ratio between the received power and the power of the interference plus the total noise on an RB scale. The interference is computed by accounting for the PSD per RB from all transmitters using overlapping RBs during an ongoing transmission. By using the PSD per RB and the number of RBs used by each interferer, the interference is accurately computed. The total noise is also estimated based on the number of transmitted RBs, by adding the noise figure at the receiver to the thermal noise. The thermal noise is obtained by multiplying the thermal noise density specified in the LTE standard of -174 dBm/Hz [94] by the number of transmitted RBs and the RB bandwidth of 180 kHz.

The second significant modification to OpenCV2X is related to the calculation of error rates in order to calculate error rates on a per packet basis. This contrasts with the previous version of the model, where transmissions were evaluated per RB by computing the SINR of each RB and mapping the result to a BLER value. As the previous version of OpenCV2X computed the SINR by assuming that all interferers use the total transmission power for each RB, and the thermal noise was set as a function of the total bandwidth, this resulted in incorrect calculations if the number of RBs per transmission was modified.

In contrast, the modifications introduced in OpenCV2X use the mean SINR for the transmitted RBs in combination with the modulation curves defined in [93] to obtain the BLER by using the curve that corresponds to the MCS of each transmission. This computation is more accurate if the number of RBs required for each transmissions changes, which can occur if parameters like the MCS configuration or the size of the packet (which modifies the size of the TB) are modified during transmissions.

All these modifications were critical for the correct implementation of the physical layer of LTE-V2V mode 4 in OpenCV2X and for the validation of the model, whose performance was compared against the analytical model presented in [95]. They also play a key role in the operation of MCS adaptation, which has direct effects on the resource organization, resource occupancy and on the overall operation of the physical layer of LTE-V2V mode 4. These effects are discussed in the following sections, where the model for MCS adaptation in LTE-V2V mode 4 is introduced.

## 4.3 Modeling MCS adaptation in LTE-V2V

The LTE-V2V mode 4 standard allows the adaptation of the MCS configuration in the PSSCH within the ranges specified in Subsection 2.4.3.2. With these considerations, the MCS configuration can be modified during ongoing transmissions and can be used for different applications. However, adapting the MCS during ongoing transmissions is not a trivial task and has several effects on the operation of the MAC and physical layers of LTE-V2V mode 4 that need to be considered in order to model MCS adaptation accurately. These effects are discussed in the following sections.

### 4.3.1 Effects of MCS selection on resource organization

The selection of different MCS configurations modifies the RB occupation and in some cases the subchannel occupation in LTE-V2V mode 4 due to its channelization structure.

According to the standard, the subchannel configuration depends on the bandwidth and the PSCCH+PSSCH transmission scheme. In the case of an adjacent scheme, which is used by the standard to evaluate the performance of LTE-V2V Mode 4 in [70], the size of each subchannel in the PSSCH can be of 5, 6, 10, 15, 20, 25, 50, 75 or 100 RBs and the channel can contain 1, 3, 5, 8, 10, 15 or 20 subchannels. Despite the number of available configurations, the standard indicates that the PSSCH should be configured with 5 subchannels of 10 RBs each for a channel bandwidth of 10 MHz [67].

Under this configuration, the selection of an MCS has a limited impact on the number of subchannels required to transmit a TB. This is depicted in Figure 4.6, where the number of subchannels and RBs (including the 2 RBs of the SCI) required to transmit a 190-Byte packet has been obtained by following the procedure described in [96].

Figure 4.6 shows that, for a 190-Byte packet (which is the standard packet size used to evaluate the performance of LTE-V2V mode 4 [70], the channelization structure limits the number of subchannels occupied to 5 (MCS 1), 4 (MCS 2), 3 (MCS 3 and 4) or 2 (MCS 5 to MCS 11 inclusive). However, Figure 4.6 also shows that the RB occupation varies for most MCS configurations independently of the subchannel occupation. This can be clearly seen for MCS 5 and MCS 11, which require two subchannels but occupy 20 and 11 RBs, respectively. These variations of RB occupancy as a function of the selected MCS and their effects need to be considered when MCS adaptation is implemented in practice, as discussed in the following sections.

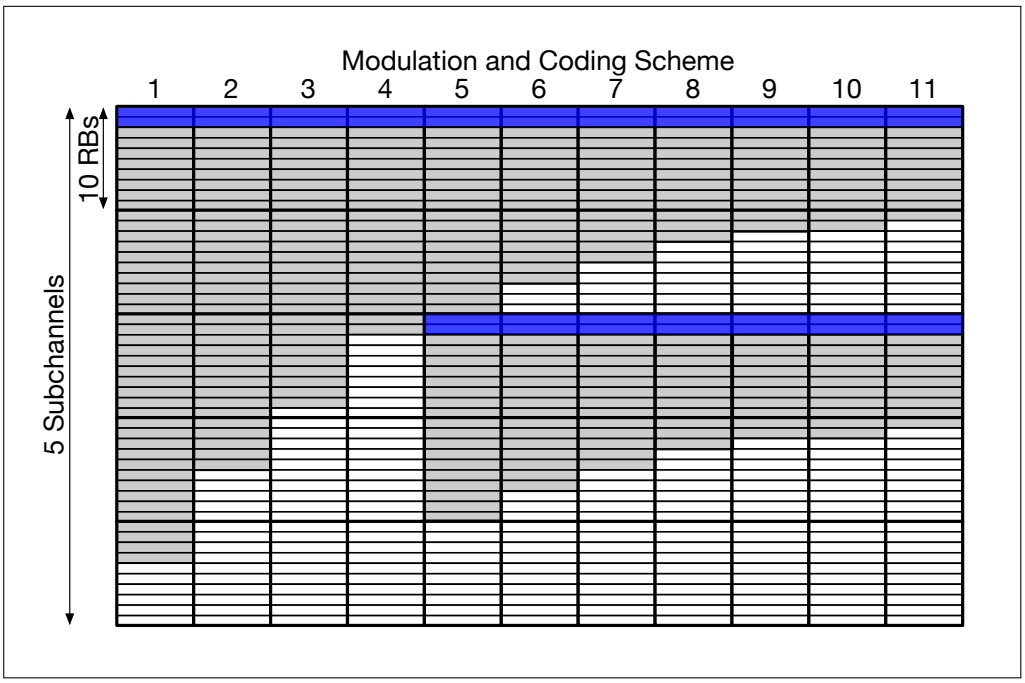


Figure 4.6: Subchannel and RB occupation as a function of the MCS for a 190-Byte packet and 5 subchannels of 10 RBs.

### 4.3.2 Effects of MCS adaptation on computation of power levels

As discussed above, even if the number of required subchannels remains unchanged, the selection of MCS modifies the number of RBs required for transmission in most cases. This has implications on the computation of power levels in the channel and consequently on the operation of the SB-SPS mechanism in LTE-V2V mode 4 that are important to consider.

For instance, if the total transmission power is assumed to be fixed, any variation on the number of used RBs directly modifies the transmission bandwidth and therefore, the PSD of each transmission. This needs to be considered every time the MCS is adapted to accurately compute the power levels in the channel and to ensure that the PSD remains within the limit of 23 dBm/MHz as specified by the standard [96]. This is often overlooked when analyzing the performance of LTE-V2V mode 4, as highlighted in [97], but it has been considered in this analysis.

More specifically, the variations of PSD due to MCS adaptation have an impact on the computation of important parameters such as the RSRP, RSSI and SINR as discussed in Subsection 4.2.3. The RSRP is computed by obtaining the average power contribution of each RE within the transmitted RBs [98]. Therefore, if the number of RBs changes due to

MCS adaptation, the value of RSRP must be computed accordingly. The variations of PSD also have an impact on the levels of interference in the channel. For instance, a transmission that occupies a lower number of RBs in a subchannel produces less interference than a transmission occupying the same subchannel but utilizes a higher number of RBs.

This variation on interference has an impact on RSSI, which is computed as the received power plus the interference and thermal noise in the received SC-FDMA symbol [98] and, therefore, it is directly related to the interference levels. This is also the case for the SINR, which is computed as the ratio between the received power and the interference plus the thermal noise.

Based on this analysis, the accurate estimation of the received power, interference and thermal noise must be carefully considered when MCS adaptation is implemented. This is particularly important for parameters such as the RSRP and RSSI, which are used to perform CSR selection as well as for the SINR, which is used for decoding transmissions. The effects of MCS adaptation on the CSR selection process are discussed in the following section.

### 4.3.3 Effects of MCS adaptation on CSR selection

The SB-SPS mechanism in LTE-V2V mode 4 filters out CSRs based on the average RSRP and RSSI of the subchannels in the sensing window. Therefore, several scenarios can arise due to variations in RSRP and RSSI as a consequence of the implementation of MCS adaptation, with further implications for the selection process of CSRs.

Figure 4.7 illustrates three potential scenarios depending on different reservation and occupation states of subchannels within the sensing window. Scenario A illustrates the case where two subchannels are reserved and fully occupied by a transmission where the implemented MCS requires use of all the RBs. As all the RBs in both subchannels are used, they both have the same levels of RSRP. This is also the case for the RSSI, because the occupied RBs contribute the same amount of interference to both subchannels.

However, in the case of scenarios B and C, the levels of RSRP and RSSI of each subchannel in the sensing window can be different if the MCS is adapted, thus varying the number of occupied RBs. For instance, the levels of RSRP in the upper subchannel of Scenario B, where all RBs are occupied, are higher than the ones corresponding to the lower subchannel. Thus, the upper subchannel has higher levels of RSSI, since there is a higher contribution of interference due to the use of a higher number of RBs.

This also occurs in Scenario C, where two subchannels have been reserved but only

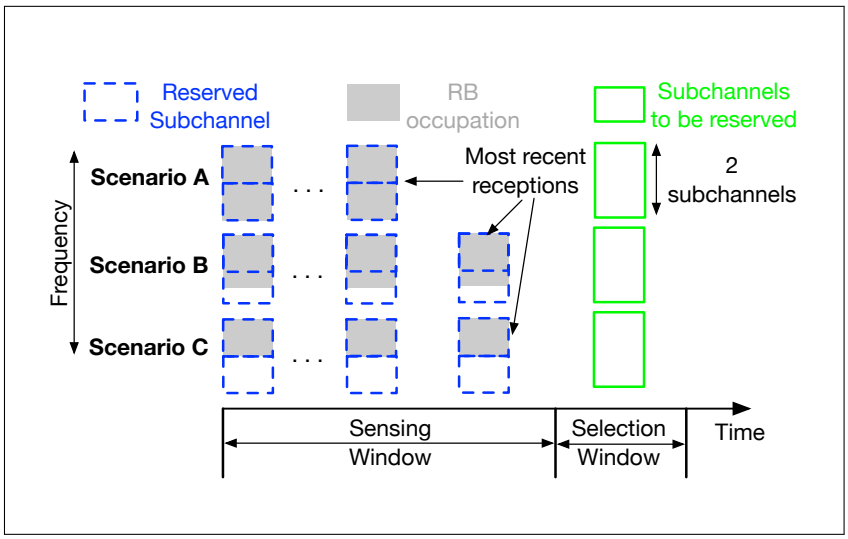


Figure 4.7: Subchannel and RB occupation during CSR selection with MCS adaptation.

the upper subchannel is fully occupied due to the implementation of a higher MCS while the reservation is maintained by SB-SPS. In this scenario the lower channel has effectively zero RSRP since all the transmission power is used in the upper subchannel and also has lower RSSI because there is no interference.

Importantly, these scenarios also have implications during the selection of CSRs, because the SB-SPS mechanism filters subchannels based on RSRP and RSSI levels. SB-SPS first discards the subchannels with the highest RSRP measured during the most recent receptions within the sensing window, which is affected by MCS adaptation as described for scenarios B and C. After this process, SB-SPS selects only 20% of the remaining subchannels with the lowest average RSSI computed. In this case, the average subchannel RSSI depends on the individual RSSI measurements in each subchannel, which can also vary as a function of the selected MCS as shown in scenarios B and C.

Based on this analysis, it is evident that the variations on the subchannel RSRP and RSSI due to MCS adaptation have important effects on the selection of CSRs performed by the SB-SPS mechanism. Therefore, these implications have been considered in this chapter to accurately model the operation of MCS adaptation in LTE-V2V mode 4 and evaluate its performance.

## 4.4 Performance analysis

In this section, MCS adaptation has been implemented as a mechanism for addressing congestion control in LTE-V2V mode 4, as proposed by the standard [69] and in the literature [37, 38]. To this end, this section describes the operation of congestion control in LTE-V2V mode 4 as well as the simulation scenario and the obtained performance results.

### 4.4.1 Congestion control in LTE-V2V mode 4

The goal of congestion control is to allow each vehicle to adjust its transmission parameters in order to reduce channel congestion. To perform congestion control each vehicle measures two metrics, the Channel Busy Ratio (CBR) and the Channel Occupancy Ratio (CR). The CBR measures the ratio between the subchannels whose RSSI exceeded a predefined threshold and all the available subchannels during the last 100 ms, providing an estimation of the overall level of congestion in the channel.

In contrast, the CR estimates the channel usage of each vehicle by measuring the ratio between the subchannels that have been used and reserved by the vehicle and all the available subchannels within a predefined period. Based on these two metrics, each vehicle can adjust its transmission parameters in order to reduce channel congestion if the CR exceeds a limit defined by the measured CBR. Recommended parameter values as defined by the standard [69] are shown in Table 4.1.

Table 4.1: CR limits per CBR range in LTE-V2V mode 4.

| **Measured CBR** | **CR limit** |
|---|---|
| $CBR <= 0.3$ | no limit |
| $0.3 < CBR <= 0.65$ | 0.03 |
| $0.65 < CBR <= 0.8$ | 0.006 |
| $0.8 < CBR <= 1$ | 0.003 |

By using the CBR and CR, each vehicle can implement different mechanisms to reduce congestion, such as increasing the MCS. As described in Subsection 4.3.1, increasing the MCS can reduce the number of required subchannels for a given transmission and therefore, reduce the CR. Moreover, even if the number of subchannels remains the same due to the channelization scheme of LTE-V2V mode 4, increasing the MCS reduces the number of required RBs which can reduce the average subchannel RSSI and ultimately the CBR.

Therefore, MCS adaptation is evaluated as a congestion control mechanism, where each vehicle adapts the MCS depending on the measured CR and CBR. To this end, two MCS configurations are implemented. MCS 7 is set by default in all vehicles, as specified in [70], when congestion is not detected in the channel. In turn, MCS 11, which is the maximum MCS specified by the standard in [67], is implemented if congestion conditions are met. With this mechanism, each vehicle increases the MCS from 7 to 11 when the CR exceeds the limit for its corresponding CBR and returns to MCS 7 otherwise.

The following sections describe the simulation environment used to evaluate the performance of MCS adaptation for congestion control and the results of this analysis.

### 4.4.2 Simulation environment

The performance of MCS adaptation for congestion control was evaluated with OpenCV2X [82], using the parameters specified in [70] and summarized in Table 4.2.

Table 4.2: Simulation scenario and parameters.

| Parameter | Value |
|---|---|
| **Vehicular topology** | |
| Road length | 2 km |
| Number of lanes | 6 (3 in each direction) |
| Lane width | 4 m |
| Vehicular density (veh/m of road) | 0.06, 0.09 and 0.20 |
| **Channel configuration** | |
| Carrier frequency | 5.9 GHz |
| Channel bandwidth | 10 MHz |
| Number of subchannels | 5 |
| Subchannel size | 10 RBs |
| **Access & Physical layers** | |
| Resource keep probability | 0 |
| RSRP & RSSI thresholds | -126 dBm & -90 dBm |
| Propagation model | Winner+ B1 |
| Noise figure | 9 dB |
| Shadowing variance LOS | 3 dB |
| MCS | 7, 11, adaptive |
| Modulation and Coding Rate | QPSK/0.7, 16QAM/0.5, adaptive |
| Transmission power | 27.32 dBm, 25.97 dBm, adaptive |

Three different vehicular densities are considered along with two fixed MCS configu-

rations (MCS 7 and MCS 11) and an adaptive configuration, where the MCS alternates between MCS 7 and MCS 11 depending on the congestion in the channel.

Moreover, in order to maintain the PSD constant and within the limit of 23 dBm/MHz, the transmission power was also adapted depending on the selected MCS configuration. To this end, the transmission power was set to 27.32 dBm for MCS 7 and 25.97 dBm for MCS 11. Finally, the application layer was configured for the transmission of 190-Byte packets with a transmission frequency of 10 Hz. The results were obtained by averaging the outcome of 5 simulation runs and are presented in the following section.

### 4.4.3 Simulation results and analysis

Figure 4.8 shows the average Packet Delivery Rate (PDR) versus the distance between each transmitter and receiver in the scenario, for all MCS configurations and vehicular densities. As expected, the PDR decreases for both MCS 7 and MCS 11 as the distance and vehicular density increase, due to the reduction in SINR and the increase of interference, respectively. It can also be noted that MCS 7 always outperforms MCS 11 with the difference in PDR increasing at higher vehicular densities. This can be attributed to the more robust modulation and coding rate of MCS 7 (QPSK/0.7), which outperforms MCS 11 (16QAM/0.5) at higher interference levels.

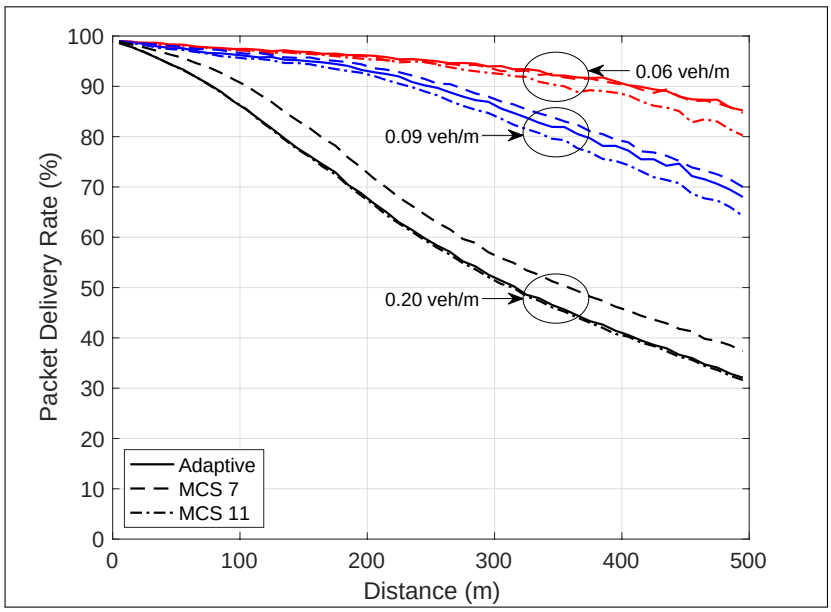


Figure 4.8: Average PDR versus transmitter-receiver distance.

Figure 4.8 also shows how the performance of MCS adaptation varies depending on the

vehicular density. For instance, at 0.06 veh/m MCS adaptation achieves the same PDR as MCS 7 because the vehicular density is not high enough to trigger the congestion control mechanism. However, as the density increases to 0.09 veh/m, some vehicles in the scenario trigger MCS adaptation changing the MCS from 7 to 11, which slightly reduces the overall PDR.

This is more evident at 0.20 veh/m, where MCS adaptation has the same performance as MCS 11 due to all vehicles increasing their MCS due to the higher vehicular density. Ultimately, it can be seen that adapting the MCS does not improve PDR in response to congestion. This could be due to the constraints imposed by the standard regarding the subchannel and MCS configurations, which limit the reduction in subchannel occupation despite the reduction in the number of required RBs.

Figure 4.9 shows the percentage of transmission errors versus the cause of error for all MCS configurations. The results are shown for a density of 0.09 veh/m and correspond only to errors within a range of 500 m. It can be seen that the percentage of half duplex errors is the same for all MCS configurations. This is expected since the transmission rates for MCS 7 and MCS 11 are the same, which results in the same number of lost transmissions due to half duplex limitations in the simulated scenario.

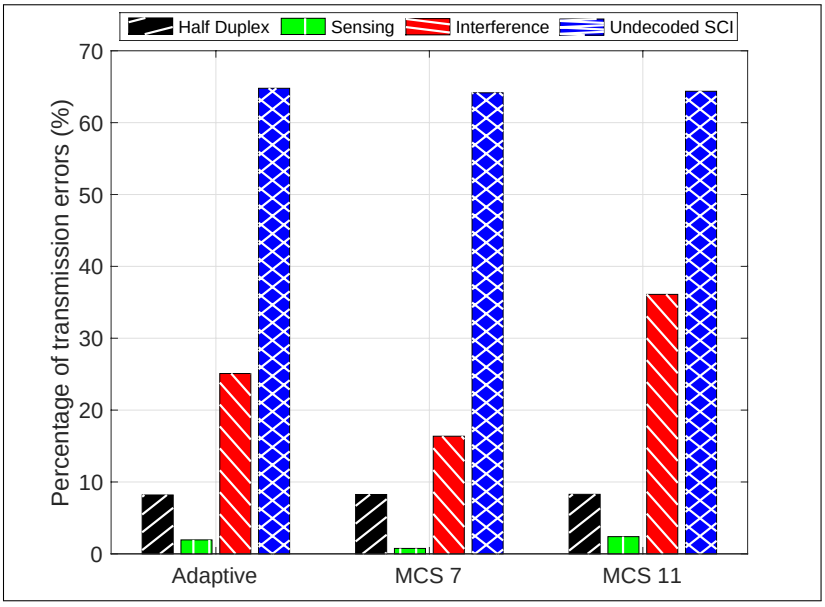


Figure 4.9: Percentage of transmission errors versus cause of error for all MCS configurations at 0.09 veh/m.

In terms of sensing errors, which occur when the received power is below the sensing threshold of -96 dBm specified in [95], MCS 7 performs slightly better than MCS 11. This

occurs because MCS 7 can implement a higher transmission power than MCS 11 while maintaining the PSD within the 23 dBm/MHz limit. Specifically, the transmission power can be set to 27.32 dBm for MCS 7 and 25.97 dBm for MCS 11 because MCS 7 occupies a larger bandwidth (15 RBs) than MCS 11 (11 RBs). In the case of MCS adaptation, the percentage of sensing errors is within the range of MCS 7 and MCS 11 as some vehicles increase the MCS when the mechanism is triggered at the configured density.

Figure 4.9 also shows the percentage of transmission errors due to interference, which occur when the packet cannot be decoded due to low levels of SINR. In this case, MCS 7 (QPSK/0.7) outperforms MCS 11 (16QAM/0.5), as the former is more robust when the same levels of interference are present in the channel. In the case of MCS adaptation, the errors due to interference are within the range of MCS 7 and MCS 11 as the MCS is increased in some of the vehicles in the scenario.

Finally, Figure 4.9 shows the percentage of transmission errors due to undecoded SCIs. This type of error occurs when the SCI cannot be decoded at the receiver, resulting in the corresponding TB being immediately discarded. This is attributable to the fact that errors are analyzed within a 500 m range, where interference from SCI collisions is more likely to cause undecoded SCIs and impact TB transmissions. Figure 4.9 also shows that the selection of different MCS configurations has no impact on SCI collisions, as the MCS only modifies the number of RBs for the TB and not the SCI.

To validate the operation of MCS adaptation for congestion control, Figure 4.10 shows the average CBR for all vehicular densities and MCS configurations, while Figure 4.11 shows the average MCS usage for MCS adaptation for all vehicular densities.

In Figure 4.10, the CBR levels at 0.06 veh/m are lower than 0.3, which is the minimum CBR required to trigger MCS adaptation according to Table 4.1. Therefore, at 0.06 veh/m and with MCS adaptation enabled almost all vehicles in the scenario implement MCS 7, as shown in Figure 4.11.

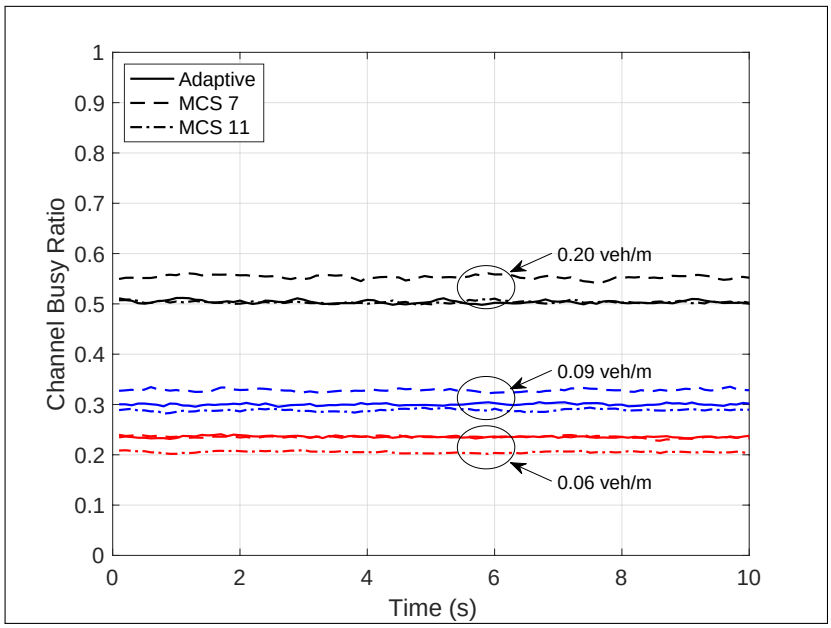


Figure 4.10: Channel Busy Ratio.

It can also be seen that for 0.09 veh/m, the CBR increases around the minimum CBR limit of 0.3 which triggers MCS adaptation. This is validated in Figure 4.11 where it is shown that 60% of vehicles increase the MCS to 11, while the remaining 40% implement MCS 7. At 0.20 veh/m, Figure 4.10 also shows that the CBR reaches 0.5 as its highest value, which is higher than the minimum CBR limit. Consequently, MCS adaptation is triggered in all vehicles, which increase their MCS to 11 as shown in Figure 4.11.

Importantly, the results of Figure 4.10 indicate that the CBR levels are generally lower for MCS 11 across all vehicular densities. This is the result of the reduction in subchannel RSSI that occurs due to the lower RB occupation of the higher MCS. Moreover, this result highlights the main advantage of increasing the MCS in congested scenarios, which is an overall reduction of channel congestion.

Finally, in the case of MCS adaptation, Figure 4.10 shows how the CBR levels vary depending on the vehicular density. For instance, at 0.06 veh/m the CBR of MCS 7 and MCS adaptation are practically the same due to the lower density in the scenario, which is below the CBR limit required to trigger MCS adaptation. However, as the density increases to 0.09 veh/m, MCS adaptation is able to reduce the overall CBR, as 60% of the vehicles in the scenario switch to MCS 11 to cope with the higher congestion in the channel. This trend is even clearer at 0.20 veh/m, where all vehicles switch to MCS 11 due to the high congestion, achieving a higher reduction on CBR.

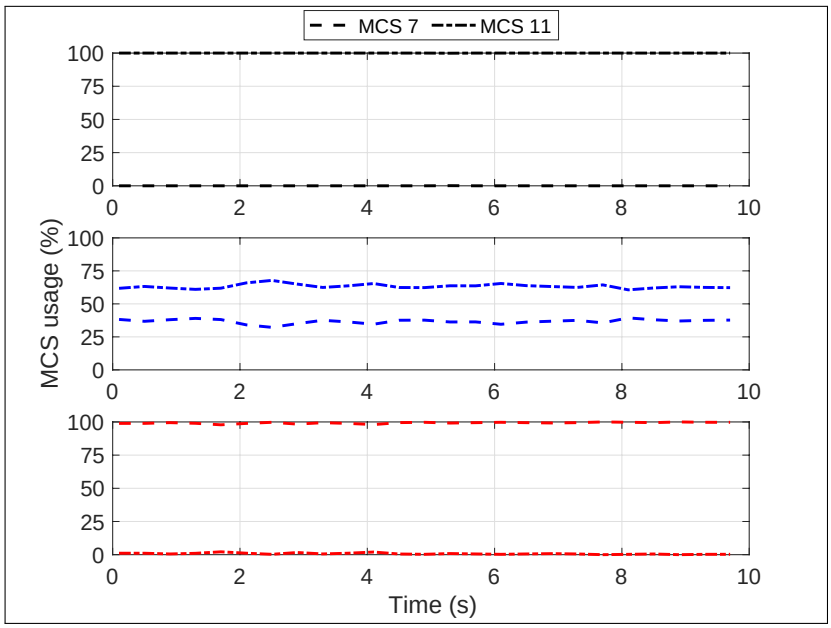


Figure 4.11: MCS usage for MCS adaptation at 0.06 veh/m (bottom), 0.09 veh/m (middle) and 0.20 veh/m (top).

This reduction in CBR can be validated through Figure 4.12 where the average subchannel RSSI is shown for all MCS configurations and vehicular densities. It can be seen that the average subchannel RSSI increases with the vehicular density due to the higher levels of interference in the scenario. More importantly, it shows that the average subchannel RSSI of MCS 7 is higher than MCS 11 for all the vehicular densities, indicating that the higher RB occupation of MCS 7 with respect to MCS 11 increases the subchannel RSSI and ultimately the CBR, as shown in Figure 4.10.

Figure 4.12 also shows how the average subchannel RSSI of MCS adaptation depends on the configured vehicular density. For instance, at 0.06 veh/m the number of vehicles in the scenario is not enough to trigger MCS adaptation, and therefore subchannel RSSI is the same as MCS 7. However, as the density increases, the average subchannel RSSI is lower for MCS adaptation in comparison with MCS 7 because the vehicles in the scenario increase their MCS due to the higher congestion in the channel.

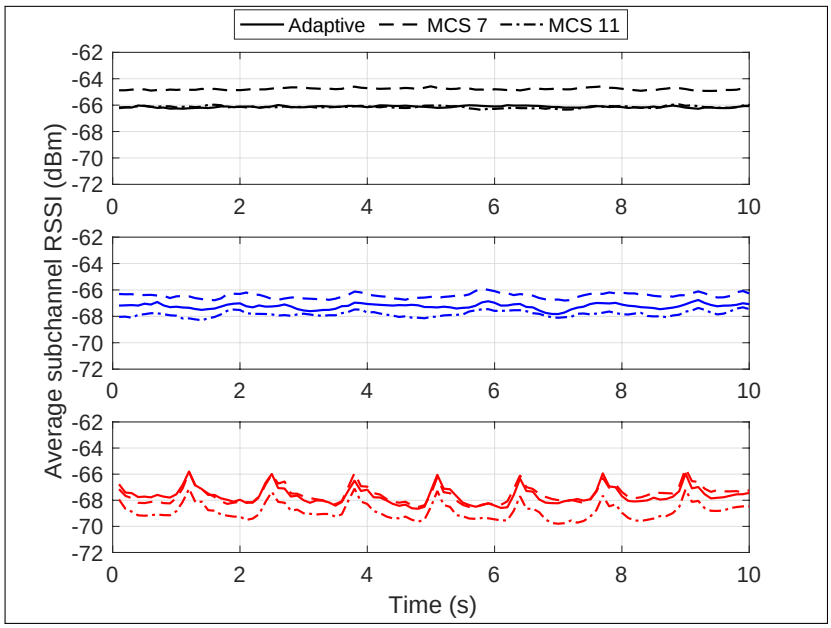


Figure 4.12: Average subchannel RSSI at 0.06 veh/m (bottom), 0.09 veh/m (middle) and 0.20 veh/m (top).

## 4.5 Chapter conclusions

In this chapter, the performance of MCS adaptation in the sidelink channel of LTE-V2V Mode 4 is analyzed. To this end, a comprehensive study of the implications of the operation of MCS adaptation in LTE-V2V mode 4 is presented. To validate the study, the operation of MCS adaptation is implemented in a simulation model, where its performance is evaluated as a mechanism for congestion control.

To model the operation of MCS adaptation in LTE-V2V mode 4, multiple simulation frameworks are leveraged. These include the INET and SimuLTE frameworks, which implement the application, transport and network layers as well as the PDCP, RRC and RLC layers of the protocol stack of the LTE-V2V mode 4. The model is complemented with other frameworks like SUMO and Veins for modeling the vehicular mobility, providing a realist simulating scenario of the proposed model.

All these frameworks are leveraged by the OpenCV2X simulator which is the core of the presented analysis. For the study presented in this chapter, OpenCV2X is extended in order to provide a standard-compliant implementation of the MAC and physical layers of LTE-V2V mode 4. Specifically, extensions are introduced to the OpenCV2X model at the

physical and MAC layers in order to accurately model the operation of MCS adaptation.

The study presented in this chapter provides valuable insights regarding the implications of MCS adaptation on the operation of LTE-V2V mode 4. Specifically it shows the impact of MCS adaptation on the resource configuration and the computation of power levels at the physical layer, as well as on the operation of the SB-SPS mechanism at the MAC layer of LTE-V2V mode 4.

To validate the study, MCS adaptation is evaluated as a mechanism for congestion control in LTE-V2V mode 4 as proposed by the standard. The results indicate that under high vehicular density, MCS adaptation is capable of reducing the subchannel interference and therefore, the congestion in the channel. However, the results also highlight the limitations of MCS adaptation due to the channelization constraints of LTE-V2V mode 4 and demonstrate that the technique does not improve the overall performance of LTE-V2V mode 4 under the analyzed congestion conditions.

Despite the limitations of MCS adaptation for congestion control, the study provides valuable insights on the operation of the technique in LTE-V2V mode 4, laying the foundation for other applications that can benefit from its implementation. This is the case of applications that require the transmission of packets of variable size, which can leverage MCS adaptation to fit different packet sizes within the same reservation. This is also the case of applications that can use MCS adaptation to improve the performance of transmission 4 in scenarios where the channel conditions are highly variable, making the use of fixed MCS configurations inefficient.

# Chapter 5

# Conclusions and future work

## 5.1 Conclusions

The main objective of this thesis was to analyze the performance of link adaptation in LTE-V2X. This procedure is critical to the operation of LTE-V2X, as it allows the system to adapt its transmission parameters to the dynamic channel conditions found in vehicular communication scenarios.

The thesis focused specifically on the analysis of the MCS as the link adaptation parameter. The selection of the MCS as the analyzed parameter was based on its particular implications on the operation of LTE-V2X. Specifically, the selected MCS has implications on the resource management process at the MAC layer as well on the operation of the physical layer of LTE-V2X. Therefore, the analysis of this parameter provided a unique perspective into the performance of LTE-V2X.

The study presented in this thesis was divided into two main parts. In the first part, the performance of MCS adaptation was evaluated in the LTE-V2I scenario, where vehicles communicate with the eNodeB. In turn, the second part presented the evaluation of MCS adaptation in the LTE-V2V scenario, where vehicles communicate directly among themselves. The study was performed independently due to the differences between both communication scenarios, providing a deeper perspective of the implications of the procedure in the LTE-V2X system.

The study also proposed the use of different methodologies for the study of MCS adaptation in LTE-V2I and LTE-V2V. In the case of LTE-V2I, the proposed methodology was based on the analysis of real-world channel measurements collected by VUEs through

a crowdsourcing approach. In turn, the analysis for LTE-V2V proposed the development of a simulation model that replicated the operation of MCS adaptation in vehicular communication scenarios.

In order to perform the evaluation of MCS adaptation in LTE-V2I, first a method to filter the collected measurements was proposed. The method was developed to extract the CQI measurements in the downlink direction from crowdsourced data and provided valuable insights on how to extract valuable information from data collected using this method.

The filtered channel quality measurements were then used to develop a model based on a Finite State Markov Chain that characterized the downlink channel quality in the analyzed scenario. The model was then leveraged to evaluate the performance of MCS adaptation by computing the maximum transmission capacity of the downlink channel when MCS adaptation is implemented.

The obtained results showed that executing MCS adaptation in LTE-V2I reduces the transmission capacity in vehicular scenarios due to the high levels of mobility. However, the results also indicated that by performing MCS adaptation, connectivity can be maintained in the analyzed scenario, which is critical to the performance of LTE-V2I communications.

The analysis of measurements collected by real LTE UEs also provided a unique opportunity to understand and evaluate the performance of LTE under real-world conditions. The results of this analysis could provide valuable insights, for instance, to mobile network operators that plan to deploy applications in LTE-V2I communication scenarios.

In contrast, the study of MCS adaptation in LTE-V2V mode 4 proposed the development of a simulation model. The model was developed in an open source simulator, where the operation of MCS adaptation in LTE-V2V and vehicular mobility models were combined. These combination provided a realistic simulation scenario where the performance of the procedure was evaluated.

The development of the MCS adaptation model leveraged a variety of open source simulation frameworks and introduced multiple extensions to an open source LTE-V2V mode 4 model, particularly at the physical layer. These modifications were critical to correct the computation of key physical layer parameters in the LTE-V2V mode 4 model and to validate its operation against a well known analytical model of LTE-V2V mode 4. After validating its operation, the corrected model was used to evaluate the performance of MCS adaptation for congestion control, where vehicles adapt their selected MCS dynamically in response to the levels of congestion in the channel.

The obtained results showed that MCS adaptation was able to control the congestion in

the channel by reducing interference when the number of vehicles in the scenario increased, which is one of the main goals of congestion control in LTE-V2V mode 4. However, the results also highlighted the limitations of the mechanism, which was unable to improve the performance in term of the number of correctly received transmissions when the levels of congestion increased under high vehicular density.

The introduction of a simulation model provided several advantages in comparison to the model developed based on real-world measurements. For instance, the simulation model allowed a more detailed analysis of the implications of MCS adaptation in operation of LTE-V2V and provided more control over the simulation scenario. However, these advantages contrast with the limitations of this type of models, which are only representations of real communication systems.

Overall, the results of the analysis of MCS adaptation highlight the relevance of this mechanism for the operation of both LTE-V2I and LTE-V2V. Specifically, the results showed that MCS adaptation has broad implications to the operation of the MAC and physical layers, both of which are critical to the performance of transmissions in the downlink and sidelink channels of LTE-V2I and LTE-V2V, respectively.

These results can be useful to understand the implications of MCS adaptation for the resource management process performed at the MAC layer as well as the effects of using different combinations of modulations and coding rates at the link level. These implications, which are unique to MCS adaptation in LTE-V2X, can also provide valuable insights that can be further used to optimize its operation for different applications.

For instance, in the case of LTE-V2I, the results could be used to better understand the performance of the mechanism when applications with high transmission rate requirements are implemented, as it is the case of information or entertainment applications. This could be also the case for the study of other type of applications that require high levels of connectivity instead, such as those focused on improving safety or optimizing vehicular traffic.

In the case of LTE-V2V, the study of MCS adaptation can also be extended to analyze and optimize the mechanism for other applications. These include applications that require the transmission of packets of variable size, where adapting the MCS can be used to fit different packet sizes using the same amount of resources. These also include applications that can leverage MCS adaptation to optimize transmissions in LTE-V2V in response to variations in the communication scenario due to the changes in vehicular density or propagation conditions.

The analysis of these applications is important as they are expected to play a key role

in the operation of V2X communications and will be extended to other use cases such as autonomous or remote driving, which are considered the future of vehicular transportation systems.

## 5.2 Future work

The future work of this thesis will be mainly focused on extending the study of LTE-V2V communications. To this end, future work aims at leveraging the developed simulation model to evaluate other applications of MCS adaptation in LTE-V2V beyond congestion control. Specifically, this refers to the evaluation of the transmission of packets of variable size, which is particularly relevant for different safety applications in LTE-V2V. This application represents a major challenge due to the operation of the SB-SPS mechanism, which was originally designed for the transmission of packets of relatively fixed size. In this context, MCS adaptation can play a key role, as it can leverage existing reservations to transmit packets of variable size using the same amount of resources and avoid braking reservations, which can severely impact the performance of transmissions in LTE-V2V mode 4.

In addition, the MCS adaptation model can be used to enable other applications in LTE-V2V mode 4 communications. This has been highlighted, for instance, by related studies that implement MCS adaptation mechanisms to improve the performance of transmissions in 802.11 p. For instance, in LTE-V2V mode 4, MCS adaptation can be used to the MCS as a function of variable vehicular density conditions and optimize transmissions as a function of the variable interference in the channel that occurs as a result. Furthermore, MCS adaptation in LTE-V2V mode 4 can be leveraged in the case of scenarios where propagation conditions vary due to the communication environment. This can occur in urban or sub-urban scenarios, where line-of-sight and non line-of-sight conditions arise, which require adapting the robustness of transmissions dynamically through MCS adaptation to increase the probability of correct packet decoding at the receptor

In addition to these new applications of MCS adaptation, the knowledge acquired of the LTE-V2V mode 4 standard and the multiple simulation frameworks can be leveraged to update the current simulation model to include features of new standards of LTE-V2V communications, such NR-V2X. This include, for instance, the implementation of new frame structures at the physical layer of the simulation model that include different numerologies, designed to reduce the latency by adapting the duration of the frame in LTE-V2V. This also

include new features at the MAC layer, which solve some of the limitations of the current SB-SPS mechanism to allow the implementation of newer applications with additional requirements in terms of packet sizes, transmission frequency, reliability and latency.

# Bibliography

[1] Ho Ting Cheng, Hangguan Shan, and Weihua Zhuang. Infotainment and road safety service support in vehicular networking: From a communication perspective. *Mechanical Systems and Signal Processing*, 25(6):2020–2038, 2011. Interdisciplinary Aspects of Vehicle Dynamics.

[2] Konstantinos Katsaros, Ralf Kernchen, Mehrdad Dianati, David Rieck, and Charalambos Zinoviou. Application of vehicular communications for improving the efficiency of traffic in urban areas. *Wireless Communications and Mobile Computing*, 11(12):1657–1667, 2011.

[3] Marco Annoni and Bob Williams. *The History of Vehicular Networks*, pages 3–21. Springer International Publishing, Cham, 2015.

[4] Jiadai Wang, Jiajia Liu, and Nei Kato. Networking and communications in autonomous driving: A survey. *IEEE Communications Surveys Tutorials*, 21(2):1243–1274, 2019.

[5] Ruilin Liu, Daehan Kwak, Srinivas Devarakonda, Kostas Bekris, and Liviu Iftode. Investigating remote driving over the lte network. In *Proceedings of the 9th International Conference on Automotive User Interfaces and Interactive Vehicular Applications*, AutomotiveUI '17, page 264–269, New York, NY, USA, 2017. Association for Computing Machinery.

[6] Valerian Mannoni, Vincent Berg, Stefania Sesia, and Eric Perraud. A comparison of the V2X communication systems: Its-g5 and c-v2x. In *2019 IEEE 89th Vehicular Technology Conference (VTC2019-Spring)*, pages 1–5, 2019.

[7] G. Araniti, C. Campolo, M. Condoluci, A. Iera, and A. Molinaro. LTE for vehicular networking: a survey. *IEEE Communications Magazine*, 51(5):148–157, May 2013.

[8] The 3rd generation partnership project. https://www.3gpp.org/. Accessed: 2022-01-07.

[9] 3GPP. *Release 8 Description (v8.0.0)*, Jun. 2008. TR 21.908.

[10] Mads Lauridsen, Lucas Chavarria Gimenez, Ignacio Rodriguez, Troels B. Sorensen, and Preben Mogensen. From LTE to 5G for connected mobility. *IEEE Communications Magazine*, 55(3):156–162, 2017.

[11] Syed Adeel Ali Shah, Ejaz Ahmed, Muhammad Imran, and Sherali Zeadally. 5G for vehicular communications. *IEEE Communications Magazine*, 56(1):111–117, 2018.

[12] Hanbyul Seo, Ki-Dong Lee, Shinpei Yasukawa, Ying Peng, and Philippe Sartori. LTE evolution for vehicle-to-everything services. *IEEE Communications Magazine*, 54(6):22–28, 2016.

[13] 3GPP. *Release 14 Description (v14.0.0)*, Jun. 2018. TR 21.914.

[14] Daniel Jiang and Luca Delgrossi. IEEE 802.11p: Towards an international standard for wireless access in vehicular environments. In *VTC Spring 2008 - IEEE Vehicular Technology Conference*, pages 2036–2040, 2008.

[15] Alessandro Bazzi, Giammarco Cecchini, Michele Menarini, Barbara M. Masini, and Alberto Zanella. Survey and perspectives of vehicular wi-fi versus sidelink Cellular-V2X in the 5G era. *Future Internet*, 11(6), 2019.

[16] Zeeshan Hameed Mir and Fethi Filali. LTE and IEEE 802.11p for vehicular networking: a performance evaluation. *EURASIP Journal on Wireless Communications and Networking*, 2014(1):1–15, May 2014.

[17] Alessandro Bazzi, Barbara M. Masini, Alberto Zanella, and Ilaria Thibault. On the performance of IEEE 802.11p and LTE-V2V for the cooperative awareness of connected vehicles. *IEEE Transactions on Vehicular Technology*, 66(11):10419–10432, 2017.

[18] Li Zhao, Jiayi Fang, Jinling Hu, Yuanyuan Li, Lin Lin, Yan Shi, and Chenxin Li. The performance comparison of LTE-V2X and IEEE 802.11p. In *2018 IEEE 87th Vehicular Technology Conference (VTC Spring)*, pages 1–5, 2018.

[19] Shanzhi Chen, Jinling Hu, Yan Shi, Li Zhao, and Wen Li. A vision of c-v2x: Technologies, field testing, and challenges with chinese development. *IEEE Internet of Things Journal*, 7(5):3872–3881, 2020.

[20] Gaurang Naik, Biplav Choudhury, and Jung-Min Park. IEEE 802.11bd ; 5G NR V2X: Evolution of radio access technologies for v2x communications. *IEEE Access*, 7:70169–70184, 2019.

[21] 3GPP. *Release 15 Description (v15.0.0)*, Sep. 2019. TR 21.915.

[22] 3GPP. *Release 16 Description (v16.0.0)*, Jun. 2021. TR 21.916.

[23] A. Elnashar and M. A. El-Saidny. Looking at LTE in practice: A performance analysis of the LTE system based on field test results. *IEEE Vehicular Technology Magazine*, 8(3):81–92, Sept 2013.

[24] V. Sevindik, J. Wang, O. Bayat, and J. Weitzen. Performance evaluation of a real long term evolution (LTE) network. In *37th Annual IEEE Conference on Local Computer Networks - Workshops*, pages 679–685, Oct 2012.

[25] S. Avallone, N. Pasquino, S. Zinno, and D. Casillo. Smartphone-based measurements of LTE network performance. In *2017 IEEE International Instrumentation and Measurement Technology Conference (I2MTC)*, pages 1–6, May 2017.

[26] Nakrop Jinaporn, Simon Armour, and Angela Doufexi. Performance evaluation on resource allocation with carrier aggregation in lte cellular networks. In *2019 IEEE 90th Vehicular Technology Conference (VTC2019-Fall)*, pages 1–5, 2019.

[27] Jose Oscar Fajardo, Ianire Taboada, and Fidel Liberal. Analysis of CQI traces from LTE MIMO deployments and impact on classical schedulers. In Mari Carmen Aguayo-Torres, Gerardo Gómez, and Javier Poncela, editors, *Wired/Wireless Internet Communications*, pages 60–73, Cham, 2015. Springer International Publishing.

[28] Ignacio Rodriguez, Erika P. L. Almeida, Mads Lauridsen, Dereje A. Wassie, Lucas Chavarria Gimenez, Huan C. Nguyen, Troels B. Soerensen, and Preben Mogensen. Measurement-based evaluation of the impact of large vehicle shadowing on V2X communications. In *European Wireless 2016; 22th European Wireless Conference*, pages 1–8, 2016.

[29] James H. Schaffner, Hyok J. Song, Arthur Bekaryan, Timothy Talty, Duane Carper, and Eray Yasan. Scanner based drive test LTE capacity measurements with MIMO antennas placed inside the vehicle. In *2015 IEEE International Conference on Microwaves, Communications, Antennas and Electronic Systems (COMCAS)*, pages 1–4, 2015.

[30] W. Viriyasitavat, M. Boban, H. M. Tsai, and A. Vasilakos. Vehicular communications: Survey and challenges of channel and propagation models. *IEEE Vehicular Technology Magazine*, 10(2):55–66, June 2015.

[31] L. Bernado, T. Zemen, F. Tufvesson, A. F. Molisch, and C. F. Mecklenbräuker. Delay and doppler spreads of nonstationary vehicular channels for safety-relevant scenarios. *IEEE Transactions on Vehicular Technology*, 63(1):82–93, Jan 2014.

[32] S. Schwarz, T. Philosof, and M. Rupp. Signal processing challenges in cellular-assisted vehicular communications: Efforts and developments within 3GPP LTE and beyond. *IEEE Signal Processing Magazine*, 34(2):47–59, March 2017.

[33] Byungjun Kang, Sunghoon Jung, and Saewoong Bahk. Sensing-based power adaptation for cellular V2X mode 4. In *2018 IEEE International Symposium on Dynamic Spectrum Access Networks (DySPAN)*, pages 1–4, 2018.

[34] Amir Haider and Seung-Hoon Hwang. Adaptive transmit power control algorithm for sensing-based semi-persistent scheduling in C-V2X mode 4 communication. *Electronics*, 8(8), 2019.

[35] Md Saifuddin, Mahdi Zaman, Behrad Toghi, Yaser P. Fallah, and Jayanthi Rao. Performance analysis of Cellular-V2X with adaptive amp; selective power control. In *2020 IEEE 3rd Connected and Automated Vehicles Symposium (CAVS)*, pages 1–7, 2020.

[36] Byungjun Kang, Jinmo Yang, Jeongyeup Paek, and Saewoong Bahk. Atomic: Adaptive transmission power and message interval control for C-V2X mode 4. *IEEE Access*, 9:12309–12321, 2021.

[37] Rafael Molina-Masegosa and Javier Gozalvez. LTE-V for sidelink 5G V2X vehicular communications: A new 5G technology for short-range vehicle-to-everything communications. *IEEE Vehicular Technology Magazine*, 12(4):30–39, 2017.

[38] Adel Mansouri, Vincent Martinez, and Jérôme Härri. A first investigation of congestion control for LTE-V2X mode 4. In *2019 15th Annual Conference on Wireless On-demand Network Systems and Services*, pages 56–63, 2019.

[39] Alessandro Bazzi. Congestion control mechanisms in IEEE 802.11p and sidelink C-V2X. In *2019 53rd Asilomar Conference on Signals, Systems, and Computers*, pages 1125–1130, 2019.

[40] Alessandro Bazzi, Alberto Zanella, and Barbara M. Masini. Optimizing the resource allocation of periodic messages with different sizes in LTE-V2V. *IEEE Access*, 7:43820–43830, 2019.

[41] Rafael Molina-Masegosa, Javier Gozalvez, and Miguel Sepulcre. Comparison of ieee 802.11p and LTE-V2X: An evaluation with periodic and aperiodic messages of constant and variable size. *IEEE Access*, 8:121526–121548, 2020.

[42] Yuan Yao, Xingshe Zhou, and Kailong Zhang. Density-aware rate adaptation for vehicle safety communications in the highway environment. *IEEE Communications Letters*, 18(7):1167–1170, 2014.

[43] Yuan Yao, Xi Chen, Lei Rao, Xue Liu, and Xingshe Zhou. LORA: Loss differentiation rate adaptation scheme for vehicle-to-vehicle safety communications. *IEEE Transactions on Vehicular Technology*, 66(3):2499–2512, 2017.

[44] Joseph Camp and Edward Knightly. Modulation rate adaptation in urban and vehicular environments: Cross-layer implementation and experimental evaluation. *IEEE/ACM Transactions on Networking*, 18(6):1949–1962, 2010.

[45] Andres Burbano-Abril, Brian McCarthy, Miguel Lopez-Guerrero, Victor Rangel, and Aisling O'Driscoll. MCS adaptation within the cellular V2X sidelink. In *2021 IEEE Conference on Standards for Communications and Networking (CSCN)*, pages 111–117, 2021.

[46] A. Burbano-Abril, R.M. Edwards, V. Rangel-Licea, R. Aquino-Santos, M. Lopez-Guerrero, R.S. Kalawsky, and M. Behjati. Modeling and analysis of LTE connectivity in a high mobility vehicular environment. *Computers and Electrical Engineering*, 68:322–336, 2018.

[47] Brian McCarthy, Andres Burbano-Abril, Victor Rangel Licea, and Aisling O'Driscoll. OpenCV2X: Modelling of the V2X cellular sidelink and performance evaluation for aperiodic traffic. *CoRR*, abs/2103.13212, March 2021.

[48] Erik Dahlman, Stefan Parkvall, and Johan Sköld. Chapter 6 - scheduling, link adaptation, and hybrid ARQ. In Erik Dahlman, Stefan Parkvall, and Johan Sköld, editors, *4G: LTE/LTE-Advanced for Mobile Broadband (Second Edition)*, pages 85–101. Academic Press, Oxford, second edition edition, 2014.

[49] Erik Dahlman, Stefan Parkvall, and Johan Sköld. Chapter 10 - downlink physical-layer processing. In Dahlman Erik, , Parkvall Stefan, and Johan Sköld, editors, *4G LTE/LTE-Advanced for Mobile Broadband*, pages 143 – 202. Academic Press, Oxford, 2011.

[50] academia. *LTE Air Interface Training Manual*, Jun. 2016. academia.

[51] Andrea Ancora, Stefania Sesia, and Alex Gorokhov. *Reference Signals and Channel Estimation*, chapter 8, pages 165–187. John Wiley & Sons, Ltd, 2011.

[52] Muhammad Kazmi. *Radio Resource Management*, chapter 22, pages 503–530. John Wiley and Sons, Ltd, 2011.

[53] 3GPP. *Requirements for support of radio resource management (v14.9.0)*, Sep. 2018. TS 36.133.

[54] 3GPP. *Technical Specification Group Radio Access Network; Evolved Universal Terrestrial Radio Access (E-UTRA); Radio Frequency (RF) requirements for LTE Pico Node B (v16.0.0, Release 16)*, Jun. 2020. TR 36.931.

[55] 3GPP. Evolved Universal Terrestrial Radio Access (E-UTRA); Physical Layer Procedures. TS 36.213 V8.8.0, 3rd Generation Partnership Project (3GPP), 2009.

[56] Erik Dahlman, Stefan Parkvall, and Johan Sköld. Chapter 10 - downlink physical-layer processing. In Erik Dahlman, Stefan Parkvall, and Johan Sköld, editors, *4G: LTE/LTE-Advanced for Mobile Broadband (Second Edition)*, pages 161–240. Academic Press, Oxford, second edition edition, 2014.

[57] F. Capozzi, G. Piro, L.A. Grieco, G. Boggia, and P. Camarda. Downlink packet scheduling in LTE cellular networks: Key design issues and a survey. *IEEE Communications Surveys Tutorials*, 15(2):678–700, 2013.

[58] A. Marinčić. Performance evaluation of different scheduling algorithms in LTE systems. In *2016 39th International Convention on Information and Communication Technology, Electronics and Microelectronics (MIPRO)*, pages 595–600, May 2016.

[59] Dr Harri Holma and Dr Antti Toskala. *LTE for UMTS - OFDMA and SC-FDMA Based Radio Access*. Wiley Publishing, 2009.

[60] Gwanmo Ku and John MacLaren Walsh. Resource allocation and link adaptation in LTE and LTE advanced: A tutorial. *IEEE Communications Surveys Tutorials*, 17(3):1605–1633, 2015.

[61] ETSI. *LTE; Evolved Universal Terrestrial Radio Access (E-UTRA) Physical layer procedures (V14.17.0 Release 14)*, June. 2021.

[62] Jiajia Liu, Nei Kato, Jianfeng Ma, and Naoto Kadowaki. Device-to-device communication in LTE-advanced networks: A survey. *IEEE Communications Surveys Tutorials*, 17(4):1923–1940, 2015.

[63] Daniel Sempere-García, Miguel Sepulcre, and Javier Gozalvez. LTE-V2X mode 3 scheduling based on adaptive spatial reuse of radio resources. *Ad Hoc Networks*, 113:102351, 2021.

[64] Moray Rumney. *3GPP LTE: Introducing Single-Carrier FDMA*, Jul. 2010. keysight.

[65] Robert Love and Vijay Nangia. *Uplink Physical Layer Design*, chapter 14, pages 315–326. John Wiley and Sons, Ltd, 2011.

[66] Alexandre K. Ligo and Jon M. Peha. Spectrum for V2X: Allocation and sharing. *IEEE Transactions on Cognitive Communications and Networking*, 5(3):768–779, 2019.

[67] ETSI. *Intelligent Transport Systems (ITS); Access layer specification for Intelligent Transport Systems using LTE Vehicle to everything communication in the 5,9 GHz frequency band (V1.1.1)*, Nov. 2018.

[68] ETSI. *Intelligent Transport Systems (ITS); Vehicular Communications; Basic Set of Applications; Specification of Cooperative Awareness Basic Service*, Apr. 2019.

[69] ETSI. *Congestion Control Mechanisms for the C-V2X PC5 interface; Access layer part (V1.1.1)*, Nov. 2018.

[70] 3GPP. *Study on LTE-based V2X services (v14.0.0)*, Jul. 2016. TR 38.885.

[71] W. Li, R. K. P. Mok, D. Wu, and R. K. C. Chang. On the accuracy of smartphone-based mobile network measurement. In *2015 IEEE Conference on Computer Communications (INFOCOM)*, pages 370–378, April 2015.

[72] Opensignal. Accessed: 2011-11-27.

[73] Openstreetmap. Accessed: 2017-11-27.

[74] Motorway 1 services. Accessed: 2017-11-27.

[75] R. Jain. *The Art of Computer Systems Performance Analysis: Techniques for Experimental Design, Measurement, Simulation, and Modeling*. Wiley, 1990.

[76] A. Leon-Garcia. *Probability, Statistics, and Random Processes for Electrical Engineering*. Pearson/Prentice Hall, 2008.

[77] Riverbed. *Riverved Modeler version 18.5*, 2017.

[78] E. Çinlar. *Introduction to Stochastic Processes*. Dover Books on Mathematics Series. Dover Publications, Incorporated, 2013.

[79] G. Bolch, S. Greiner, H. de Meer, and K.S. Trivedi. *Queueing Networks and Markov Chains: Modeling and Performance Evaluation with Computer Science Applications*. Wiley, 2006.

[80] Andrea Ancora, Issam Toufik, Andreas Bury, and Dirk Slock. *Orthogonal Frequency Division Multiple Access (OFDMA)*, chapter 5, pages 121–143. John Wiley & Sons, Ltd, 2011.

[81] Matthew Baker and Tim Moulsley. *Downlink Physical Data and Control Channels*, chapter 9, pages 189–214. John Wiley & Sons, Ltd, 2011.

[82] B. McCarthy and A. O'Driscoll. Opencv2x mode 4: A simulation extension for cellular vehicular communication networks. In *2019 IEEE 24th International Workshop on Computer Aided Modeling and Design of Communication Links and Networks (CAMAD)*, pages 1–6, 2019.

[83] Andras Varga. *OMNeT++*, pages 35–59. Springer Berlin Heidelberg, Berlin, Heidelberg, 2010.

[84] Levente Mészáros, Andras Varga, and Michael Kirsche. *INET Framework*, pages 55–106. Springer International Publishing, Cham, 2019.

[85] B.P. Crow, I. Widjaja, J.G. Kim, and P.T. Sakai. IEEE 802.11 wireless local area networks. *IEEE Communications Magazine*, 35(9):116–126, 1997.

[86] Christoph Sommer, Reinhard German, and Falko Dressler. Bidirectionally Coupled Network and Road Traffic Simulation for Improved IVC Analysis. *IEEE Transactions on Mobile Computing (TMC)*, 10(1):3–15, January 2011.

[87] Pablo Alvarez Lopez, Michael Behrisch, Laura Bieker-Walz, Jakob Erdmann, Yun-Pang Flötteröd, Robert Hilbrich, Leonhard Lücken, Johannes Rummel, Peter Wagner, and Evamarie Wießner. Microscopic traffic simulation using SUMO. In *The 21st IEEE International Conference on Intelligent Transportation Systems*. IEEE, 2018.

[88] Jerome Harri, Fethi Filali, and Christian Bonnet. Mobility models for vehicular ad hoc networks: a survey and taxonomy. *IEEE Communications Surveys Tutorials*, 11(4):19–41, 2009.

[89] Antonio Virdis, Giovanni Stea, and Giovanni Nardini. Simulating LTE/LTE-advanced networks with SimuLTE. In Mohammad S. Obaidat, Tuncer Ören, Janusz Kacprzyk, and Joaquim Filipe, editors, *Simulation and Modeling Methodologies, Technologies and Applications*, pages 83–105, Cham, 2015. Springer International Publishing.

[90] Raphael Riebl, Hendrik-Jorn Gunther, Christian Facchi, and Lars C. Wolf. Artery: Extending veins for VANET applications. In *2015 International Conference on Models and Technologies for Intelligent Transportation Systems (MT-ITS), Budapest, Hungary, June 3-5, 2015*, pages 450–456, 2015.

[91] Raphael Riebl, Christina Obermaier, Stefan Neumeier, and Christian Facchi. Vanetza: Boosting research on inter-vehicle communication. *Proceedings of the 5th GI/ITG KuVS Fachgespräch Inter-Vehicle Communication (FG-IVC 2017)*, pages 37–40, 2017.

[92] Yvo de Jong Bultitude and Terhi Rautiainen. Ist-4-027756 winner ii d1. 1.2 v1. 2 WINNER ii channel models. *EBITG, TUI, UOULU, CU/CRC, NOKIA, Tech. Rep*, 2007.

[93] Richard Rouil Jian Wang. *BLER Performance Evaluation of LTE Device-to-Device Communications*, Nov 2016. Wireless Networks Division Communications Technology Laboratory (NIST).

[94] Stefania Sesia, Issam Toufik, and Matthew Baker. *Radio Frequency Aspects*, pages 457–502. 2011.

[95] M. Gonzalez-Martín, M. Sepulcre, R. Molina-Masegosa, and J. Gozalvez. Analytical models of the performance of C-V2X mode 4 vehicular communications. *IEEE Transactions on Vehicular Technology*, 68(2):1155–1166, 2019.

[96] 3GPP. *User Equipment (UE) radio transmission and reception (v14.0.0, Release 14)*, Mar. 2017. TR 38.786.

[97] NXP. *Analysis of CAMP Report on the C-V2X Performance Assessment Project*, 2019.

[98] 3GPP. *Physical layer Measurements (v14.0.0)*, Dec. 2017. TS 36.214.